Journal of Cardiovascular Magnetic Resonance (2005) **1,** 109–327

ISSN: 1097-6647 print / 1532-429X online
DOI: 10.1081/JCMR-200048628

Taylor & Francis
Taylor & Francis Group

Posters

321. Chronic Testosterone Treatment in Men with Coronary Artery Disease: A Study with Perfusion Cardiovascular Magnetic Resonance

Andrew G. Elkington,[1] Carolyn M. Webb, PhD,[2] Peter D. Gatehouse, PhD,[1] David N. Firmin, PhD,[1] Dudley J. Pennell, MD,[1] Peter Collins, MD.[2] [1]*CMR Unit, Royal Brompton and Harefield NHS Trust, London, UK,* [2]*Department of Cardiology, Royal Brompton and Harefield NHS Trust, London, UK.*

Introduction: Testosterone has beneficial effects on myocardial ischemia and endothelial function in men with coronary artery disease, however the effects of chronic testosterone treatment on myocardial perfusion per se are unknown. Therefore, we measured the effects of chronic testosterone on myocardial perfusion in men with coronary artery disease (CAD) and low-normal or low plasma testosterone using cardiovascular magnetic resonance (CMR).

Methods: 22 men (57 ± 9 years) with known CAD were randomised to either oral testosterone (80 mg BD) or identical placebo. After 8 weeks their treatment was crossed over. After each 8 week period they underwent a rest and adenosine stress first-pass myocardial perfusion CMR scan. All CMR studies were performed on a 1.5 T scanner (Siemens Sonata). For each study, we used a gadolinium bolus (0.1 mmol/kg, 7 ml/s) and a FLASH sequence (pixel size 1.4 × 1.4 mm, TE 1.1 ms, TR 1.9 ms, image time 295 ms) with a mid-ventricular short axis slice. All images were analysed off-line using dedicated software (CMRtools, London, UK). The subendocardial and subepicardial myocardial perfusion reserve indices (MPRi) were calculated for the septum, anterior, lateral and inferior walls.

Results: There was a significant improvement in the subendocardial MPRi on testosterone treatment (1.83 ± 0.92 vs 1.54 ± 0.88, + 19%, $p = 0.01$). The improvement in MPRi on testosterone treatment in the subepicardium was also significant (1.86 ± 0.83 vs 1.65 ± 0.89, + 13%, $p = 0.05$).

Conclusions: In men with CAD and low plasma testosterone, chronic oral testosterone treatment improves myocardial perfusion reserve. This is supportive of the potential clinical use of testosterone in this group of patients.

322. To Assess Age Related Variation of Myocardial Perfusion By Cardiovascular MR (CMR) in Healthy Human Volunteers

Jonathan Lyne, MRCP, Andrew Elkington, MRCP, Gillian Smith, Peter Gatehouse, PhD, Guang-Zhong Yang, PhD, Assomull Ravi, MRCP, Pennell Dudley, MD FRCP FACC FESC. *CMR Unit, Royal Brompton Hospital, London, UK.*

Introduction: Coronary vasodilator reserve, the ratio of maximal to baseline coronary blood flow is a measure of coronary vasodilatory capacity. Coronary vasodilatation may decline with age; the onset, amplitude and time course of these potential changes are fundamental to our understanding of perfusion.

Purpose: To assess age related variation of myocardial perfusion by cardiovascular MR (CMR) in healthy human volunteers.

Methods: Eighteen healthy volunteer subjects were recruited (mean age 50, range 36–69 years, 15 women) as controls for a CMR study of cardiac syndrome X. Written informed consent was obtained in accordance with ethics committee requirements. Subjects refrained from caffeinated beverages or supplements for 24 hours prior to scanning. All volunteers gave no history of cardiac or pulmonary disease, hypertension, hyperlipidaemia, smoking or diabetes. No subject was on any chronic medication. All had normal resting electrocardiography and exercise tolerance. Based on these findings all participants had a low probability of coronary artery disease.

CMR scans were performed using a Siemens Sonata 1.5 T scanner. Subjects were scanned supine using a 4 element phased array coil. Perfusion sequence parameters were as follows: Hybrid EPI, matrix size = 160; phase resolution 100%, 1.9 × 1.9 mm pixels, 8 mm slice thickness; field-of-view = 340 × 75%; acquisition time per slice 186 ms; TR = 6.2 ms; flip angle 30 degrees. First pass perfusion studies were performed with 0.1 mmol/kg injection of 0.5 mol gadolinium DTPA (Schering). The contrast was injected at 5 ml/sec using a power injector (Medrad, Pittsburgh, PA) followed by 10 ml normal saline, 50 images per slice were obtained during a single breathold. Hyperemia was induced by an intravenous adenosine infusion, via the left antecubital vein, (Adenoscan, Sanofi-Synthelabo, UK) at 140 mcg/kg/min for 4 minutes. Perfusion scans at rest then stress were performed at least 20 minutes apart, allowing for clearance of contrast agent between the two scans.

Results: CMR was successful and well tolerated in all volunteers. Studies were analysed on CMRtools (Cardiovascular Imaging Solutions, London, UK), using a single mid ventricular slice. A single region of interest (ROI) was drawn to delineate the entire myocardium. Spatially averaged signal intensity (SI) time curves from the ROI were obtained. Model constrained deconvolution was used to calculate the impulse response function from the SI curves. The myocardial perfusion reserve index (MRPI) was then calculated and plotted

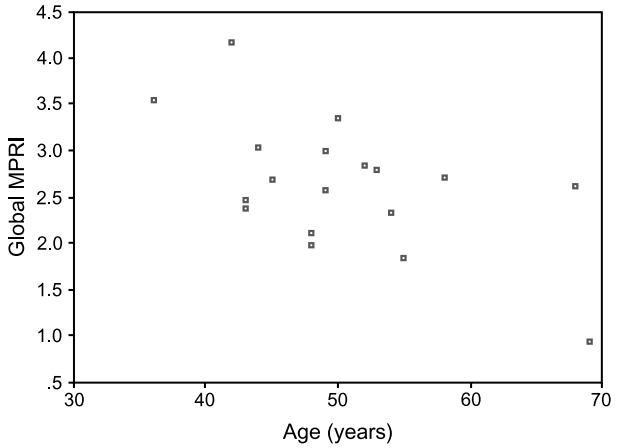

Figure 1.

against age (Figure 1) yielding a Spearman's rank correlation of − 0.529 ($p = 0.011$). There was no significant correlation between age and diastolic blood pressure (−0.390 $p = 0.122$). But there was a negative correlation (−0.584, $p = 0.014$) between age and systolic pressure.

Conclusions: This is the first CMR study to describe decreasing myocardial perfusion reserve with increasing age. With aging there is a reduced heart rate response to beta adrenergic receptor stimulation a lesser increase in left ventricular ejection fraction and reduced relaxation of systemic vascular resistance. Endothelial cells become increasingly dysfunctional and their functional integrity weakens. In experimental models there is greater local release of adenosine into the coronary microcirculation of older animals, exogenous adenosine may have a lesser effect on vascular smooth muscle due to receptor downregulation. These changes impose a greater pulsatile and late-systolic load on the ventricle. This results in systolic prolongation, increasing the proportion of coronary flow during the systolic time period, closely linking ventricular systolic function with myocardial flow, potentially compromising flow reserve. Our results are in accord with a previous positron emission tomography study. The significance of these findings is that an appreciation of a decreasing MPRi with aging may need to be taken into account in the utilization of this technique in threshold values for the detection of coronary artery disease.

323. Correlates of Sub-Endocardial Myocardial Perfusion Reserve By First Pass MRI

Olakunle O. Akinboboye, MBBS, MPH, MBA,[1] Yi Wang, DSc,[1] Nora Ngai, PhD,[1] Sunil T. Mathew, MD,[1] Uzodinma R. Dim, MD,[1] Kathy McGrath, RN,[1] Marguerite Roth, RN,[1] William Schapiro, RT (CMR),[1] Kenneth Nichols, PhD.[2]
[1]*Research, St. Francis Hospital/Stonybrook University, Roslyn, NY, USA,* [2]*Nuclear Medicine, Long Island Jewish Medical Center, New Hyde Park, NY, USA.*

Introduction: The determinants of sub-endocardial (SE) (inner 50% of the myocardium) myocardial perfusion are unclear.

Purpose: We hypothesized that serum HDL and LDL are determinants of myocardial perfusion reserve index (MPRI) in the SE.

Methods: We measured indices of myocardial perfusion by first-pass gadolinium-enhanced MRI following I.V. adenosine-induced hyperemia and at rest in 20 asymptomatic diabetic patients without known CAD (75% male, mean age 59 ± 9). A 1.5 T MRI scanner (Sonata, Siemens Medical Solutions, Malvern, PA) with a circular polarized body array flex coil was used. Short axis imaging was performed using a partial Fourier saturation recovery TurboFLASH sequence with these parameters: TR/TE/TI/FA = 2.9 ms/1.3 ms/90 ms/15°, data matrix 128 × 70, and voxel spatial resolution 3.5 × 1.9 × 8 mm^3 based on the size of the patient. Gadolinium contrast dose was 0.05 mmol/kg per injection (Omniscan, Amersham). The steepness of the initial upslope phases of the first pass signal intensity curves for the blood pool and myocardium (using 6 equal sectors) were determined automatically by using commercially available software (MEDIS, Medis Imaging Systems Inc, Leiden, The Netherlands). Rest perfusion relative upslope (RPRU) and hyperemic perfusion relative upslope (HPRU) were computed as the ratios of myocardial curve upslope to blood pool curve upslope at rest and during hyperemia, and MPRI computed as HPRU/RPRU. Same day measurements taken and entered into a multivariate model for determinants of SE MPRI were (table):

Results: (Mean for the six sectors):RPRU = 12 ± 5%, HPRU = 12.5 ± 4%, and MPRI = 1.1 ± 0.4. The only significant correlate of SE MPRI by univariate analysis was HDL (r = 0.639, $p = 0.003$). On multivariate analysis the significant correlates of SE MPRI were HDL (T = 4.031, $p = 0.001$) and LDL (T = 2.134, $p = 0.049$).

Conclusions: The correlates of SE perfusion reserve by cardiac MPRI are serum LDL and HDL levels.

Clinical characteristics

Measure	Value	Measure	Value
Mean Weight (lbs)	206 ± 33	Fasting Glucose (mg/dl)	170 ± 79
Waist Circumfrence	103 ± 10	C-reactive Protein(mg/dl)	4.2 ± 3
T.Chol (mg/dl)	185 ± 34	Insulin (mg/dl)	16 ± 22
HDL (mg/dl)	45 ± 12	HB AIC (%)	7 ± 1
Triglyceride (mg/dl)	157 ± 99	Von Willebrand Factor (%)	114 ± 55
LDL (mg/dl)	109 ± 27	micro-albumin (mg/dl)	23 ± 30

324. On Artifacts in First-Pass Myocardial Perfusion Imaging

Oliver M. Weber, PhD. *Department of Radiology, University of California, San Francisco, San Francisco, CA, USA.*

Introduction: Assessment of myocardial perfusion deficits by means of MR imaging during first pass of contrast agent has found widespread acceptance for the diagnosis of coronary artery disease. Even though absolute quantification is difficult, the relative information available has proven to be of high diagnostic value, and agreement with other modalities is good. However, a number of prerequisites render perfusion imaging 7demanding, and compromises have to be made. Contrast passage needs to be sampled at high frequency. In general, a data point every heartbeat, or at least every other heartbeat, is required. Since acquisition of several (usually, 3–4) slices is required for sufficient spatial coverage, imaging time is restricted to typically 150–200 ms per slice. Therefore, spatial resolution achievable inplane is limited, and effects of partial volume are commonly seen in perfusion images, especially at the interface between ventricular cavities and myocardium.

Purpose: To assess effects of spatial resolution and contrast agent concentration on artifacts in sequence used for perfusion imaging.

Methods: A phantom was built to reflect myocardial geometry using an external circular container ('myocardium'; diameter, 11 cm) with a suspended plastic bag at the center ('left ventricular cavity'; diameter, 7.5 cm). The outer container was filled with 1.25 mM Gd-DOTA (Dotarem, Guerbet Group, Aulnay Sous Bois, France) in 0.9%-saline solution (T1 $\approx$ 400 ms). The inner bag was filled with 30, 20, 10, 5, 3.75, and 2.5 mM Gd-DOTA in 0.9%-saline solution. At each concentration level, single-shot MR imaging was performed using a fast gradient echo sequence at spatial resolutions of 4.0 mm, 3.2 mm, 2.7 mm, 2.0 mm, 1.6 mm, 1.3 mm, and 1.0 mm (TR = 2.0–3.9 ms; TE = 1.0–2.0 ms; FOV = 256 mm; slice thickness = 8 mm; matrix = 64–256; halfscan = 62%). In preliminary experiments, it had been determined that neither SENSE nor halfscan (partial Fourier) nor phase encoding direction had an impact on image quality. Ten dynamics were acquired in a triggered (60 bpm) sequence. Imaging times ranged from 80–624 ms per dynamic. The outlines of signal loss around the inner cavity was manually drawn using ImageJ (Research Services

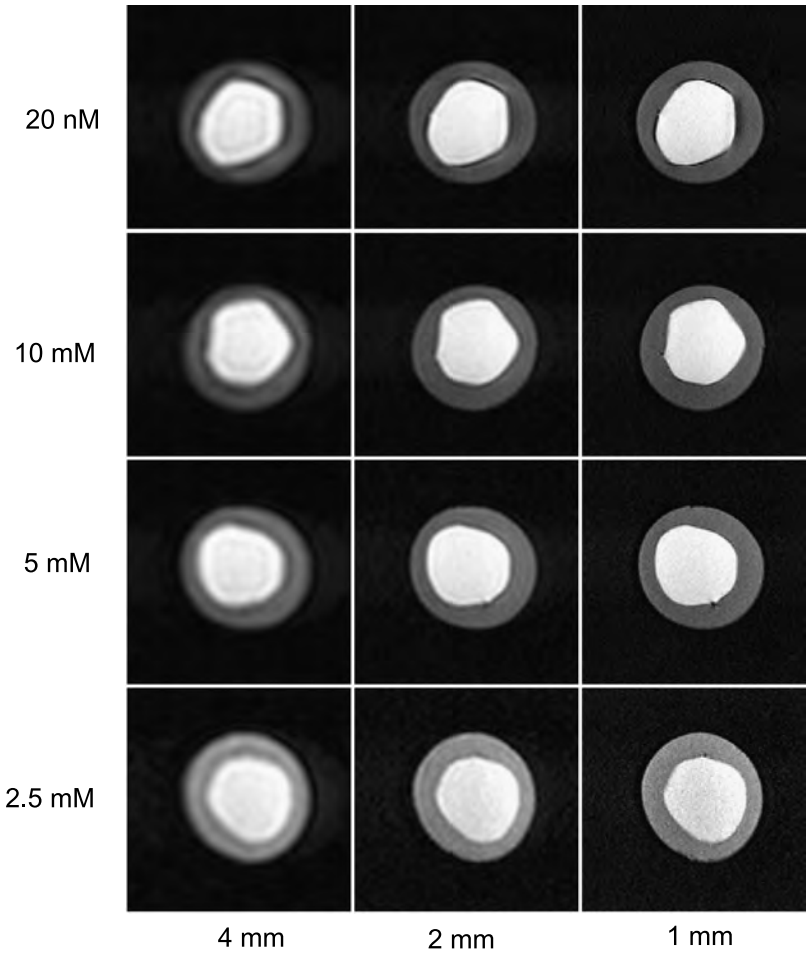

Branch, NIH, Bethesda, MD), and the area was expressed as percentage of total outer area ('myocardium').

Results: In many cases, artifacts previously occasionally seen in vivo could be reproduced. As may be expected, there was a clear trend towards smaller artifacts with higher spatial resolution and lower contrast agent concentration. However, it was also found that, for all concentrations investigated, at spatial resolutions above 2 mm considerable fractions (between 13 and 33%) of the outer area were affected by signal loss artifacts, with smaller loss of signal intensity at lower concentrations. At high contrast agent concentrations, artifact size remained around 10% even at the highest spatial resolution. For lower concentrations, artifact size was greatly reduced for higher spatial resolution and was below 5% for spatial resolutions of 1 mm at 10 and 5 mM, 1.6 mm or better at 3.75 mM, and 2 mm or better at 2.5 mM.

Discussion: The artifacts seen both in this study and in vivo are most likely due to partial volume effects in combination with high differences in susceptibility. The goal should therefore be to aim for the highest spatial resolution achievable, potentially by sacrificing coverage. Fast imaging techniques such as parallel imaging and partial Fourier may also be helpful. Reducing the amount of contrast agent administered is beneficial as well, but also reduces the contrast to noise ratio of hypo-enhancing regions. The two effects must therefore carefully be balanced against each other.

Conclusion: To avoid partial volume/susceptibility artifacts in first pass perfusion imaging, a high spatial resolution (2 mm inplane or better) in combination with the minimum acceptable contrast dose should be chosen.

Artifact size (%) in dependence of spatial esolution and contrast agent concentration

	4.0 mm	3.2 mm	2.7 mm	2.0 mm	1.6 mm	1.3 mm	1.0 mm
30 mM	18.7	15.6	15.0	13.8	12.9	10.8	9.6
20 mM	17.7	17.0	15.0	12.6	11.4	10.4	11.0
10 mM	22.3	18.9	15.5	14.0	9.9	8.4	4.6
5 mM	16.6	17.9	15.7	10.8	10.8	8.3	3.5
3.75	23.7	13.2	14.0	11.3	3.5	1.8	0.3
2.5	33.7	18.4	14.8	2.1	1.9	0.6	0.2

325. Post Operative Myocardial Infarction: New Parameters with Cardiovascular Magnetic Resonance

Ricardo O. Obregon, Sr., MD, Angel Piacenza, Sr., MD, Jorge Parras, MD, Edgar Garcia, MD, Raul Cayre, MD, Raul Pelozo, MD. *Resonancia Cardiovascular, Instituto de Cardiologia, Corrientes, Argentina.*

Introduction: The diagnosis of post operative myocardial infarction (POMI) in human is not well understood. Current clinical diagnosis is mostly based on the electrocardiogram (EKG) and serologic findings. Diagnostic tools currently available are unsatisfactory. Previous studies indicated that the delayed enhancement by contrast cardiovascular magnetic resonance (deCMR) and the abnormal wall motion are associated with irreversible ischemic injury. We have hypothesized that CMR parameters can predict POMI (rPOMI) compared with classical POMI parameters (cPOMI): Elevated creatine kinase MB isoform (CK-MB) and electrocardiogram (EKG).

Purpose: The goals of this study were: (1) to evaluate the utility of the cardiovascular magnetic resonance for diagnosing POMI compared with classical parameters. And (2) to compare the results with clinical variables of the early post operative period.

Methods: Fifty seven consecutive patients admitted for coronary artery bypass surgery were studied. Group A: (21 patients) without previuos myocardial infarction and Group B: (36 patients) with previous myocardial infarction.

POMI was defined by CMR (rPOMI) by the presence of new abnormalities of the wall motility and Classical POMI (cPOMI) by new elevation of CK-MB > 60 UI/ml and new Q waves in the electrocardiogram. These groups were compared with regard hemodynamic and enzymatic variables of the early post-operative period.

Irreversible myocardial injury was visualized by T1-weighted sequences (TE 23 ms, slice thickness 10 mm, matrix 256 × 180, field of view 360 × 360 cm) 25 min after intravenous application of 0.1 mmol/kg gadolinium-pentetic acid. We calculated the signal intensity ratio of the infracted myocardium compared with remote myocardium and the proportion of the infarcted tissue related to the entire myocardium in the infarct-containing slice.

The left ventricular ejection fraction was quantified in a set of contiguous gradient-echo images (TE 4.8 to 6.1 ms, slice thickness 10 mm) in the true short-axis orientation. A 16 segment model was scored for wall motion and contrast-enhancement by two blinded observers.

Results: In Group A, patients with POMI identified by deCMR had a higher number of coronary artery graft 3.8 ± 1.4 vs. 2.5 ± 3.8 ($p < 0.03$), longer time of cardiopulmonary bypass (CPB) 154 ± 4.5 vs. 71 ± 74 min ($p < 0.015$), longer time of aortic cross clamp 101 ± 31 vs. 49 ± 60 min ($p < 0.05$) and higher level of cTnT 2.24 ± 2.9 vs. 0.66 ± 1.0 ($p < 0.039$). In the same group, only patients with higher levels of cTnT and CK-MB were identified by cPOMI approach (Chart 1). In group B, patients with longer time of CPB 142 ± 69 vs. 80 ± 74 min ($p < 0.04$) were identified by cPOMI approach, whereas rPOMI failed to identify more complicated patients.

Conclusions: 1) CMR is a useful method to study POMI in post-operative coronary by-pass patients. 2) The identification of POMI by CMR were better than the classical approaches to identify estimate the patients with longer surgical times and greater intra-operative ischemia (cTnT).

Variables in patients without previuos infarction

Variables post surgery	cPOMI (−)	cPOMI (+)	p	rPOMI (−)	rPOMI (+)	p
Venous N° By pass	1.25 ± 1.12	2.5 ± 1.73	0.08	1.15 ± 1	2.14 ± 1.57	0.11
N° arterial by pass	1.37 ± 0.45	1.25 ± 0.5	0.8	1.15 ± 0.68	1.71 ± 1.1	0.17
Total N° of by pass	2.62 ± 1.15	3.75 ± 1.25	0.18	2.3 ± 1.25	3.85 ± 1.4	**0.02**
Circulatory bypass	88 ± 78	149 ± 38	0.15	71 ± 74	154 ± 45	**0.01**
Time aortic Clamp	57 ± 57	106 ± 37	0.12	49 ± 60	101 ± 31	**0.05**
CK-MB	20 ± 18	65 ± 29	**0.0007**	22 ± 21	47 ± 35	0.06
cTnT	1.02 ± 1.4	1.81 ± 3.3	0.48	0.66 ± 1	2.24 ± 2.9	0.04

326. Stress Myocardial Perfusion MRI using FIESTA in the Detection of Significant Coronary Artery Stenosis

Kakuya Kitagawa, MD,[1] Tairou Kurita, MD,[2] Hajime Sakuma, MD,[1] Katsuya Onishi, MD,[2] Kan Takeda, MD,[1] Takeshi Nakano, MD,[2] Atsushi Nozaki, PhD,[3] Thomas K. Foo, PhD.[4] [1]*Radiology, Mie University Hospital, Tsu, Japan,* [2]*Internal Medicine, Mie University Hospital, Tsu, Japan,* [3]*GEYMS, Tokyo, Japan,* [4]*GE, Baltimore, MD, USA.*

Introduction: Previous studies demonstrated that first-pass myocardial perfusion MRI during vasodilator stress permits noninvasive detection of flow-limiting stenoses in the coronary arteries. However, considerable artifacts and image noise are frequently observed on myocardial perfusion MR images, because there are opposing requirements for the perfusion MR sequence, including good temporal resllution, high spatial resolution and full coverage of LV myocardium.

Purpose: The purposes of this study were to evaluate if FIESTA (Fast Imaging Employing Steady State Acquisition) perfusion MR seqeunce can provide improved image quality in comparison with conventional perfusion MR seqeunce using a hybrid echo-planar approach, and to determine the diagnostic performance of stress perfusion MRI using FIESTA in detecting significant coronary arterial stenoses.

Methods: Thirty-one patients (mean age 65 +/− 10 years) with suspected coronary artery disease were evaluated with a 1.5 T MR system. First-pass dynamic MR images were acquired during ATP stress and in the resting state by using FIESTA perfusion sequence (TR 3.0 ms; TE 1.2 ms; TI 180 ms; flip-angle 45 degrees) after intravenous bolus injection of gadolinium contrast medium (0.05 mmol/kg, 4 ml/sec). Coronary angiography was performed in all patients within 2 weeks of MR study. Stenosis of 70% or more of the luminal diameter of the coronary artery was considered to be significant. The contrast-to-noise ratios at peak contrast enhancement in normally perfused myocardium were calculated on FIESTA perfusion MR images and conventional perfusion MR images (gradient echo sequence with echo planar readout; TR 6.7 ms; TE 1.4 ms; 4 echo-trains; TI 180 ms; flip angle 20 degrees).

Results: FIESTA perfusion MRI showed significantly improved contrast-to-noise ratio (16.4 +/− 5.3 vs 12.5 +/ − 3.6, $p < 0.05$) when compared with conventional perfusion MRI using echo-planar readout. In addition, no serious subendocardial hypointensity artifact was observed on FIESTA perfusion MR images during first-pass transit of MR contrast medium through the left ventricle. At selective coronary angiography, 70% or greater diameter stenosis was detected in 39 of the 93 major coronary arteries. The overall sensitivity of stress myocardial perfusion MRI using FIESTA for detecting patients having at least one coronary artery with significant luminal narrowing was 86% (19 of 22 patients). The sensitivity and specificity of stress myocardial perfusion MRI using FIESTA in predicting significant stenosis in the individual coronary artery were 85% (33 of 39 arteries) and 93% (50 of 54 arteries), respectively.

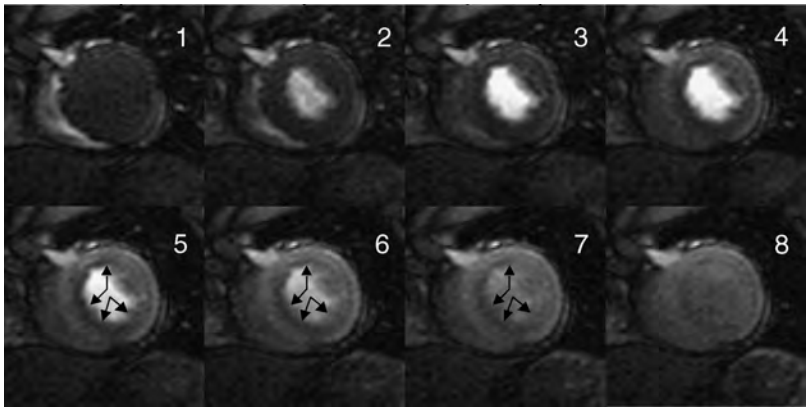

Figure 1. Stress perfusion MRI using FIESTA in double vessel disease. Ischemic myocardium was clearly depicted as subendocardial perfusion defects in anteroseptal wall and inferior wall (arrows).

Conclusions: Myocardial perfusion MRI using FIESTA demonstrated improved contrast-to-noise ratio and reduced artifact when compared with conventional perfusion MRI using a hybrid echo-planar method. Stress myocardial perfusion MRI using FIESTA permits accurate detection of significant coronary artery disease in patients with suspected coronary artery disease (Figure 1).

327. Cardiac MRI Can Detect Myocardial Scar in Patients with Troponin Positive Chest Pain and Minimal Angiographic Coronary Disease

Jonathan P. Christiansen, MB ChB, MD, FRACP,[1] Colin Edwards, MB BS, FCP,[1] Toni Sinclair, BHSc, PGDipHMgt,[2] Guy Armstrong, MB ChB, FRACP,[1] Tony Scott, MB ChB, FRACP,[1] Hitesh Patel, MB ChB, FRACP,[1] Hamish Hart, MB BCh, MRCP, FRACP.[1] [1]*Cardiovascular Division, Waitemata Health, Auckland, New Zealand,* [2]*The Radiology Group, Auckland, New Zealand.*

Introduction: Patients presenting with chest pain (CP) and an elevated serum troponin may be subsequently found to have minimal coronary artery disease on angiography. We hypothesised that a proportion of these patients will have focal myocardial scar. We used contrast-enhanced cardiac magnetic resonance imaging (CE-CMR) to investigate for previously undiagnosed scar.

Methods: We studied 17 patients (mean age 55 ± 7) presenting with CP, an elevated troponin I ($\geq$ 0.9 ng/mL, Bayer Corp) and minimal angiographic coronary disease (CAD). Patients with a clinical diagnosis of pericarditis, tachyarrhythmia at presentation, prior history of MI and those with an alternative explanation for an elevation in Troponin I were excluded. CMR was performed $\geq$ 2 weeks after the index event using a 1.5 T Philips Intera. Functional and volumetric data were obtained from breath-hold steady state free precession cine imaging. Myocardial scar was assessed using delayed enhancement (DE) inversion recovery imaging 10 minutes following administration of 0.1 mM/kg Gd-DTPA.

Results: DE consistent with myocardial scar (DE + ve) was seen in 5 of 17 patients (29%). All DE was in a subendocardial distribution. Mean Troponin I was not different between DE + ve vs DE-ve patients (4.8 ± 3.1 vs 4.0 ± 3.1, p = ns). LV systolic function was normal in all patients but significantly higher in the DE-ve group [EF% = 62 ± 3 (DE + ve) vs 71 ± 8 (DE-ve) $p < 0.05$]. DE was seen in the inferior or inferolateral segments in all 5 DE + ve patients and 4 patients had a RWMA in that location. One DE + ve patient had a prior history of paroxysmal atrial arrhythmia suggesting an embolic source.

Conclusions: Patients with an acute presentation of CP and an elevated serum troponin may have significant myocardial scar even when minimal CAD is found on angiography. This may have important implications for both prognosis and treatment.

328. Assessment and Follow-Up of Patients Presenting with Non-ST Elevation Acute Coronary Syndromes Treated with Early Revascularisation Using Cardiac Magnetic Resonance Imaging

Patrick Sparrow, MD,[1] Stephen Ball, MD, PhD,[2] Mohan U. Sivananthan, MD,[1] Sven Plein, MD.[1] [1]*BHF Cardiac MRI Unit, Leeds General Infirmary, Leeds, UK,* [2]*BHF Heart Research Unit, Leeds General Infirmary, Leeds, UK.*

Introduction: Current AHA guidelines recommend that patients presenting with high or intermediate-risk non-ST elevation acute coronary syndromes (NSTE-ACS) undergo early x-ray angiography and revascularisation. Cardiac Magnetic Resonance (CMR) imaging can provide information about myocardial ischemia, function and viability.

Purpose: The aim of this study was to evaluate CMR in the initial assessment and follow-up of patients with NSTE-ACS who underwent early revascularisation.

Methods: Twenty-five patients (24 men and one woman, mean age 56.08 years, range 40–75 years) with a diagnosis of NSTE-ACS based on the presence of suspected cardiac chest pain and/or electrocardiogram abnormalities who underwent early coronary angiography and revascularization were recruited. Patients underwent CMR imaging 24–48 hours before and 6–8 months after revascularisation using a comprehensive single-session protocol that assessed myocardial function, perfusion (rest and Adenosine-stress), and viability (with delayed-contrast enhanced imaging). Quantitative visual analysis of all combined CMR data was performed with estimation of left ventricular volumes and mass, both fixed and inducible ischaemic burden as measured by percentage LV mass visualized demonstrating an defect on first pass perfusion imaging and scar as measured by delineation of delayed enhancement. Changes in left ventricular function, scar

Table 1. Summary of results pre and post revascularisation

	PCI(n = 17)			CABG(n = 8)		
Mean value	Before	After	Paired t test	Before	After	Paired t test
LVEF (%)	59.2	58.83	$p = 0.74$	58.8	59.7	$p = 0.7$
DE (grams)	4.47	4.14	$p = 0.85$	6.24	7.1	$p = 0.44$
Perfusion defect (% mass)						
Fixed	1.97	1.08	$p = 0.25$	2.28	1.98	$p = 0.76$
Inducible	22.92	1.36	$p < 0.0001$	22.86	0	$p < 0.006$

burden and perfusion abnormalities were compared between the two examinations and assessed for statistical difference using a paired t test. A p value < 0.01 was considered to indicate statistical significance.

Results: Seventeen patients underwent percutaneous coronary intervention (PCI) and eight coronary artery bypass grafting (CABG). There was no significant statistical difference in left ventricular function, as assessed by ejection fraction or left ventricular scar burden, as assessed by total mass of scar on delayed enhancement in either PCI or CABG before and after the revascularization procedure. However there was a significant reduction in inducible ischaemic burden in both PCI and CABG groups following their respective procedures (See Table 1). No patients in the CABG group had inducible ischaemia on follow up but 2 patients in the PCI group did- one a new defect and the other a persistant defect present prior to intervention.

Conclusions: CMR imaging can be used to assess the functional effects of revascularisation in NSTE-ACS. Patients treated with either PCI or CABG demonstrates a significant improvement in perfusion as assessed by CMR.

329. Accuracy of Qualitative Analysis of Myocardial Perfusion by Adenosine Stress MRI in Suspected Coronary Artery Disease

Kiran R. Nandalur, MD,[1] Frederick H. Epstein, PhD,[1] Szilard Voros, MD,[2] John M. Christopher, RT,[1] Jennifer R. Hunter, RN,[1] Christopher M. Kramer, MD.[1] [1]*Radiology, University of Virginia Health Systems, Charlottesville, VA, USA,* [2]*Cardiology, University of Virginia Health Systems, Charlottesville, VA, USA.*

Background: Diagnostic accuracy of quantitative analysis of first-pass contrast-enhanced stress myocardial magnetic resonance imaging is well-documented. The accuracy of qualitative analysis of stress perfusion CMR is not fully established.

Purpose: To assess the diagnostic accuracy of qualitative analysis of first-pass contrast-enhanced stress myocardial magnetic resonance imaging using a hybrid gradient echo/echo planar pulse sequence in the detection of coronary artery disease (CAD) with x-ray angiography as the gold standard.

Methods: We prospectively studied 20 patients (age 59+/−12 years, 35% female, 15% previous myocardial infarction, 80% hypertension, 85% hypercholesterolemia, 60% tobacco use, 15% diabetes) with chest pain and suspected significant CAD who also underwent cardiac catheterization. The patients were studied on a Siemens Sonata 1.5 T MR scanner employing a multi-slice hybrid gradient echo/echo-planar sequence to examine the myocardial first pass of Gd-DTPA (0.075 mM/kg injected at 3 mL/s IV) during hyperemia (adenosine 140 μg/kg/min × 4–6 minutes) and again at rest 10 minutes later. Specific parameters included a nonselective 90° saturation pulse followed by a 60–80 ms delay, field of view = 340–400 × 212–360 mm, matrix = 128 × 80, slice thickness = 8 mm, flip angle = 25°, TR = 6.2 ms, TE = 1.3 ms, and echo train length = 4. Three short axis slices (apex, mid, and base) were imaged over 50 heartbeats during stress and rest. Delayed enhancement inversion recovery fast gradient echo imaging was performed in the same 3 slices, 10–20 minutes after a total of 0.15 mM/kg Gd-DTPA. The inversion time was chosen to null normal myocardial signal. X-ray coronary angiography was performed in all patients within 11 +/− 10 days of MR. MR exam quality was assessed on a semi-quantitative scale (1 = excellent, 2 = good, 3 = fair, 4 = poor). MR images were examined by an experienced observer blinded to clinical data using a 16 segment left ventricular model. A total of 320 segments were classified as 1) normal; 2) ischemia (qualitative perfusion defect at stress but not at rest; 3) infarct (perfusion defect with corresponding delayed enhancement in the same segment; or 4) artifact. Receiver-operator characteristic (ROC) analysis was utilized to assess the diagnostic performance of MR relative to catheter angiography, with 50% or greater luminal diameter stenosis considered significant.

Results: The incidence of significant CAD (> 50% stenosis) on a per patient basis was 7/20 or 35%. The overall MR image quality mean was 1.9 +/− 0.8. The overall sensitivity and specificity of MR imaging for detecting significant CAD was 86% and 77%. The area under the ROC curve for the detection of significant stenosis in individual coronary arteries was 0.81 (standard error = 0.11).

Conclusions: First-pass contrast-enhanced stress myocardial MR using a hybrid gradient echo/echo planar pulse sequence with qualitative image analysis is accurate in the detection of coronary artery disease using x-ray angiography as the gold standard. The potential additive value of quantitative image analysis requires further study.

330. First-Pass Perfusion and Delayed Enhancement Magnetic Resonance Imaging Detect Papillary Muscle Ischemia in Ischemic Mitral Regurgitation

Philipp Boyé,[1] Hassan Abdel-Aty,[1] Jeanette Schulz-Menger,[1] Matthias G. Friedrich.[2] [1]*Cardiology, Franz-Volhard-Klinik, Helios Klinikum Buch, Berlin, Germany,* [2]*Department of Cardiac Sciences, Faculty of Medicine, University of Calgary, Calgary, AB, Canada.*

Introduction: Ischemic mitral regurgitation (MR) predicts poor prognosis in patients with acute and chronic coronary artery disease (CAD). In these patients, papillary muscle dysfunction may be caused by acute myocardial necrosis as well as chronic hypoperfusion. Delayed enhancement imaging and first-pass perfusion in Cardiovascular Magnetic Resonance (CMR) are highly sensitive tools to detect small areas of myocardial necrosis and perfusion defects.

Purpose: We attempted to visualize papillary muscle necrosis and hypoperfusion in the setting of acute myocardial infarction (AMI) and chronic CAD respectively and explore its association with MR as assessed by standard techniques.

Methods: We investigated two groups of patients with either acute MI (Group A: 29 Patients, 26 males) or chronic CAD (Group B: 31 Patients, 26 males, Age 57 ± 12) on 1,5 T scanner applying

1. inversion recovery gradient echo pulse sequence (IR-GRE) 10 minutes after intravenous injection of Gd-DTPA (0,2 ml/kg) to assess delayed Enhancement (DE). (both Goups)
2. GRE-EPI hybrid sequence to asses First-pass Perfusion (Group B only).

Echocardiography and/or cardiac catheterization served as the gold standard to identify MR. Two blinded observers evaluated both papillary muscles in CMR images visually for a consensus diagnosis of:

a) the presence of DE
b) the presence of perfusion defects.

Results:

GroupA: Echocardiography revealed MR in 24/29 patients. Of these 24 patients, DE of at least one PM was found in 20. The posterior PM was most frequently involved (85%).

Group B: Echocardiography or cardiac catheterization revealed MR in 13/31 patients of whom 12 showed hypoperfusion in at least one PM (6 posterior, 1 anterior, 5 both). There was a significant correlation between the presence of PM hypoperfusion in CMR and MR as defined by Echo/Cath (Chi-Square $p < 0.002$).

Conclusion: Delayed Enhancement and first-pass perfusion CMR are sensitive tools to identify papillary muscle ischemia related to ischemic mitral regurgitation both, in the setting of acute myocardial infarction and chronic coronary artery disease.

331. Variation of Coronary Artery Lumen Measurements Between Dark-Blood and Bright Blood Techniques

Yi Wang, Dsc, Sunil T. Mathews, MD, Bin Luo, Nathaniel Reichek, MD. *Department of Research, St. Francis Hospital, Roslyn, NY, USA.*

Introduction: Quantification of coronary lumen is an important MRA application in stenosis diagnoses. Coronary-artery angiography requires high-resolution 3D imaging since vessels are tortuous and their diameters are usually 3 to 4 mm. Both bright blood and dark blood techniques are used in MR coronary imaging. However, their performance on measuring coronary vessels was unclear.

Purpose: To validate a hypothsis that the value of measured vessel lumen tends to be smaller on images with dark blood techniques than that with bright blood techniques.

Methods: We examined the consistency of in-plane proximal left main (LM) or left anterior descending (LAD) coronary artery lumen measurement with different MR imaging techniques, including 2D breath hold TurboFLASH, 3D breath hold and navigator guided TrueFISP, as well as breath hold (2D) and navigator guided (3D) dark blood in 22 volunteers with IRB approved consent (ages: 38 to 79 mean and std 60.4 ± 10.7, 10 females) without known coronary abnormality by 2 experienced observers. After scout imaging located the proximal LM, a 3D breath hold ECG-triggered TrueFISP (TFI) sequence was used to acquire images of LM or LAD on axial slices. The same slice location was then used for 2D breath hold TurboFLASH and Turbo Spin Echo dark blood imaging. A 3D navigator guided TFI and Turbo Spin Echo were finally collected also at axial slab. All images were acquired with a 1.5 T Siemens Sonata scanner (Siemens Medical Solutions, Malvern, PA) and a CP body array flex coil. The sequence parameters for the 3D breath hold TFI: TR/TE/FA = 2.9 ms/1.3 ms/50°, data matrix 220 × 320, and voxel spatial resolution 1.6 × 1.1 × 1.5 mm^3. FOV was kept the same for all imaging at 350 mm, the segmented data acquisition window was kept short (160 ms) and turned on only at diastole. 3D navigator guided TFI images has the same resolution. An acceptance window of ± 3 mm for navigator echo was used. The slice thickness of the 2D breath hold TurboFLASH image was 3 mm, while the other parameters kept the same. Dark blood was achieved by applying double inversion pulse with TI set at the blood signal suppression point and images were acquired every other heartbeat. Vessel size was measured at the same coronary segment perpendicular to the coronary orientation using Siemens Argus.

Results: Dark blood images showed good contrast between coronary and surrounding fat. Images from a typical case with all five techniques for LAD lumen measurement are shown in Figure 1. Measurements of lumen at the same location from each imaging technique among all 22 cases by different observers correlate well ($R^2 = 0.54$). The mean and standard deviation between dark blood and bright blood of all 22 cases are 3.29 ± 0.21 mm and 3.426 ± 0.15 mm in breath hold, 3.16 ± 0.02 mm and 3.49 ± 0.04 mm in navigator

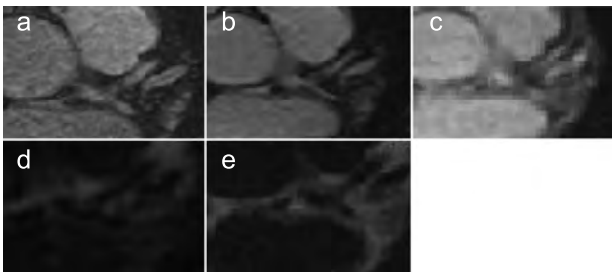

Figure 1. One example coronary artery images from (a). 3D breath-hold TrueFISP; (b) 3D navigator guided TrueFISP, (c). 2D breath-hold TurboFLASH, (d). 2D breath-hold turbo spin-echo, and (e). 3D navigator guided turbo spin-echo.

guided, and 3.25 ± 0.17 mm and 3.44 ± 0.12 mm in all imaging techniques.

Conclusions: The in-plane proximal coronary artery lumen does appear smaller on dark blood images than bright blood image, regardless 2D or 3D, breath hold or navigator guided, as well as different observers. Further study is needed to validate which is closer to the true lumen size.

332. Manifestation of Coronary Stenoses on Breath-Hold Steady State Free Precession Sequence: Retrospectively Compared to Conventional X-Ray Coronary Angiography

Liuquan Cheng, MD, PhD,[1] Yuangui Gao, MD,[1] Andrea Guaricci,[2] Suresh Mulukutla, MD,[3] Martin R. Prince, MD, PhD,[2] Yi Wang, PhD.[2] [1]*MRI, Radiology, Chinese PLA General Hospital, Beijing, China,* [2]*Department of Radiology, Weill Medical College, Cornell University, New York City, NY, USA,* [3]*Department of Cardiology, UPMC Presbyterian, University of Pittsburgh, Pittsburgh, PA, USA.*

Objecitve: To evaluate the accuracy of coronary stenoses detection and to determine the spectrum of plaque features using breath-hold three-dimensional SSFP (FIESTA).

Materials and Methods: 28 patients with known coronary artery disease were examined using the breath-hold 3D-SSFP sequence and x-ray coronary angiography (XCA). Double-blinded data review was performed by two clinicians. Plaque features of the verified severe stenoses (> 50% in diameter) on XCA were retrospectively identified on the SSFP images compared segment by segment.

Results: The sensitivity and specificity for diagnosing coronary stenoses by two reviewers were 61–66% and 94% respectively. Of the 44 severe stenoses on XCA, SSFP could detect the residual narrowed lumen (91%, 40/44), bright plaque (70%, 31/44) and coronary arterial remodeling (32%, 14/44) in retrospective review. Narrowed lumen associated with bright plaque and arterial remodeling (Figure 1) had an 85% (11/13) positive predictive value for stenoses detection. The positive predictive value by narrowed lumen with bright plaque but without arterial remodeling, and narrowed lumen without visible bright plaque or remodeling, are only 74% and 60%, respectively.

Conclusions: SSFP has the advantage of imaging both the lumen and plaque on the tomographic CMRA images for stenoses detection depending on the proper interpretation of plaque, arterial remodeling and residual lumen. Stenosis detection that incorporates atherosclerotic plaque can potentially improve understanding of coronary artery disease.

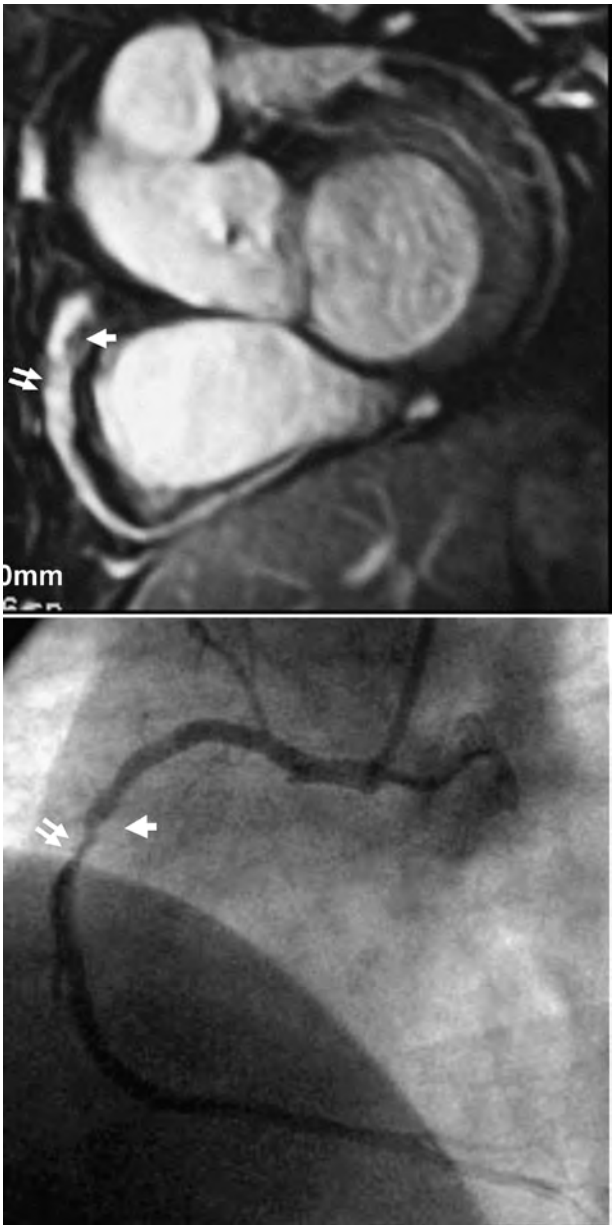

Figure 1. 51-year-old man with focal severe (↓↓) and diffuse mild (↓) stenosis on RCA. On reformatted MIP image (A), the bright plaque signal and the outward extended arterial remodeling (↓↓), prevent the severely narrowed lumen shown on the CCA from being detected. A heterogeneous bright plaque can also be detected along the diffuse mild stenosis (↓) which only shows slightly narrowed lumen and irregular border on CCA.

REFERENCES

Schar, M., et al. (2003). *JMRI* 17:538.
Fayad, Z. A. (2001). *Circ. Res.* 89:305.
Flamm, S. D. (2004). *JMRI* 19:686.
Yuan, C. *JMRI* 19:710.

333. Rapid Fourier Phase Analysis of Cine MRI Images for Evaluation of Regional Wall Motion and Asynergy

James Pemberton, MD,[1] Xiaokui Li, MD,[2] Patrick Von Behren, PhD,[3] Lei Sui, PhD,[3] Helene Houle, PhD,[3] Cory Swingen, PhD,[4] Inderjit Anand, MD,[5] Michael Jerosch-Herold, PhD,[6] David J. Sahn, MD.[2] [1]*Pediatric and Adult Cardiology, Oregon Health & Science University, Portland, OR, USA,* [2]*Pediatric Cardiology, Oregon Health & Science*

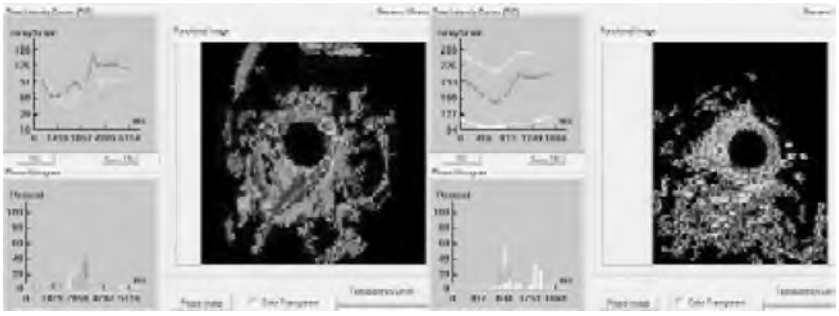

University, Portland, OR, USA, [3]*Siemens Ultrasound, Mountain View, CA, USA,* [4]*Radiology, University of Minnesota, Minneapolis, MN, USA,* [5]*Cardiology, University of Minnesota, Minneapolis, MN, USA,* [6]*Diagnostic Radiology, Oregon Health & Science University, Portland, OR, USA.*

Introduction: Detailed analysis of wall motion on MRI images requires significant expertise and is often laborious.

Purpose: We tested a new software method for phase analysis that has been adapted to compute phase/motion on MRI images.

Methods: In this study we compared transverse views of the LV from 6 normal subjects studied on a 1.5 Tesla Siemens system to 11 patients with regional asymmetry of at least one segment in the short axis view, which included inferior hypokinesis in 3, anteroseptal hypokinesis in 4 or anterolateral wall hypokinesis in 4. Breath-hold, ECG-gated, cine MRI data for a midventricular slice in the short axis oreientation were acquired with standard protocols. Studies were loaded as AVI files for analysis of systolic phase delay relative to R-wave, computed rapidly by optical flow methods. Delay is expressed in degrees after normalization by R-to-R duration (R-to-R = 360°).

Results: In the normal patients peak systolic phase delay was $< 180°$, (mean ± SD) $177 \pm 23°$. The patients with ischemic cardiomyopathy and wall segment abnormalities showed a mean phase of $218° \pm 29°$ around the mean phase angle. Parametric color maps of phase delay allowed rapid, efficient and observer-independent localization of myocardial sectors with abnormal phase delay.

Conclusion: This new phase analysis program should be rapid and reproducible for wall motion analysis in patients with ischemic heart disease. It introduces a new method for identifying regional wall motion abnormalities from MRI cine studies, which is completely observer-independent.

334. Frequency of Normal Perfusion in Infarcted Myocardial Segments. A Single Adenosine Stress Comparison of Cardiac Magnetic Resonance and Myocardial Perfusion SPECT

Louise E. J. Thomson, MBChB,[1] David S. Fieno, MD,[2] Aiden Abidov, MD,[1] Allison Hamilton,[1] Edward Gill,[1] Sean Hayes, MD,[1] John Friedman, MD,[1] Rola Saouaf, MD,[1] Rory Hachamovitch, MD,[3] Daniel S. Berman, MD.[1] [1]*S. Mark Taper Foundation Imaging Center, Cedars Sinai Medical Center, Los Angeles, CA, USA,* [2]*Department of Medicine, Cedars Sinai Medical Center, Los Angeles, CA, USA,* [3]*Cardiovascular Division, Keck School of Medicine, University of Southern California, Los Angeles, CA, USA.*

Introduction: Initial reports of stress perfusion cardiac magnetic resonance imaging (CMR) suggest adenosine perfusion (Ad) CMR is sensitive for coronary artery disease detection when combined with delayed enhancement imaging (DE). It is recognized that subendocardial infarcts may have normal rest perfusion but the frequency of normal stress perfusion in these regions is unknown.

Purpose: We sought to examine agreement between dual isotope myocardial perfusion SPECT (MPS), and AdCMR with DE for detection of perfusion abnormalities using a unique combined imaging protocol with a single adenosine stress.

Methods: Patients referred for MPS had rest thallium-201 SPECT prior to Ad stress in the magnet (Siemens Sonata 1.5 T). During Ad infusion, Tc99m Sestamibi injection was immediately followed by first pass gadolinium injection (0.1 mmol/kg, trueFISP). Rest CMR perfusion and DE were obtained 10, 20 minutes later, followed by post-stress SPECT. Blinded 5-point, 17 segment scoring was recorded for AdCMR (aided by rest perfusion CMR), DE and rest and stress MPS.

Results: 45 patients (23 male, mean age 70 ± 14 yr) were studied. In a sub-analysis of 14 patients with DE, 8 had normal AdCMR and 2 had normal MPS. In 54 abnormal DE segments ($27 < 50\%$ and $27 \geq 50\%$ transmural), there was normal AdCMR in 29/54 and normal rest MPS in 35/54 (p = ns vs. AdCMR). However the frequency of normal stress MPS was lower (17/54 segments, $p < 0.05$ vs AdCMR). Segmental degree of transmurality by DE correlated more strongly with rest MPS ($r = 0.43$, $p = 0.001$) than with either AdCMR ($r = 0.36$, $p = 0.007$) or stress MPS ($r = 0.32$, $p = 0.01$).

Conclusions: In segments with DE evidence of myocardial scar, myocardial perfusion is frequently normal at rest and with Ad stress. This finding is observed more frequently with AdCMR than with Ad stress MPS.

335. Obesity Trends are Changing Our Physical Diagnostic Principles: A New Perspective with Magnetic Resonance Imaging

Gurpreet Baweja,[1] Raad H. Mohiaddin,[2] Gordon A. Ewy,[1] Vincent L. Sorrell.[1] [1]*University of Arizona Sarver Heart Center, Tucson, AZ, USA,* [2]*Royal Brompton Hospital, London, UK.*

Introduction: Determination of the central venous pressure from jugular venous pulsation depends on the notion that the distance from the sternal angle to the mid right atrium (SA-RA) is a constant measuring 5 cm.

Purpose: The purpose of this study was to measure the distance from the middle of the RA to the SA in a clinically representative patient population using cardiac magnetic resonance imaging (MRI).

Methods: Consecutive offline measurements were performed on all patients receiving routine, ambulatory cardiac MRI exams during the two month study period. Patients with obvious chest deformities or incomplete image sequences were excluded.

Results: Fifty-eight patients (28 males) with mean age of 35 + 17 years were analyzed. The mean SA-RA distance was 6.3 + 1.7 cm with 6.8 + 1.8 cm in males and 5.8 + 1.5 cm in females ($p < 0.05$) (see table for complete results).

Conclusions: The SA-RA distance is larger than previously noted and correlates with body size and gender. Historically, the 5 cm estimate for jugular venous pressure estimation was likely valid, and reflected the smaller body habitus predominant 1/2 century ago. With the larger BMI currently noted today in industrialized nations, our data support using a more accurate SA-RA distance of 6 cm for females and 7 cm for males.

Factors	Mean	Correlation with SA-RA distance-coefficient (r)	P value
Age, yrs	35.4 ± 17.6	0.12	0.37
Height, m	1.69 ± 0.14	−0.33	0.32
Weight, kg	75.1 ± 16.8	0.88	0.001
BMI, kg/m^2	27.1 ± 9.5	0.84	0.001
AP diameter of chest, mm	197.8 ± 34.4	0.88	< 0.001
AP diameter of RA, mm	51.5 ± 8.9	0.16	0.24

336. Effects of Magnetic Resonance Imaging and Balloon Inflation on Stability of Drug-Eluting Stent Polymer: An In-Vitro Study

Mladen I. Vidovich, MD,[1] Daniel C. Lee, MD,[1] Edwin Wu, MD,[1] Benjamin D. Myers,[2] Vinayak P. Dravid, PhD,[2] Charles J. Davidson, MD.[1] [1]*Division of Cardiology, Northwestern University, Feinberg School of Medicine, Chicago, IL, USA,* [2]*Department of Materials Science and Engineering, Northwestern University, Robert R. McCormick School of Engineering and Applied Science, Evanston, IL, USA.*

Introduction: Cardiac magnetic resonance (MR) of bare-metal stents appears to be free of any potential adverse clinical effects. However, the effect of MR scanning on the polymer coating of drug-eluting stents might potentially cause disruption or peeling of the polymer and potentially affect the anti-restenosis benefits.

Purpose: We performed an in-vitro study of drug-eluting stents to determine the stability of the polymer coating under simulated cardiac MR scanning conditions and to determine the effects of balloon expansion on polymer integrity.

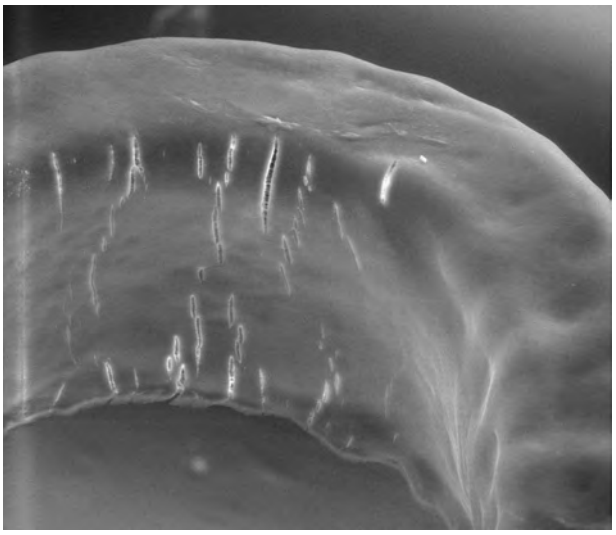

Figure 1.

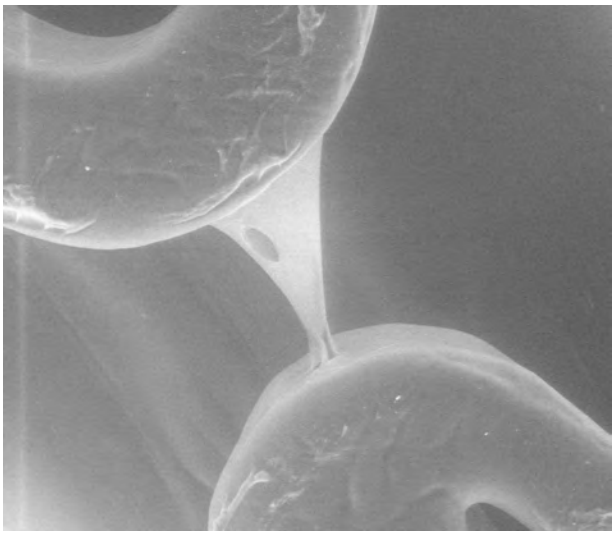

Figure 2.

Methods: Three Cypher (Cordis Corp, Miami, FL) and three Taxus (Boston Scientific Corp, Natick, MA) stents were studied. The stents were imaged with an environmental scanning electron microscope (ESEM) before and after balloon expansion to nominal stent inner diameter. Expanded stents along with weight ballast were then placed in center of clinical 1.5 T MR scanner (Siemens Sonata). Imaging protocols were performed to simulate a complete clinical cardiac examination (multiple cines were obtained using a steady-state free precession and viability images with an inversion-recovery gradient echo). Typical imaging parameters for the cine images were: field of view 350 × 263 mm, acquisition matrix of 125 × 256 pixels, repetition time (TR) 42.75 ms, echo time (TE) 1.2 ms, excitation angle 70° and voxel size 2.1. × 1.4 × 5 mm. For the viability images: field of view 350 × 295 mm, acquisition matrix 138 × 256 pixels, voxel size 2.1 × 1.4 × 5 mm, TR 700 ms, TE 3.93 ms, excitation angle of 25° and inversion time (TI) of 250 ms. Stents were observed with ESEM after 1 simulated cardiac MR scan and again after 5 repeated MR scans. The stents were observed in an FEI Quanta 600F ESEM (FEI Company, Hillsboro, OR) equipped with a field emission electron gun and an Oxford energy dispersive x-ray spectrometer. The ESEM was operated at 15 kV and a chamber pressure of 1.5 Torr, which allowed direct observation and elemental analysis without a conductive coating.

Results: The stent polymer coating was intact in both drug-eluting stent types prior to balloon expansion. After balloon inflation, the Cypher stent demonstrated multiple microfractures (< 2 μm) (Fig. 1) while the Taxus stents demonstrated frequent adhesion of polymer to connecting struts (Fig. 2). One Taxus stent revealed significant (200 μm) peeling of polymer from the stent surface after balloon expansion (Fig. 3). One and five simulated MR scanning protocols were then performed on the expanded stents. There were no significant additional deformities or surface irregularities observed on either of the stent models (Fig. 4).

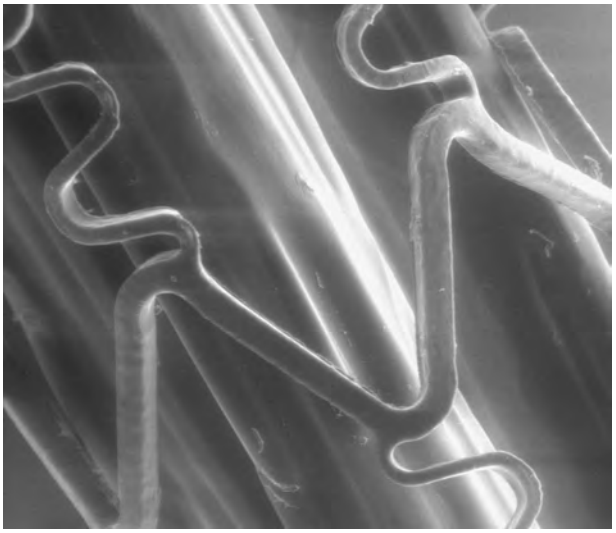

Figure 4.

Conclusions: There are no observable deformities of the polymer induced by MR scanning of the two commercially available drug-eluting stents in this in-vitro experiment. The lack of additional polymer deformities following a simulated cardiac MRI examination suggests that additional risks or drug efficacy are not different than under normal circumstances. The clinical implications of the adhesions and peeling following balloon expansion of the Taxus stent and microfractures on the Cypher stent are unknown.

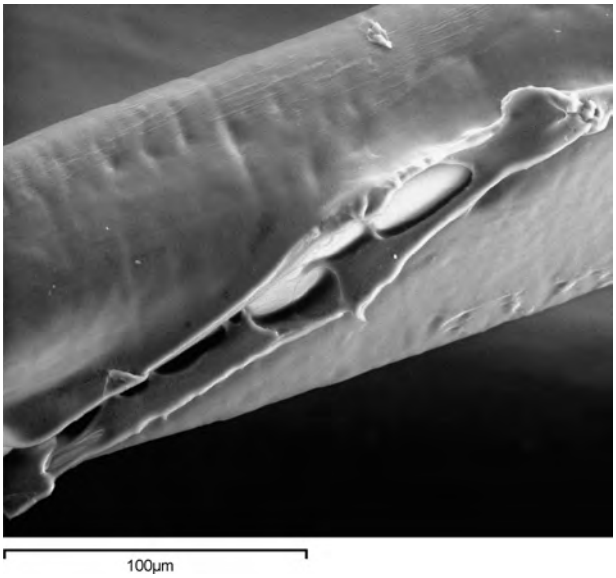

Figure 3.

337. In-Plane Pulse Wave Velocity with MRI in Ischemic Heart Disease: Validation of a New Technique

Heynric B. Grotenhuis, MD,[1] Jos J. M. Westenberg, PhD,[1] Joost Doornbos, PhD,[1] Theodorus A. M. Kaandorp, MD,[1] Rob J. van der Geest, MSc,[1] Hildo J. Lamb, PhD, MD,[1] Jaap Ottenkamp, MD, PhD,[2] Albert de Roos, MD, PhD,[1] Johan H. C. Reiber, PhD.[1] [1]*Radiology, Leiden University Medical Center, Leiden, The Netherlands,* [2]*Pediatric Cardiology, Leiden University Medical Center, Leiden, The Netherlands.*

Introduction: Aortic Pulse Wave Velocity (PWV) is a powerful independent predictor of all-cause and cardiovascular mortality in various patient groups. It can be used as an integrated index of vascular structure and function, on and through which other standard risk factors operate. Through-plane PWV (PWV_{tp}) with MRI has been reported to give a global indication of vascular status, however, regional differences in vascular structure along the entire aortic vascular bed cannot be depicted.

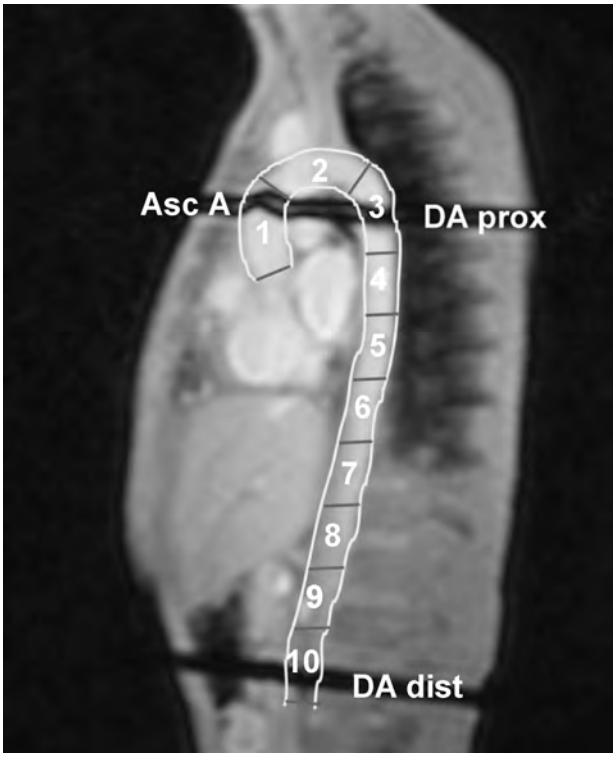

Figure 1.

Purpose: In this study we describe a new method of measuring PWV using MRI, enabling regional depiction of the aortic vascular status in patients with ischemic heart disease. Reproducibility of the method was evaluated and compared to PWV_{tp} in volunteers.

Methods: Seven patients were examined (mean (SD) age 67.9 (5.4) years). PWV_{tp} and in-plane PWV (PWV_{ip}) were measured twice in seven volunteers (mean (SD) age to 30.4 (6.6) years) to evaluate reproducibility. MRI examinations were performed on a 1.5 Tesla Philips Gyroscan Intera. PWV of the aorta was determined in two ways:

1-Directional PWVtp: Two flow measurements were performed consecutively, perpendicular to the aorta. Flow was determined at three locations: ascending aorta; end of aortic arch (AA) and near the bifurcation of descending aorta (DA). The distance between the two acquisition planes measured along the aorta and the time-difference between the points-of-arrival of the systolic wave determined the PWV_{tp} of the AA and the DA. Point-of-arrival of the systolic wave was determined from the intersection of the offset in flow during diastole and the upslope of the systolic wave. Scan parameters: TE/TR/α = 2.8/5.0/20°, slice thickness 8 mm, FOV = 300 mm, scan matrix = 128 × 128. Retrospective cardiac synchronization; 140 to 190 reconstructed phases per cardiac cycle.

2-Directional PWVip: In a stack of three consecutive acquisition planes, 2-directional velocity-encoded MRI was performed. The stack was double-oblique planned covering the complete aorta. Scan parameters: TE/TR/α = 2.7/4.6/10°, slice thickness 15 mm, FOV 450 mm, scan matrix 128 × 128. Retrospective cardiac synchronization; 150 to 220 phases reconstructed per cardiac cycle. Velocity-encoding in two directions: FH and AP.

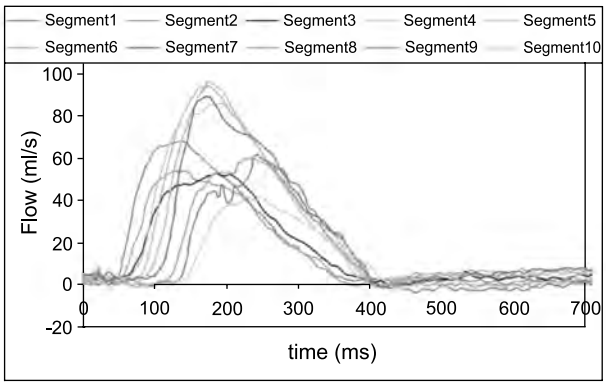

Figure 2.

Table 1.

	PWV_{tp} AA	PWV_{tp} DA	PWV_{ip} AA	PWV_{ip} DA
mean diff (SD)	0.20 (1.1)	0.69 (1.5)	0.59 (1.0)	0.31 (.086)

Table 2.

	Patientsmean (SD)	*p*-valueMann-Whitney U-test	Volunteersmean (SD)
PWV_{tp} AA	8.3 (2.2)	0.002	4.7 (0.71)
PWV_{tp} DA	8.6 (3.7)	0.025	5.0 (1.5)
PWV_{ip} AA	4.7 (0.7)	0.006	4.6 (0.4)
PWV_{ip} DA	5.0 (1.5)	0.003	4.6 (0.8)

The aorta was divided into ten consecutive segments of 4.2 cm (Figure 1). Per segment, the mean maximal velocity parallel to the axis of the aorta was determined, resulting in ten systolic-flow-waves (Figure 2). The particular points-of-arrival define the PWV_{ip} between the segments. PWV_{ip} of the AA and DA were determined by averaging the PWV-values of the first three and subsequent seven segments respectively, enabling comparison between PWV_{tp} and PWV_{ip}. Regional PWV_{ip} for the patients was increased when exceeding the mean PWV_{ip} in a particular patient plus twice the mean SD (derived from PWV_{ip} of the volunteer population).

Results: PWV_{tp} and PWV_{ip} showed good correlation for volunteers for the DA (Pearson correlation coefficient $r_P = 0.90$, $p < 0.01$), but non-significant correlation for the AA ($r_P = 0.61$, $p = 0.146$). Repeated measurements among volunteers showed good correlation for PWV_{tp} and

PWV_{ip}: mean differences and SDs were small and non-significant (Table 1). Bland-Altman showed no systematic distribution in these differences. Mann-Whitney U-test showed a significant increased PWV among patients compared to volunteers, both for PWV_{tp} and PWV_{ip} (Table 2). Four out of seven patients showed regionally increased PWV_{ip}.

Conclusion: Assessment of PWV_{ip} is a feasible tool to detect regional abnormalities of aortic PWV, with good reproducibility and correlation with PWV_{tp} measurements, especially for the DA. In this study a significantly increased overall PWV was found in patients compared to volunteers, as well as increased regional PWV. Further research is needed to elucidate the clinical implications of this new technique.

338. Contrast-Enhanced Cardiac MRI Accurately Differentiates Ischaemic from Non-Ischaemic Aetiologies in Newly Diagnosed Cardiomyopathy

Jonathan P. Christiansen, MB ChB, MD, FRACP,[1] Colin Edwards, MB BCh, FCP,[1] Toni Sinclair, BHSc, PGDipHMgt,[2] Guy Armstrong, MB ChB, FRACP,[1] Tony Scott, MB ChB, FRACP,[1] Hitesh Patel, MB ChB, FRACP,[1] Hamish Hart, MB BCh, MRCP, FRACP.[1] [1]*Cardiovascular Division, Waitemata Health, Auckland, New Zealand,* [2]*The Radiology Group, Auckland, New Zealand.*

Introduction: Patients with newly diagnosed cardiomyopathy (CM) frequently undergo angiography to exclude significant coronary artery disease (CAD). Contrast-enhanced cardiac MRI (CE-CMR) is sensitive and specific for the detection of myocardial scar. We hypothesized that CE-CMR could accurately identify those patients with an ischaemic CM (ICM), and eliminate the need for angiography in patients with non-ischaemic CM (DCM).

Methods: We studied 33 patients (mean age 57 ± 11) with CM. Patients with new onset heart failure and echocardiographic evidence of systolic dysfunction were prospectively identified. Patients who subsequently underwent both CE-CMR and coronary angiography were included. ICM was defined angiographically as > 50% stenosis in $\geq$ 1 vessel. CE-CMR was performed using a 1.5 T Philips Intera. Functional and volumetric data were obtained from breath-hold steady state free precession cine imaging. Myocardial scar was assessed using delayed enhancement (DE) inversion-recovery imaging 10 minutes following administration of 0.1 mM/kg Gd-DTPA. Patients with any DE in a subendocardial distribution were classified as having ICM by CE-MRI.

Results: Overall 12 patients had ICM by angiography. The majority (75%) had three vessel CAD. All patients with angiographic ICM had subendocardial DE on CE-CMR and were correctly classified as having ICM. Volumetric parameters did not differ between ICM and DCM (LVEDV = 260 ± 85 vs 289 ± 69 mL, LVESV = 187 ± 83 vs 214 ± 68 mL, LVEF% = 30 ± 12 vs 27 ± 10, p = ns for all). The sensitivity and negative predictive value for CE-MRI were 100% for the detection of ICM. The specificity was 86% and the positive predictive value 80%. In patients with angiographic DCM four had mid-wall DE, and three had subendocardial DE.

Conclusions: All patients with angiographic ICM were correctly identified by CE-CMR. The lack of subendocardial DE on CE-CMR identifies CM patients without significant CAD. These patients may not require diagnostic angiography.

339. Correlation of Clinical Parameters in Acute Myocardial Infarction with Delayed Contrast Enhancement and No-Reflow assessed by early contrast-enhanced Cardiac MR Imaging

Oliver Bruder, MD,[1] Kai-Uwe Waltering, MD,[2] Thomas Schlosser, MD,[2] Markus Jochims, MD,[1] Georg V. Sabin, MD,[1] Jörg Barkhausen, MD.[2] [1]*Department of Cardiology and Angiology, Elisabeth Hospital Essen, Essen, Germany,* [2]*Department of Diagnostic and Interventional Radiology, University Hospital Essen, Essen, Germany.*

Introduction: In patients with acute myocardial MRI-determined microvascular obstruction predicts more frequent cardiovascular complications.

Purpose: Aim of our study was to investigate the influence of clinical parameters on the extent of the no-reflow area and the correlation with laboratory values.

Methods: 59 patients (47 male, 12 female, mean age 58 ± 11 years) with first myocardial infarction (MI) treated by percutaneous coronary intervention (PCI) resulting in TIMI grade 3 flow were included into the study. MR imaging was performed on a 1.5 T MR-system 3.1 ± 2.2 days after MI. One minute after Gadodiamide injection (0.2 mmol/kg BW, Omniscan, Amersham) the entire left ventricle was covered in a single breath-hold using a single shot inversion-recovery steady state free precession (IR-SSFP) sequence (TR 2.4 ms, TE 1.1 ms, FA 50°). The extent of the no-reflow area was assessed by planimetry. The area of late enhancement was measured on the data sets collected 15 minutes post-contrast. Laboratory values [Troponin I (Trop I), creatine kinase (CK)]

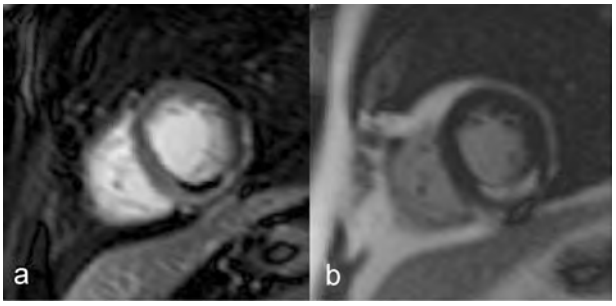

Figure 1. 48 yo male patient 2 days after MI of the posterior wall, 1 min (a) and 15 min (b) after constrast injection.

and clinical parameters (time to TIMI flow, ST-elevation and ST-recovery) were recorded.

Results: No-reflow areas (mean extent 11.1 ± 8.5% of the LV myocardium) were detected in 38 patients (53%); (Fig. 1). A strong positive association was found between the extent of the no-reflow area and the extent of the late enhancment (pearson correlation coefficient $p = 0.87$). The maximum Trop I (r = 0.67), the maximum CK (r = 0.63) showed a moderate and the maximum ST-elevation (r = 0.41) a weak correlation with the extent of the no-reflow area. No association was found between the time to TIMI flow as well as the ST-recovery and the extent of the no-reflow area.

Conclusions: Compared to previous studies our results show a higher incidence of MRI-determined microvascular obstruction. The extent of the no-reflow area mainly depends on the infarct size, whereas time to TIMI flow and ST-recovery, a clinical marker of successful PCI, show no correlation. Larger clinical studies are required to investigate the prognostic value of the no-reflow area independent of infarct size.

340. Physiologic Compensation is Supranormal in Advanced Aortic Stenosis; Does it Return to Normal after Aortic Valve Replacement? An MRI LV Torsion Study Using 3D-HARP

Robert W. W. Biederman, MD,[1] June Yamrozik,[1] Ronald B. Williams,[1] Geetha Rayarao,[1] Valerie Bress,[1] Diane A. Vido,[1] Sunil Mankad, MD,[1] James A. Magovern,[1] Nael Osman,[2] Mark Doyle, PhD.[1] [1]*Allegheny General Hospital, Pittsburgh, PA, USA,* [2]*Johns Hopkins University, Baltimore, MD, USA.*

Background: Compensatory LVH in severe aortic stenosis (AS) alters the manner in which circumferential, radial and meridional fiber architecture interact, and prior to end-stage AS, the LV has supranormal contractile performance, chiefly represented by compensatory augmentation in torsion. The temporal stages of torsion recovery following aortic valve replacement (AVR) are unknown.

Hypothesis: We hypothesize that as LVH regresses following AVR, torsion will beneficially decrease, representing not abnormal function, but a return towards a normal uncompensated state, with relative torsion regressing slower than LV bulk rotation.

Methods: Twenty patients with late but not decompensated AS underwent MRI for RF tissue tagging (1.5 T-GE-CV/i) and 3D-LV-torsion analysis via HARP (Diagnosoft) pre-and post-AVR at early (6 ± 1 mo) and late (13 ± 2 mo) time points.

Results: Seventeen patients who survived and/or returned had post-AVR torsion, rotation and LV function data by MRI. LV mass index (LVMI) decreased post AVR by 15% (91 ± 24 vs 75 ± 16 g/m^2, $p < 0.001$). However, at the level of the LV cavity, no change in LVEF was seen (55 ± 20 vs 64 ± 8, $p = 0.1$). The 3D torsion work (total LV torsion integrated over systolic ejection time) regressed by 35% early (10.7 ± 6.8 vs 6.9 ± 4.7 deg^{2}s^{2}g, $p < 0.05$) while the corresponding relative torsion did not regress (16.6 ± 7.2 vs 16.3 ± 14.3 ∞, $p = 0.98$). However, by the late time point, regression of relative rotation to historic normal levels (12 ± 3 ∞) was achieved, 45% (16.6 ± 7.2 vs 9.0 ± 3.4 ∞, $p < 0.05$). The LV mass negatively correlated with the time to generate 50% maximal absolute rotation (r = − 0.63) pre AVR, 6 mo (r = 0.40) and at one year (r = − 0.89). The rate of torsion (∞/mm s) was unchanged over time.

Conclusion: In aortic stenosis pre AVR, LV torsion is supranormal but the rate of torsion pre and post AVR is inversely related appropriately to LV mass and its subsequent regression. LV bulk rotation regresses first, followed by LV torsion. An added benefit of AVR is regression of rotational components, hidden at the level of the LV cavity and regressing at very different times. Torsion regression follows a temporal pattern which may be related to relative early abolishment of LVH mRNA signaling post AVR compared to late signaling of metalloproteinase inhibition.

341. Graded Abnormalities in Regional Myocardial Strain by DENSE (Displacement Encoding with Stimulated Echoes) CMR Associated with Transmural Extent of Infarction

Sriram Padmanabhan, MD, Anthony H. Aletras, PhD, Pamela Vincent, RT(R)(CT)(MR), Andrew E. Arai, MD. *Laboratory of Cardiac Energetics, NIH/NHLBI, Bethesda, MD, USA.*

Introduction: DENSE CMR measures regional myocardial circumferential shortening (CS) and radial thickening (RT) with high spatial resolution. However, correlation of strain obtained by DENSE and gadolinium (Gd) delayed enhancement (DE) in patients with myocardial infarction (MI) is not well established.

Purpose: We studied the relationship between radial and circumferential myocardial strain obtained by DENSE with transmural extent of MI.

Methods: We recruited 21 subjects for the study (15 patients with MI, 6 normal). Cardiac MRI included multiple short-axis DENSE acquisitions, and corresponding Gd DE images. A single mid-ventricular slice was analyzed with its corresponding DE images in a blinded fashion. Strain data were obtained using inhouse software. The transmural extent of enhancement was scored as 0 = normal, 1 ≤ 25%, 2 = 26–50%, 3 = 51–60%, and 4 ≥ 75% of myocardium. Six sectors were analyzed. Results are mean + SD.

Results: In normal volunteers CS was 21.7 + 5.7% (range 11.9 to 35.5%), and RT was 20.6 + 6.6% (range 15.8 to 30.1%). In MI patients, 34 of 90 segments had DE (grade 1: n = 18, grade 2: n = 6, grade 3: n = 5, grade 4: n = 5). In normal segments of MI patients, CS measured 22.7 + 6.2% and RT 21.9 + 5%. There was significant

decrease in CS and RT with increasing transmural extent of enhancement. In segments with grade 1 hyperenhancement, CS decreased to 11.8 + 6.5% ($p = 0.004$), and RT to 16.1 + 5.9% ($p = 0.02$). In grade 2 segments, CS decreased further to 8.3 + 9.1%($p = 0.001$) and RT to 10.8 + 6.7%($p = 0.001$). In grade 3 and 4 segments, CS measured 10.1 + 6($p = 0.001$), and RT was 8.05 + 13.8($p = 0.004$).

Conclusions: Myocardial strain measured by DENSE MRI shows progressively more severe abnormalities in regional strain associated with increasing transmural extent of myocardial enhancement. DENSE can objectively measure regional function and is complimentary to myocardial viability imaging in patients with MI.

342. Visual Estimation Versus Quantitative Assessment of Left Ventricular Ejection Fraction: A Comparison By Cardiovascular Magnetic Resonance Imaging

Burkhard Sievers, Simon Kirchberg, Ulrich Franken, MD, Binu John-Puthenveettil, Asli Bakan, Hans-Joachim Trappe, MD. *Cardiology and Angiology, University of Bochum, Herne, Germany.*

Background: MRI is known to be most accurate for quantitative assessment of the left ventricular ejection fraction (EF). However, quantitative assessment of left ventricular EF is time consuming and often not applicable in daily clinical routine. Automatic contour detection for rapid ventricular EF assessment would be of great practical value, but has not yet been perfected and is still unreliable in the analysis of gradient-echo cine images.

Purpose: To compare the visual and quantitative assessment for left ventricular ejection fraction (EF) in normal subjects and patients with impaired left ventricular function.

Methods: 100 subjects (40 normal subjects, 40 patients with ischemic cardiomyopathy and 20 patients wit non-ischemic cardiomyopathy) were investigated using a 1.5 Tesla cardiovascular magnetic resonance imager. Images were acquired by a fast gradient-echo sequence with steady-state free precession (SSFP) using the standard short-axis method. Left ventricular EF was calculated from the sums of the outlined areas using the Simpson's rule. Interobserver variability between the calculated and the visual EF was assessed. Analyses were performed randomly and blinded by two independent observers.

Results: Left ventricular EF was significantly underestimated by the visual read in all 3 groups (mean difference: normals 2.6 ± 2.6%, ischemic cardiomyopathy 1.7 ± 2.1%, non-ischemic cardiomyopathy 1.2 ± 2.1%; $p = 0.0197$), Figure 1. The correlation coefficient for normal subjects was 0.92, for ischemic cardiomyopathies 0.96 and for non-ischemic cardiomyopathies 0.95. The interobserver variability was small for the calculated EF (95% limits of agreement − 3.5, 3.4). For the visually estimated EF, there was a wider range of the 95% limits of agreement (− 13.8, 13.1). Measurements obtained with the standard short axis method required 23 ± 5 min. The visual estimation required less than one minute per patient (30 ± 10 seconds).

Conclusion: Left ventricular EF is underestimated by visual estimation compared to the quantitative assessment. The visual approach for EF assessment is reasonably accurate

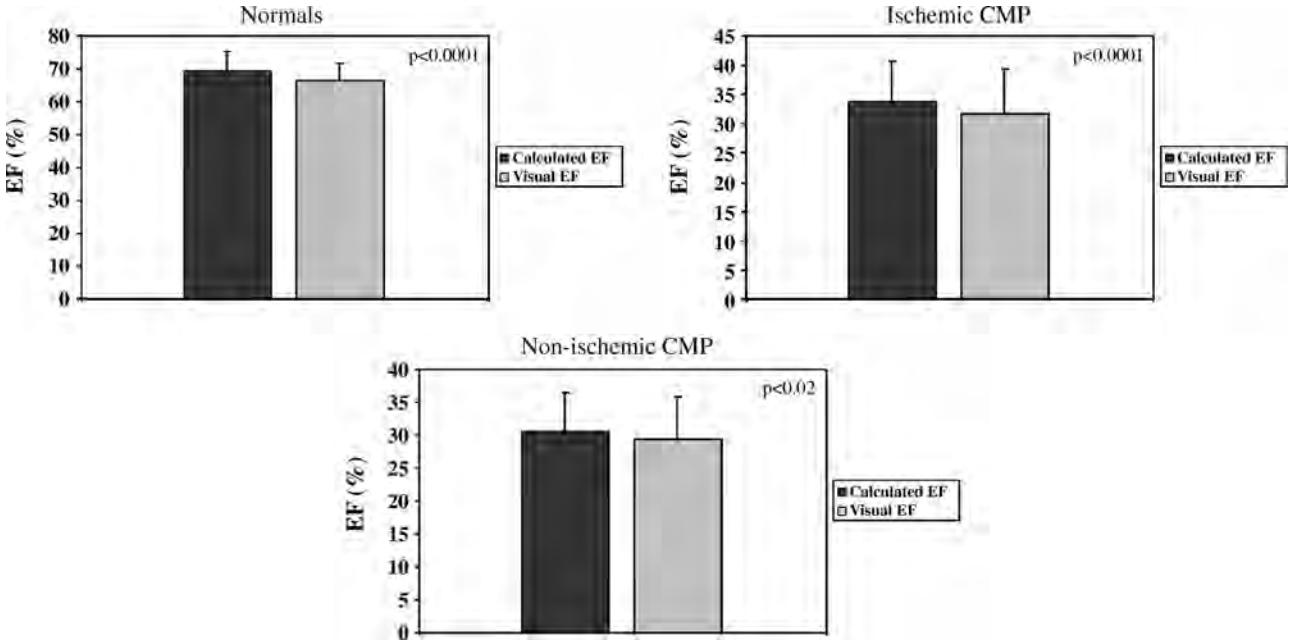

Figure 1.

in normal and impaired functioning left ventricles. It may be used for rapid assessment of left ventricular function in clinical practise. For most accurate analysis the quantitative approach is required.

343. Definition of a MRI Score Combining Pattern of Myocardial Delayed Enhancement and Segmental Wall Motion Analysis to Discriminate Between Cardiac Dysfunction Due to Coronary Artery Disease or Related to Other Causes: Results in 80 Patients

Xavier Lyon, MD,[1] Azarine Arshid, MD,[2] Alban Redheuil, MD,[2] François Ledru, MD,[3] Elie Mousseaux, MD, PhD.[2] [1]*Service of Cardiology, University Hospital, Lausanne, Switzerland,* [2]*Department of Radiology, European Hospital, Paris, France,* [3]*Department of Cardiology, European Hospital, Paris, France.*

Introduction: It is of particular importance to identify a potential causative role of coronary artery disease (CAD) in patients with cardiac dysfunction, as revascularization therapy can greatly improve prognosis if hibernating myocardium is present. According to current guidelines a coronary angiography is usually performed, but MRI evaluation of the pattern of myocardial delayed enhancement (DE) was recently shown to bear the potential to differentiate left ventricular (LV) dysfunction due to CAD or related to other causes.

Purpose: In the present report we attempted to define a MRI score that would more accurately discriminate between these two conditions by combining DE pattern with segmental LV wall motion analysis.

Methods: A cardiac MRI was performed in 80 patients with LV dysfunction (age: 58 ± 13 y, NYHA score: 2.7 ± 0.9, ejection fraction: 26 ± 15%; mean ± SD). After a complete workup, including coronary angiography, LV dysfunction was attributed to the extent of CAD in 44 pts (CAD group) and to other causes in 36 (non-CAD group). Using the 16 segments model, LV was evaluated for function (1: normal, 2: dyskinesia, 3: akinesia, 4: severe hypokinesia, 5: moderate hypokinesia) and DE (1: DE without endocardial involvement, 2: no DE, 3: DE with endocardial involvement). The MRI score of a given patient was obtained by summing the ratio of function by DE calculated for each segment (theoretical range: 5.3 to 80).

Results: MRI score was significantly different between both groups (CAD: 17 ± 5, non-CAD: 38 ± 10; $p < 0.001$). The use of 27 as cut-off value correctly classified all but two patients with a 100% negative predictive value for the presence of CAD.

Conclusions: These data suggest that MRI is a promising non-invasive method to differentiate LV dysfunction due to CAD from other causes. The use of a score combining segmental wall motion analysis and pattern of DE can efficiently discriminate both groups and appears better than the observation of DE alone as used in previous studies. Prospective studies must be performed to evaluate if such an approach could avoid coronary angiography in a population particularly at risk of complications of invasive examinations.

Detection of LV dysfunction due to CAD

	sensitivity	specificity	NPV
MRI score < 27	100	94	100
Any endocardial DE	84	90	82

NPV = negative predictive value for the presence of CAD.

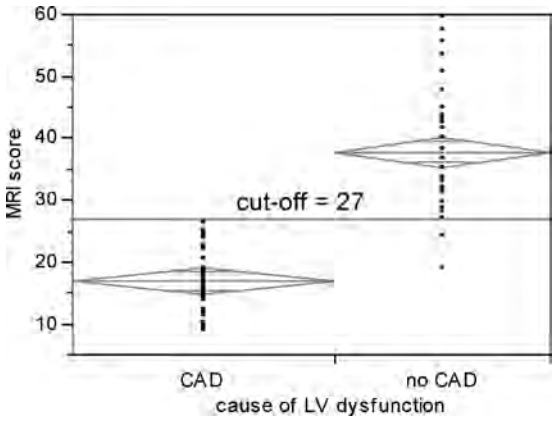

344. Impaired Coronary Vasodilation and Increased Coronary Size By Coronary MRA are Associated with High Coronary Artery Calcium in Asymptomatic Older Subjects

Masahiro Terashima, MD, PhD,[1] Patricia K. Nguyen, MD,[1] Geoffrey D. Rubin, MD,[2] Carlos Iribarren, MD,[3] Brian K. Courtney, MD,[1] Alan S. Go, MD,[3] Stephen P. Fortmann, MD,[1] Michael V. McConnell, MD, MSEE.[1] [1]*Division of Cardiovascular Medicine, Donald W. Reynolds Cardiovascular Clinical Research Center, Stanford University School of Medicine, Stanford, CA, USA,* [2]*Department of Radiology, Donald W. Reynolds Cardiovascular Clinical Research Center, Stanford University School of Medicine, Stanford, CA, USA,* [3]*Kaiser Permanente Division of Research, Donald W. Reynolds Cardiovascular Clinical Research Center, Oakland, CA, USA.*

Introduction: Noninvasive measures of subclinical coronary atherosclerosis may identify high-risk subjects to guide preventive therapy. Coronary vasodilation by nitroglycerine (NTG) is endothelium-independent, but its impairment has been associated with increased cardiovascular risk. Coronary artery remodeling is also known to occur with subclinical atherosclerosis. High-resolution coronary magnetic resonance angiography (MRA) can noninvasively measure coronary size and vasodilation.

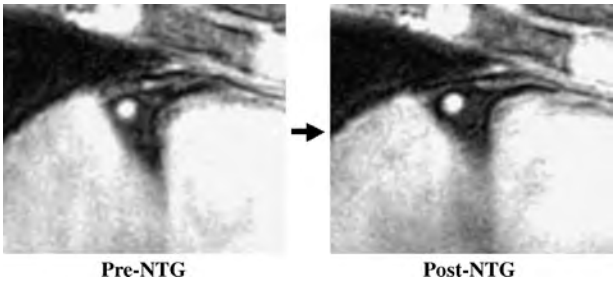

Figure 1. Representative NTG coronary vasodilation image. CAC score = 0, Vessel area: pre – 17.0 mm^2, post – 21.8 mm^2 (% dilatation = 28.6%).

Purpose: We tested the hypothesis that high coronary artery calcium (CAC) is associated with alterations of coronary vasodilation and size as assessed by coronary MRA.

Methods: A cohort of 1007 older patients (age 60–72, 38% female) without a history of cardiovascular disease were enrolled from the Kaiser Permanente health care system for prospective evaluation, including CAC. Quantitative CAC was performed on a multi-detector CT scanner with prospective ECG-gating and was scored using the Agatston method. In subset of 236 patients, NTG coronary vasodilation was measured by MRA. Cross-sectional images of the mid right coronary artery were acquired pre and 5 min post 0.4 mg sublingual NTG using a gated, breathheld spiral coronary MRA sequence (FOV = 22 mm, slice thickness = 5.0 mm, flip angle = 60, in-plane resolution = 0.7 mm) on a 1.5 T scanner equipped with high performance gradient (40 mT/m, 150 T/m/ms). Image quality was adequate in 90% of subjects, leaving 212 for quantitative analysis. Coronary artery cross-sectional area was measured and %vasodilation was determined from the ratio of post-NTG to pre-NTG vessel area.

Results: The mean age of the subjects was 66 ± 2.8 years and 32% were female. A high CAC score ($\geq$ 400) was present in 40 subjects. The degree of coronary artery vasodilation to NTG was significantly impaired in the subjects with high CAC compared to subjects with a CAC score < 400 (16.4 ± 16.3% vs. 25.2% ± 21.3%, $p = 0.015$). In addition, coronary artery cross-sectional area was larger by 17% in patients with high CAC (23.9 ± 8.5 mm^2 vs. 20.5 ± 6.7 mm^2 for CAC < 400, $p = 0.006$).

Conclusions: In an asymptomatic older community patient cohort, a high CAC score was associated with impaired NTG-induced coronary vasodilation as well as a larger baseline coronary artery size. MRA may provide additional noninvasive measures of subclinical coronary atherosclerosis (Figure 1).

345. Detection of Myocardial Infarction in Ischemic, Nonischemic, and Mixed Cardiomyopathy

Rishi Kaushal,[1] David Fieno, MD,[2] Michael Radin, MD,[3] Emanuel Shaoulian, MD,[4] Alan Kadish, MD,[5] Jagat Narula, MD,[4] Jeffrey Goldberger, MD,[6] Kalyanam Shivkumar, MD, PhD,[1] David Bello, MD.[4] [1]*David Geffen School of Medicine at UCLA, Los Angeles, CA, USA,* [2]*Medicine, Cedars-Sinai Medical Center, Los Angeles, CA, USA,* [3]*Pacific Coast Imaging, Irvine, CA, USA,* [4]*Medicine, University of California at Irvine, Irvine, CA, USA,* [5]*Medicine, University of California at Los Angeles, Los Angeles, CA, USA,* [6]*Medicine, Northwestern University, Chicago, IL, USA.*

Introduction: Cardiomyopathies are classified as ischemic (ICM) based on the following clinical criteria: evidence of prior MI, significant coronary stenosis on coronary angiography, and/or prior revascularization. Patients who do not meet these criteria are classified as nonischemic (NICM).

Purpose: This study investigated the use of Cardiac MRI (CMRI) to identify evidence of prior MI in patients with severe left ventricular dysfunction of mixed etiologies.

Methods: CMRI was performed on 128 patients with severe left ventricular dysfunction. 100 (78%) patients were classified as ICM (mean EF: 29 ± 10%) and 28 (22%) as NICM (mean EF: 31 ± 11%). Two blinded observers evaluated each study.

Results: 95/100 patients (95%) with clinical criteria for ICM demonstrated MI, despite the fact that 32/100 (32%) of the ICM patients had no history or clinical evidence of prior MI. In contrast 6/28 patients (21%) with NICM demonstrated MI. The mean infarct size as percent of LV mass was 27 ± 18 and 17 ± 13 among ICM and NICM patients, respectively ($p = 0.12$); transmural MI was seen in 57% of ICM patients whereas only 14% of NICM patients had evidence of transmural hyperenhancement ($p < 0.001$). Table 1 shows the relationship between the extent of CAD based on angiography and the presence or absence of infarct detected by CMRI. 12 patients with ICM were

Table 1.

	NICM	ICM			
	0–50% stenosis	50–70%	> 70%	2-vessel dz	3-vessel dz
Total no. of patients	28	6	11	23	41
Patients with MI based on CMRI	6	4	9	23	38
% of pts. with MI based on CMRI	21	67	82	100	93

identified with LV dysfunction out of proportion to the extent of CAD. 10/12 patients (83%) had evidence of prior MI on CMRI; all were silent. The mean infarct size was 15 ± 13% of LV mass.

Conclusions: In heart failure patients, 95% of patients with severe left ventricular dysfunction satisfying clinical criteria for ICM have evidence of prior MI as identified by contrast-enhanced MRI, with 32% of these patients lacking a history or clinical evidence of prior MI (silent MI). 21% of patients with non-ischemic cardiomyopathy have MRI evidence of prior MI.

346. Threshold for Left Ventricular Dysfunction Caused By Myocardial Necrosis Mass Quantified By MRI. Another Point of Inflexion?

Lilia M. Sierra-Galan, MD,[1] J. Enrique Hernandez L., MD.[2]
[1]*Cardiovascular Magnetic Resonance/Cardiology, Hospital Español de México, Mexico, Mexico,* [2]*Cardiology, Hospital Español de México, Mexico, Mexico.*

Introduction: Left ventricular dysfunction (LVD) secondary to myocardial infarction (MI) has been commonly related to its magnitude and location. Several studies had correlated the enzymatic level with the extension and repercussion over left ventricular (LV) function. However, to date, there are no previous reports about how much of myocardial necrosis, measured in grams, (MN) starts LVD and the remodelling process.

Purpose: To determine the critical mass of myocardial necrosis necessary to cause LVD, expressed in increment of left ventricular end systolic volume (LVESV) and decrease of left ventricular ejection fraction (LVEF).

Methods: Thirty-three patients with MI documented by clinical findings, cardiac enzymes and EKG criteria were submitted to cardiac MRI evaluation. In all these patients LV function, total mass and MN were measured in accordance with standard criteria. Considering LVD as EF < or = 55% and in accordance with the amount of MN in grams, we estimated as mild percentage of myocardial necrosis between 0 to 37% of mean total left ventricular mass (MTLVM), moderate between 38 to 46% and severe more than 47%.

Results: Twenty-seven patients were male (82%), 18 had blood hypertension (55%) and 12 were diabetic (36%). The LVEF was 56 ± 14%; LVESV 73.9 ml ± 49.6; MTLVM 126.6 g ± 48.0; MN 27.4 g ± 18.3. A third order polynomial regression fit was made with the amount of myocardial necrosis as independent variable vs. the LVEF as dependent variable ($r = 0.78$, $p < 0.001$), and for the MN vs. LVESV ($r = 0.74$, $p = 0.002$).

Conclusions: In our findings, a threshold of 34 g of MN was the point of inflexion, from where we observed a progressive worsening of LVD. This results needs to be confirmed in a large number of patients since the amount of MN founded in accordance to our criteria was mild (27% of MTLVM).

347. Left Ventricular Aneurysm: Comprehensive Assessment of Morphology, Structure and Thrombus Using Cardiovascular Magnetic Resonance.

Heatlie Grant, MBBS MRCP PhD, Raad Mohiaddin, FRCP FRCR FECS. *Cardiovascular MR, Royal Brompton Hospital, London, UK.*

Background: Left ventricular (LV) aneurysm and pseudoaneurysm formation following myocardial infarction are grave complications. Contrast enhanced cardiac magnetic resonance (CMR) imaging provides unique and definitive information on the location, size and nature of an aneurismal structure, the presence of thrombus and the viability of myocardium.

Methods: We present a retrospective review of LV aneurysm and pseudoaneurysm diagnosed in a supra regional CMR centre between 1999 and 2003.

Results: Twenty seven cases of confirmed LV aneurysm and pseudoaneurysm were identified from our database. The mean age was 65.2 ± 11.7 years with 72% of these patients being male. All the patients had previously undergone investigation including echocardiography. None of the patients were referred with a definite diagnosis of pseudoaneurysm. Seven patients had a diagnosis of ''true aneurysm'' which turned out to be correct. A further seven were identified as having previously unsuspected intraventricular clot. Six patients turned out to have left ventricular pseudoaneurysm. One patient with a mediastinal mass on computed tomography scanning actually had a ventricular pseudoaneurysm. Five patients scanned for other reasons turned out to have previously unsuspected ventricular aneurysms.

Conclusions: Cardiac magnetic resonance provides a comprehensive assessment of left ventricular aneurysms. Following their CMR scan, the final diagnosis was significantly revised in 74% of the patients in this series.

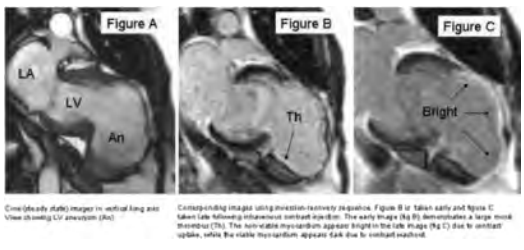

348. Early Mechanical Activation and Decreased Strain Analyzed by Tagged MRI Predict Electrophysiologic Inducibility in Ischemic Cardiomyopathy

Verônica R. S. Fernandes, MD,[1] Katherine C. Wu, MD,[1] Boaz D. Rosen, MD,[1] Caterina Silva, MD,[1] Benilton S. Carvalho, MSc,[2] Khurram Nasir, MD MPH,[1] Ronald Berger, MD,[1] João A. C. Lima, MD.[1] [1]*Cardiology, Johns Hopkins University, Baltimore, MD, USA,* [2]*Biostatistics, Bloomberg School of Public Health-Johns Hopkins University, Baltimore, MD, USA.*

Introduction: Ventricular arrhythmias are a common cause of sudden death in ischemic cardiomyopathy (ICM). Existing non-invasive parameters cannot identify high risk patients reliably.

Purpose: Use myocardial tissue tagging to examine differences in regional myocardial deformation and relate them to inducibility for ventricular tachyarrhythmias by electrophysiologic study (EPS).

Methods: 16 patients with ICM referred for prophylactic implantable cardioverter defibrillator placement underwent tagged and contrast enhanced MRI to analyze regional LV function and infarction areas, respectively. Peak systolic circumferential strain (ECC%) and time to peak systolic strain were analyzed in 12 regions in a short axis mid-ventricular slice. Areas were divided according to remote, adjacent and infarct areas by the extent of delayed hyper-enhancement. All patients had invasive (n = 3) or non-invasive (n = 13) EPS and those inducible for ventricular tachycardia or ventricular fibrillation were considered positive. Associations of peak systolic Ecc and time to peak systolic Ecc strain with inducibility were studied using *t*-test. All patients were recruited as part of the Johns Hopkins Reynolds project.

Results: 11 patients were inducible. Both infarct extent and ejection fraction in inducible and non-inducible patients were not statistically different. Importantly, regional deformation expressed as peak Ecc (absolute value) was lower in remote regions in inducible patients compared to noninducible patients ($-13.47 \pm 8.48\%$ versus $-16.66 \pm 5.61\%$, $p < 0.05$). The most marked differences were observed in the time to peak systolic Ecc. Time to peak systolic Ecc was substantially earlier in inducible compared to noninducible patients. Average time to peak Ecc in inducible patients and non inducible patients was 316.21 ± 28.02 ms and 388.53 ± 48.25 ms, respectively ($p < 0.001$). When analyzed according to regions, time to peak systolic Ecc was significantly earlier only in the infarct regions (302.8 ± 111.6 ms vs 410.87 ± 194.87 ms, $p = 0.01$).

Conclusions: Impaired strain in remote regions and earlier mechanical activation in infarcted regions determined by peak systolic strain in patients with ischemic cardiomyopathy are related to inducibility for ventricular tachycardia and fibrillation and may help in understanding the anatomic substrate that underlies ventricular tachyarrhythmias in these patients.

Shortening strain Ecc (%) and Peak Time Ecc (%) by inducibility and myocardial viability areas

	Inducible patients		Noninducible patients	
Areas	**Ecc (%)**	**Time to peak (ms)**	**Ecc (%)**	**Time to peak (ms)**
Remote	$-13.47 \pm 8.48^{*}$	326.71 ± 148.92	$-16.67 \pm 5.61^{*}$	374.66 ± 198.13
Adjacent	-15.21 ± 6.67	312.9 ± 115.4	-14.24 ± 10.35	386.23 ± 194.05
Infarct	-11.75 ± 4.82	$302.88 \pm 111.66^{**}$	-13.55 ± 6.54	$410.87 \pm 194.88^{**}$

Values are expressed by mean ± SD; $^{*}p < 0.05$, $^{**}p = 0.01$ (*t*-test)

349. Chronic Beta-Blockade Improves Longitudinal Left Ventricular Function in Patients with Chronic Heart Failure due to Systolic Dysfunction: a Cardiac Magnetic Resonance Study

Nikolay P. Nikitin, MD, PhD, Poay Huan Loh, MRCP, Elena I. Lukaschuk, MSc, John G. F. Cleland, MD, FRCP, FACC. *Academic Unit of Cardiology, University of Hull, Kingston Upon Hull, UK.*

Introduction: There is currently an increasing interest in left ventricular (LV) longitudinal function. It is mostly related to the recent observations that in various cardiac diseases longitudinal myocardial function might be impaired earlier than circular fiber activity. It is not known however if longitudinal LV function can improve in the process of pharmacological treatment and if so, whether it recovers in parallel with global LV systolic function.

The assessment of mitral annular motion has been recognized as an accurate method to quantify longitudinal LV function using various techniques. Measurement of mitral annular displacement (MAD) using M-mode echocardiography has been in use since late 60-s but is often limited in patients with suboptimal echo images. Cardiac magnetic resonance (CMR) offers an alternative method of assessing longitudinal LV function not dependent on the acoustic window.

Purpose: The purpose of this study was to observe changes in LV longitudinal function in CHF patients on optimal pharmacological treatment with beta-blockers using cine CMR.

Methods: The study population included 125 patients with symptoms of chronic heart failure (NYHA class II–III, aged 69 ± 8 yrs, ranged 45 to 94 years old) including 102 patients with LV systolic dysfunction (ejection fraction [EF] < 45%) and 23 patients with preserved LV systolic function (EF $\geq$ 45%). All patients were on optimal pharmacological treatment including beta-blockers, ACE

inhibitors or angiotensin receptor blockers, aldosteron antagonists and diuretics.

The study subjects underwent CMR on a 1.5 Tesla scanner (Signa CV/i, GE Medical Systems) at baseline and after 12 months using ECG-triggered breath-hold FIESTA imaging. LV end-diastolic and end-systolic volumes and EF were calculated from a set of short-axis cine images with commercially available MRI-MASS software (MEDIS, Leiden, NL). MAD was measured at the lateral and septal sites in the horizontal long axis (4-chamber) view and at the anterior and inferior sites in the vertical long axis (2-chamber) view and averaged.

Results: Twenty-three patients who died during the 12 months follow-up were excluded from the analysis. Therefore, 102 patients completed the study. Most patients were men (n = 91) and were diagnosed with CHF of ischaemic aetiology (n = 90). There were no changes in LV end-diastolic volume (217 ± 81 vs 214 ± 80 ml, NS) or end-systolic volume (140 ± 71 vs 136 ± 73 ml, NS) or EF (38 ± 13 vs 40 ± 14%, NS). However, MAD increased as a result of treatment from 7.1 ± 3.5 to 8.1 ± 3.6 mm ($p < 0.001$). Improvement was observed in the group of patients with impaired global LV systolic function (6.2 ± 2.4 to 7.1 ± 2.9 mm, $p < 0.001$) but not in the group of patients with preserved systolic function (11.2 ± 4.0 to 11.9 ± 3.6 mm, NS).

Conclusions: In patients with chronic heart failure due to LV systolic dysfunction, longitudinal LV function as assessed by measuring MAD with cine CMR improves as a result of chronic beta-blocker therapy even in the absence of improvement in global LV systolic function.

350. Oral Administration of 17-Beta-Estradiol Over 3 Months Without Gestagen Co-Administration Does Not Improve Coronary Flow Reserve in Post-Menopausal Women: A Placebo-Controlled Cross-Over MR Study

Juerg Schwitter, MD,[1] Sebastian Kozerke, PhD,[2] Jens Bremerich, MD,[3] Christoph Baltes, MSC,[2] Martin Birkhäuser, MD,[4] Peter Boesiger, PhD,[2] Peter Buser, MD.[5]
[1]*Cardiology, University Hospital Zurich, Zurich, Switzerland,* [2]*Institute of Biomedical Engineering, Federal Institute of Technology, Zurich, Switzerland,* [3]*Radiology, University Hospital Basel, Basel, Switzerland,* [4]*Gynecology, University Hospital Berne, Berne, Switzerland,* [5]*Cardiology, University Hospital Basel, Basel, Switzerland.*

Introduction: Estrogens have been shown to improve endothelial function in animals and positive effects in women were reported in acute settings. However, in large clinical trials long-term hormon replacement therapy combining estrogens and gestagens in postmenopausal women reported increased cardiovascular complications.

Purpose: To test the hypothesis that 17-beta oestradiol administered orally over 3 months without co-administration of gestagens would improve coronary flow reserve in postmenopausal women.

Methods: In a double-blind placebo-controlled cross-over design postmenopausal women (mean age 60 ± 5 years, n = 14) were randomized to either start with placebo or 17-beta estradiol (Estrofem, Novo Nordisk) 2 mg/d given orally over 3 months and to switch thereafter for an other 3 months of therapy. At baseline, a stress echocardiography was performed to exclude coronary artery disease. Coronary flow reserve (CFR) was determined by coronary sinus MR flow measurements performed at rest and during vasodilation (dipyridamole 0.56 mg/kg over 4 minutes IV) yielding a spatial/temporal resolution of 0.8 × 0.9 mm^2 and 25–30 ms, respectively. MR studies were performed a baseline (MR1), and after 3 and 6 months of therapy (MR2 and MR3), respectively.

Results: Three patients had to be excluded from the study due to headache over several days, severe nausea during vasodilation at MR1, and due to caffeine intake at the day of the MR study (MR3), respectively. In two patients MR was technically inadequate. Hemodynamics such as heart rate, and systolic and diastolic blood pressures were not different for the control and estradiol group. For CFR, and for resting and hyperemic coronary sinus blood flow no differences between the placebo and estradiol group were found (2-way ANOVA for repeated measurements; see Figure 1). Reproducibility for CFR measurements with phase-contrast MR expressed as mean difference ± SD of paired measurements (determined in the placebo group with a mean CFR of 2.55 ± 0.33 was − 0.21 ± 0.13 (− 1.1 ± 4.9%).

Conclusions: Oral administration of 17-beta-estradiol over 3 months without a gestagen co-administration does not improve coronary flow reserve in post-menopausal women.

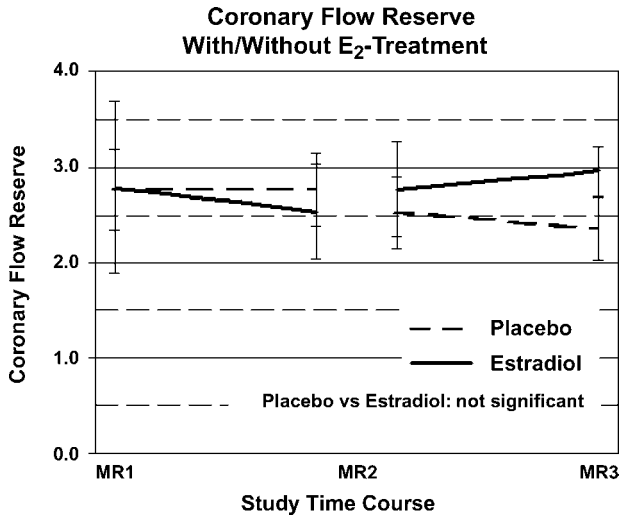

Figure 1.

351. Diagnosis of Incidental Coronary Artery Anomalies Using Standard CMR Pulse Sequences—A Retrospective 5 Year Review

Andrew Crean, MRCP FRCR, Yves Provost, MD FRCP(C), Narinder Paul, MD FRCP(C), Naeem Merchant, MD FRCP(C). *Department of Cardiac MRI, Toronto General Hospital, Toronto, ON, Canada.*

Introduction: Coronary artery anomalies are an infrequent but potentially serious cause of morbidity and mortality. It is not always appreciated that many of these anomalies can be identified on standard CMR studies without the need for complicated coronary visualisation techniques or dedicated vessel tracking. In order to detect these abnormalities it is important to have an appreciation of the range of pathology that may be encountered.

Purpose: To demonstrate the spectrum of coronary artery pathology that may be encountered during routine CMR examinations.

Methods: A retrospective review of consecutive clinical MR cases from January 1999–August 2004.

Results: We found 32 cases of coronary anomaly on routine studies performed for other clinical indications. These were:

12 cases of anomalous coronary origin including several with an inter-arterial course. ALCAPA variant was also seen.
7 cases of coronary sinus aneurysm including 2 large enough to potentially obstruct the RV outflow tract.
4 cases of coronary artery aneurysm including one case of Kawasaki's disease.
4 cases of coronary artery fistulisation to either the RVOT/pulmonary arteries or to the LVOT.
5 cases of unusual orientation of the coronary arteries in patients with transposition of the great arteries and prior Mustard procedure- including 1 case with potential arterial compression by a surgical baffle. The cases are shown with multiple illustrated examples and discussion of clinical relevance.

Conclusions: Coronary artery anomalies may be diagnosed with a high degree of confidence using standard CMR sequences with only minor adjustments of technique if the supervising physician is aware of the range of pathology that may be encountered.

352. Tissue MR Imaging of Subacute Myocardial Infarction correlates with B-Type Natriuretic Peptide and Tissue Doppler Imaging

Bernard P. Paelinck, MD,[1] Christiaan J. Vrints, MD,[1] Jeroen J. Bax, MD,[2] Johan M. Bosmans, MD,[1] Rob J. van der Geest, MSC,[3] Albert de Roos, MD,[3] Hildo J. Lamb, MD.[3] [1]*Cardiology, University Hospital Antwerp, Edegem, Belgium,* [2]*Cardiology, Leiden University Medical Center, Leiden, The Netherlands,* [3]*Radiology, Leiden University Medical Center, Leiden, The Netherlands.*

Introduction: B-type natriuretic peptide (BNP) is an amino acid protein released from the cardiac ventricles in response to myocyte stretch. BNP has been correlated to left ventricular (LV) filling pressures in patients with LV dysfunction and has been used to improve management of these patients. Combining Doppler assessed early diastolic mitral flow velocity (E) with early diastolic mitral annular velocity (Ea) has been correlated with both LV pressures and BNP. Phase-contrast MRI allows velocity encoding of both moving structures (tissue MR Imaging) and blood.

Purpose: To study whether tissue MR Imaging assessed E/Ea correlates with BNP.

Methods: 14 patients in the subacute phase (5.9 ± 2.7 days) of Q-wave myocardial infarction (mass index: 83 ± 14 g/m^2, ejection fraction: 44 ± 12%) underwent consecutive measurement of mitral inflow and mitral annular velocities with Doppler and phase-contrast MRI. The data were correlated with BNP.

Results: There was a strong relation between MRI (12.5 ± 6.3) and Doppler (12.6 ± 5.6) assessed E/Ea ($r = 0.89$, $p < 0.0001$) and between MRI (1.8 ± 0.8) and Doppler (1.5 ± 0.8) assessed E/A ($r = 0.92$, $p < 0.0001$). BNP ranged from 39.5 to 2380 pg/ml. E/A related strongly to BNP (MR: $r = 0.72$, $p = 0.004$ and Doppler: $r = 0.66$, $p = 0.014$). Best relation was found between E/Ea and BNP (MR: $r = 0.74$, $p = 0.002$ and Doppler: $r = 0.88$, $p < 0.0001$).

Conclusions: Tissue MR Imaging has the ability to measure E/Ea. Tissue MR Imaging assessed E/Ea correlates with BNP in patients with subacute myocardial infarction.

353. Aortic Anatomy and Physiology with Magnetic Resonance Aortic Wall Imaging and Pulse Wave Velocity Measurement

Alex Auseon, DO,[1] Anne Garcia, RT,[1] Tam Tran, BS,[1] Christopher J. Hardy, PhD,[2] Subha V. Raman, MD, MS.[1] [1]*Internal Medicine, Ohio State University, Columbus, OH, USA,* [2]*GE Global Research, Niskayuna, NY, USA.*

Introduction: Endothelial dysfunction is an early sign of arterial disease. Loss of large vessel compliance increases pulse wave velocity (PWV) of fluid traveling through the vessel, suggesting that measurement of PWV could serve as a surrogate marker of vessel wall disease, most commonly atherosclerosis. A magnetic resonance (MR)-based technique to measure pulse wave velocity utilizing a cylindrical excitation pulse has been developed and tested in normal volunteers, but to date has not been applied prospectively to correlate PWV with atherosclerotic burden in situ.

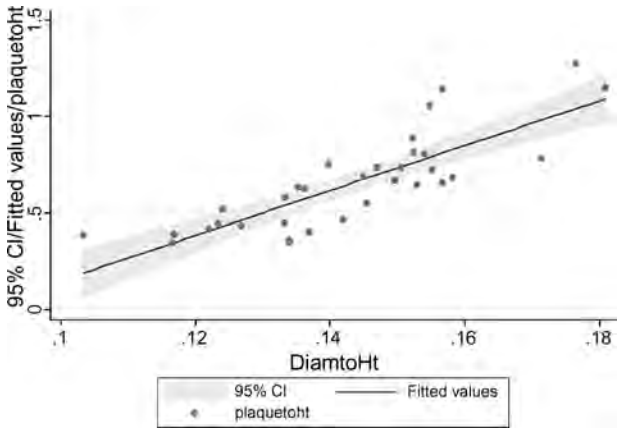

Figure 1.

Purpose: We tested the hypothesis that aortic PWV measured with MR correlates with atherosclerotic plaque burden in the proximal descending thoracic aorta.

Methods: Individuals with risk factors for coronary atherosclerosis scheduled to undergo cardiac catheterization were prospectively enrolled to undergo cardiovascular MR and CT examination. The MR protocol included determination of aortic PWV, with concomitant noninvasive brachial artery blood pressure measurement. The PWV pulse sequence used a two-dimensional pulse to excite a cylindrical volume along the descending aorta, followed by a bipolar velocity-encoding gradient that was stepped through a range of values to produce velocity traces throughout the cardiac cycle. Additionally, black blood imaging using a dual inversion recovery fast spin echo sequence was prescribed in serial axial planes of the descending thoracic aorta for aortic plaque quantification. Multiple blinded reviewers used semi-automated post-processing software (Cine Tool, GE) to delineate endovascular and perivascular aortic borders and to measure relative left-to-right propagation of the velocity waveform to allow quantification of PWV analyzed data sets. In addition, standard contiguous short-axis steady-state free precession cine imaging was obtained to quantify left ventricular size and function.

Results: 33 subjects age 27–75 years (mean 56 years) were enrolled. PWV demonstrated moderate correlation with pulse pressure ($R = 0.48$, $p < 0.01$) but no significant correlation with aortic plaque area (p = NS). Aortic plaque area correlated with aortic diameter ($R = 0.87$, $p < 0.001$), even after normalization to height ($R = 0.83$, $p < 0.001$; Figure 1). Initial analysis of secondary endpoints revealed no significant relationship between PWV and CRP, serum lipids, calcium score, or angiographic severity of coronary artery disease in this cohort.

Conclusions: Aortic pulse wave velocity by NMR pencil excitation correlates with reduced aortic compliance as measured by brachial artery pulse pressure in a heterogeneous cohort with risk factors for atherosclerosis. Aortic plaque burden did increase with increased normalized aortic diameter, suggesting an increase in atherosclerosis with positive aortic remodeling. Further analysis accounting for confounding variables is warranted to assess the relationship between PWV and conventional atherosclerotic risk factors.

354. Left Ventricular Regional Function Improvement in Patients with Chronic Anterior Myocardial Infarction. Evaluation By Magnetic Resonance Myocardial Tagging During Clinical Follow-Up

Sérgio D. Florenzano, MD,[1] José Rodrigues Parga Filho, MD,[2] Carlos Eduardo Rochitte, MD,[2] Luiz Francisco de Ávila, MD,[2] Luiz Antonio Machado Cesar, MD,[2] Cláudio Campi de Castro, MD.[2] [1]*Radiology, Heart Institute (InCor)- University of Sao Paulo Medical School, Braganca Paulista, Brazil,* [2]*Radiology, Heart Institute (InCor)- University of Sao Paulo Medical School, Sao Paulo, Brazil.*

Introduction: Myocardial tagging technique(MRI-T) is well suited to monitor left ventricular(LV) regional function during long-term follow-up.

Purpose: Our aim was to evaluate MRI-T for LV function in patients with anterior myocardial infarction(MI) during clinical follow-up.

Methods: MRI-T was performed at rest(R) in 24 patients(19 men) (mean age:54.33 ± 10.11 years) with chronic MI. Studies were compared at protocol inclusion(E1), after 4 months(E2) and 10 months(E3). We defined 3 regions: remote(R), adjacent(A) and infarcted(I). Infarcted regions were sub-classified by late enhancement in ≤ 25%(I-1), 26–50%(I-2), 51–75%(I-3) and > 75%(I-4) transmurality. Cine-images were acquired during breath-hold with 6–8 LV short-axis using an ECG-triggered gradient-echo sequence with spatial modulation of magnetization: TR/TE:6.2/2.3 msec; FA:15; FOV:36 cm; matrix:256 × 160; BW:31.25 kHz; Thk:8 mm; Gap:2 mm; NEX:1; Tag separation:7 mm. We calculated regional circumferential shortening(CS) index in the entire LV (Find tags software-Johns Hopkins University) and compared by ANOVA for each region and study.

Results: There were no significant differences in EDV, ESV and EF from E1, E2, and E3. There were significant differences in CS between R, A, and I at each follow-up study E2 vs. E3($p < 0.006$) and E1 vs. E3($p < 0.003$). Regions at infarcted areas were different for the studied degrees of transmurality (I-1 vs. I-2(p = ns), I-1 and I-2 vs. I-3($p = 0.0003$), I-3 vs. I-4($p < 0.001$). CS values for R, A, I-1, I-2, I-3 and I-4 in E1 were 0.1406 ± 0.054, 0.1233 ± 0.057, 0.1057 ± 0.056, 0.0937 ± 0.051, 0.0798 ± 0.053 and 0.0572 ± 0.036, respectively. CS values for R, A, I-1, I-2, I-3 and I-4 in E2 were 0.1367 ± 0.049, 0.1273 ± 0.051, 0.1053 ± 0.051, 0.0938 ± 0.054, 0.0718 ± 0.056 and 0.0614 ± 0.046, respectively. CS values for R, A, I-1, I-2, I-3 and I-4 in E3 were 0.1535 ± 0.042, 0.1400 ± 0.050, 0.1158 ± 0.052, 0.0106 ± 0.056, 0.0857 ± 0.053 and 0.0725 ± 0.049, respectively.

Conclusions: MRI-T showed quantitative improvement in LV function for different regions and infarction transmurality, been an excellent tool to monitor medical treatment during follow-up.

355. Interscan Reproducibility of Quantitative Plaque Measurements of Carotid Atherosclerosis in a Clinical Multi-Center Trial using Magnetic Resonance Imaging

Tobias Saam, MD,[1] William S. Kerwin, PhD,[1] Baocheng Chu, MD/PhD,[1] Jianming Cai, MD/PhD,[1] Annette Kampschulte, MD,[1] Vasily L. Yarnykh,[1] Thomas S. Hatsukami, MD,[2] Xue-Qiao Zhao, MD,[3] Nayak L. Polissar, PhD,[4] Kelly Flemming, MD,[5] John Huston, III, MD,[5] William Insull, Jr., MD,[6] Joel D. Morrisett, PhD,[6] Scott D. Rand, MD/PhD,[7] Kevin J. DeMarco, MD,[8] Chun Yuan, PhD.[1] [1]*Department of Radiology, University of Washington, Seattle, WA, USA,* [2]*Department of Surhery, University of Washington, and VA Puget Sound Health Care System, Seattle, WA, USA,* [3]*Department of Medicine, University of Washington, Seattle, WA, USA,* [4]*The Mountain-Whisper-Light Statistical Consulting, Seattle, WA, USA,* [5]*Department of Radiology, Mayo Clinic, Rochester, MN, USA,* [6]*Department of Medicine, Baylor College of Medicine, Houston, TX, USA,* [7]*Department of Radiology, Medical College of Wisconsin, Milwaukee, WI, USA,* [8]*Department of Radiology, Laurie Imaging Center, New Brunswick, NJ, USA.*

Introduction: To establish multi-contrast MRI as a viable, alternative tool for use in clinical trials, a critical requirement is to determine its variability due to measurement error. Although the reproducibility of lumen and wall measurements from multi-contrast MRI was previously reported, that study was conducted at a *single* institution. It is critical to establish the variation of lumen and wall measurements when introduced to multiple centers. Furthermore, to the best of our knowledge, inter-scan reproducibility data for quantitative MRI measurements of plaque components in vivo has not been reported.

Purpose: To test the hypothesis that quantitative measurements of wall volume and plaque composition in *multi-center* clinical trials can be obtained with high inter-scan reproducibility.

Methods: Thirty-nine asymptomatic subjects with > 15% carotid stenosis by ultrasonography were recruited from five clinical sites (site 1:n = 11, site 2:n = 16, site 3:n = 2, site 4:n = 3, site 5:n = 7) to participate in a double-blind, randomized trial (Drug versus Placebo). Subjects were imaged on GE 1.5 T scanners, using TOF, T1-/PD-/T2-and contrast-enhanced T1-weighted images (scan coverage = 24 mm). Four scans (0, 4, 8 and 13 weeks) were scheduled for each subject at each site. Measurement reproducibility was assessed by comparing quantitative data from the index carotid artery of the 19 subjects in the placebo group over the four time points. Each scan was read by 2 experienced reviewers who reached a consensus decision. The obstructive wall volume (OWV) was calculated as wall volume divided by outer wall volume and the volume of lipid-rich/necrotic core (LR-NC) and calcification (Ca) were measured as percentages of the vessel wall. For %LR-NC and %Ca, only those subjects that exhibited an LR-NC or Ca were used in the analysis.

Results: Intraclass correlation coefficient (ICC) showed excellent agreement for wall volume (ICC = 0.97), OWV

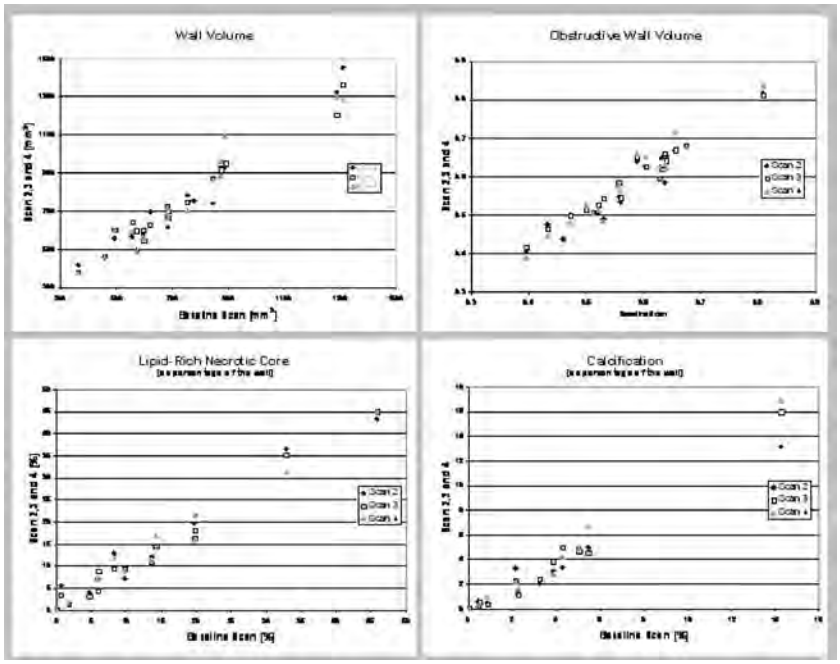

Figure 1.

Endpoint and Exclusion	Treatment Effect 2%	5%	10%	20%	50%	100%
	Number of subjects per group*					
Wall	264	43	12	4	2	2
OWV	81	14	5	3	2	2
%LR-NC (N=13)	943	152	39	11	3	2
%Ca (N=11)	2705	434	110	29	6	3

* Fewer than 10 subjects per treatment group is not recommended
OWV=Obstructive Wall Volume
LR-NC=Lipid-Rich/Necrotic Core
Ca=Calcium
N=Number of subjects displaying one feature

Figure 2.

(ICC = 0.97), %LR-NC (ICC = 0.99) and %Ca (ICC = 0.97) (Figure 1). Measurement error was 5.8% for wall volume, 3.2% for OWV, 11.4% for %LR-NC and 18.6% for %Ca. The calculated measurement errors include any true biological changes that may have occurred in 3 months. One important outcome of the present study is to provide the basis for power calculation in designing future MRI-based trials. Figure 2 can be used as a reference for designing such studies by reading off the number of subjects needed to detect an expected treatment effect.

Conclusions: In vivo MRI is capable of quantifying plaque volume and plaque composition, such as %lipid-rich/necrotic core and %calcification, in the clinical setting of a *multi-center* trial with high inter-scan reproducibility.

356. Vasonstriction of Peripheral Arteries During Reduced Shear: A Novel Technique for Assessing Endothelial Function Using Phase Contrast MRI

Harry A. Silber, MD, PhD,[1] Pamela Ouyang, MD,[1] David A. Bluemke, MD, PhD,[2] Sandeep N. Gupta, PhD,[3] Thomas K. Foo, PhD,[3] Joao A. C. Lima, MD.[1] [1]*Cardiology/Medicine, Johns Hopkins University School of Medicine, Baltimore, MD, USA,* [2]*Radiology, Johns Hopkins University School of Medicine, Baltimore, MD, USA,* [3]*General Electric Medical Systems, Milwaukee, WI, USA.*

Introduction: The endothelial layer of blood vessels is crucially important to maintaining vascular health. Dysfunction of arterial endothelium is one of the earliest physiological occurrences in the development of atherosclerosis. Consequently, there is much interest in assessing endothelial function noninvasively. One endothelial-dependent property is that peripheral arteries constrict during reduced shear.

Purpose: This study investigated whether shear rate reduction and resulting low-shear mediated arterial constriction can be measured in peripheral arteries using phase contrast magnetic resonance imaging (PCMRI).

Methods: The femoral artery was studied in 33 healthy normal subjects using ECG-gated PCMRI. A single imaging plane perpendicular to the artery of interest was prescribed. The imaging parameters were: Matrix size 256 × 128, field of view 10 × 10 cm, slice thickness 3 mm, repetition time (TR) 11.43 msec, and echo time (TE) 5.25 msec. Resulting temporal resolution was 180 msec. A fixed cross-section was acquired before and during a 5-minute distal occlusion. Systolic shear rate and radius were measured from the velocity profile via a best-fit parabola. This provides sub-pixel precision. Shear rate at onset of occlusion was derived from baseline radius and from flow at two minutes into occlusion.

Results: Systolic shear rate decreased from 404 ± 78 sec^{-1} at baseline to 233 ± 75 sec^{-1} immediately after cuff inflation ($p < 0001$), then recovered partially to 252 ± 75 sec^{-1} at two minutes into cuff inflation ($p < 0001$). Arterial systolic radius decreased from 3.52 ±.41 mm at baseline to 3.43 ±.42 mm at two minutes into cuff inflation ($p < 0001$). The average percent change in radius from baseline to two

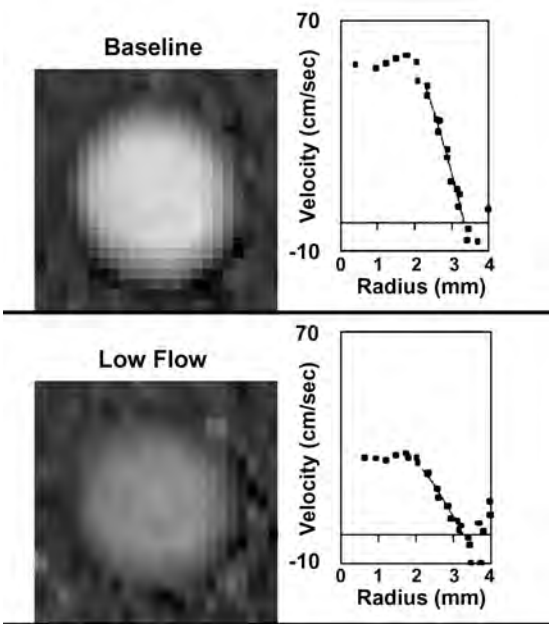

minutes into cuff inflation was − 2.8 ± 2.5%. Both the percent change in radius and the absolute change in radius from baseline to two minutes into cuff inflation were proportional to the percent change in shear rate from baseline to immediately after cuff inflation (r = 36, p = 028, and r = 44, p = 0097, respectively).

Conclusions: Endothelially mediated constriction of peripheral arteries induced by decreasing shear can be measured using PCMRI. The degree of constriction is proportional to the reduction in shear rate. Measuring low-shear mediated vasoconstriction using PCMRI may add important information toward a comprehensive evaluation of endothelial function.

357. Automatic Vessel Wall Thickness Measurement of the Human Descending Aorta in In-Vivo MR Images

Isabel M. Adame Valero, MSc,[1] Rob J. van der Geest,[1] David A. Bluemke,[2] Joao A. C. Lima,[2] Johan H. C. Reiber,[1] Boudewijn P. F. Lelieveldt.[1] [1]*Lkeb, Leiden University Medical Center, Leiden, The Netherlands,* [2]*Department of Radiology, Johns Hopkins Hospital, Baltimore, MD, USA.*

Introduction: Early stages of atherosclerosis are characterized by inflammation of the vessel wall (wall thickening), but normal lumen dimensions. Therefore, all methods that rely on reduction of lumen diameter fail on the detection of early lesions. Magnetic resonance imaging (MRI) can generate high-resolution cross sectional images of the aorta, which enables wall thickness assessment. Currently, this is done manually which is time-consuming and it is subjected to intra- and inter-observer variability. Our goal is an automated technique to trace the contours of the lumen and outer boundary of the aortic wall, and measure vessel wall thickness.

Methods: The algorithm is based on prior knowledge of vessel wall morphology: model-based segmentation and dynamic programming.

First of all, the descending aorta is found by means of the Hough transform by detecting circular structures within the image. This provides the center of the vessel. Prior to the lumen detection, the edge between vessel wall and lumen is enhanced. Then, a geometrical model (ellipse) is created. Following an iterative procedure, the ellipse is deformed, rotated and translated to match the lumen in the enhanced image, according to image gradient measurements. The greater the average gradient along the ellipse, the better it approximates the lumen contour. Afterwards refinement of the contour is performed on the original image by means of dynamic programming.

The second step is outer wall contour detection. The technique is similar to that of lumen, but using a different enhancement to suppress periaortic fat, and taking into account that the outer wall contour must surround the lumen contour. With those requirements, a new ellipse is fitted to the outer wall. As in lumen detection, refinement of the contour is carried out on the original image by dynamic programming.

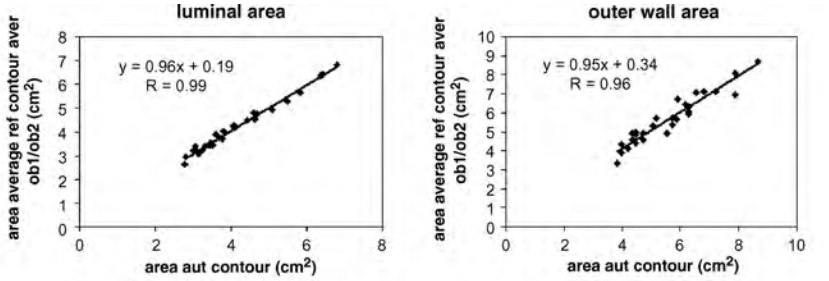

Comparison between automatic and manual measurements for luminal and outer wall area

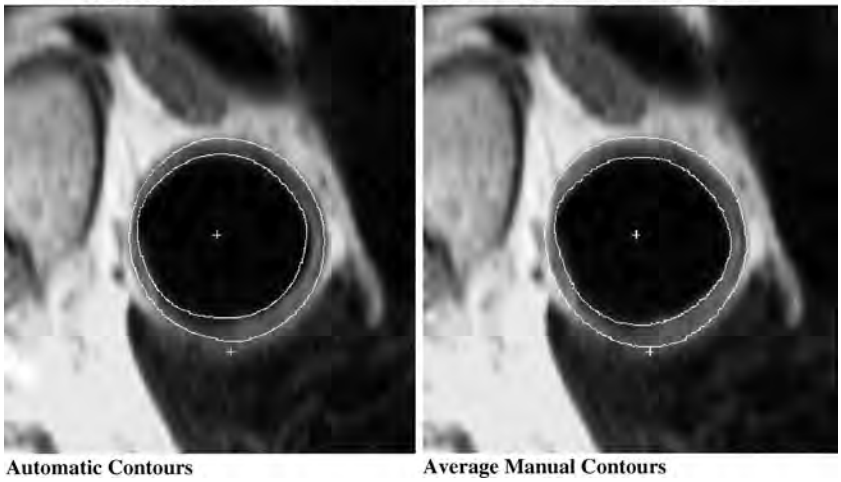

Automatic Contours Average Manual Contours

Finally, wall area and, average and maximum wall thickness are computed. The detection is fully automated and it takes around 7 seconds (standard PC workstation).

Results: The algorithm has been tested on high-resolution MR axial images from 28 human subjects of the descending thoracic aorta at the level of the right pulmonary artery and compared to manual contours averaged from those drawn by 2 experts. Imaging parameters: TR = 2 R-R intervals, TE = 42, FoV = 40 cm, slice thickness = 4 mm and pixel size = 0.7 mm. The results demonstrate:Excellent correspondence between automatic and manual area measurements: lumen (r = 0.99), outer (r = 0.96); and acceptable for wall thickness (r = 0.68). The average paired difference between the automatic/manual measurement pairs was 4.0 ± 14.2 mm^2 (1.0 ± 3.4%; p = NS) for lumen area, 7.2 ± 38.6 mm^2 (1.3 ± 6.7%; p = NS) for outer area, and 3.2 ± 32.9 mm^2 (2.0 ± 21.0%; p = NS) for wall area. When compared to the contours drawn by each observer separately, the mean thickness obtained from the automatic detection is 2.0 ± 0.5 mm, while for observer 1 is 2.1 ± 0.4 mm, and observer 2, 1.9 ± 0.4 mm. For the average contour it was 2.0 ± 0.4 mm. This shows that the accuracy of the automatic method is in the order of inter-observer reproducibility.

Conclusions: Though further optimization is required, our algorithm is a powerful tool for measuring aortic wall thickness.

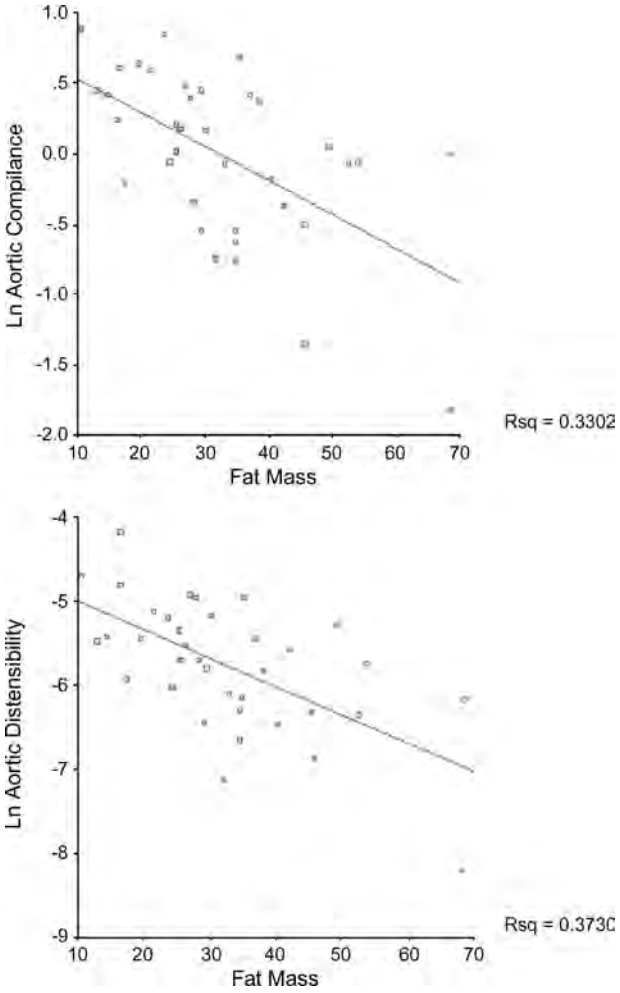

358. Obesity is an Independent Risk Factor for Aortic Mechanical Function—A Cardiovascular Magnetic Resonance Imaging Study

Monique R. Robinson,[1] Michaela Scheuermann-Freestone,[1] C Paul Leeson,[1] Kieran Clarke,[2] Stefan Neubauer,[1] Frank Wiesmann.[1] [1]*Cardiovascular medicine, University of Oxford Centre for Clinical Magnetic Resonance Research, Oxfordshire, UK,* [2]*University of Oxford, University Laboratory of Physiology, Oxfordshire, UK.*

Introduction: Determining the independent effect of obesity on the heart is difficult, because cardiovascular investigations are commonly complicated by the presence of insulin resistance (IR) and hypertension (HTN).

Purpose: We hypothesized that uncomplicated obesity would be associated with decreased aortic elastic function.

Methods: Asymptomatic normotensive obese subjects (n = 27) of mean body mass index (BMI) 33 kg/m^2 and age- and sex-matched controls (n = 12, BMI 23 kg/m^2) were scanned in a 1.5 Tesla MR system. Cine images were acquired at the ascending, proximal descending and abdominal aortic levels and aortic diameters manually contoured. Aortic compliance (A_C), distensibility (A_D), elastic modulus (E_m) and stiffness index (β) were calculated. Blood pressure (BP) was measured. Fasting lipids, glucose, insulin, leptin and IR (using HOMA) were measured. Multiple linear regression (MLR) was used to determine the main predictors of A_C, A_D, E_m and β.

Results: BP, LDL cholesterol, glucose and IR were normal in the obese. Leptin was significantly higher with obesity (8.9 ± 0.6 vs. 4.7 ± 0.6 ng/ml, $p < 0.001$). Mean A_C in the obese was significantly lower (0.9 ± 0.1 vs.1.5 ± 0.2 $mm^2/mmHg$, $p < 0.02$), as was A_D (3.3 ± 0.01 vs.5.6 ± 0.01 $mmHg^{-1} \times 10^{-3}$, $p < 0.02$) indicating reduced aortic buffering capacity and elasticity. E_m did not differ significantly, but β was higher in the obese (1.5 ± 0.01 vs.0.1 ± 0.01 × 10^{-3}, $p < 0.02$) reflecting deranged intrinsic vessel elasticity. A_C correlated negatively with BMI ($r = -0.5$, $p < 0.001$), fat mass ($r = -0.6$, $p < 0.001$), and leptin ($r = -0.5$, $p = 0.002$). A_D correlated negatively with BMI ($r = -0.6$, $p < 0.001$), fat mass ($r = -0.6$, $p < 0.001$) and leptin ($r = -0.4$, $p < 0.01$). MLR showed fat mass as the strongest predictor of A_C, leptin and BMI were also predictive. A_D was predicted by fat mass, BMI and leptin. For E_m, fat mass and BMI were highly predictive.

Conclusions: Aortic elastic function is markedly deranged in uncomplicated obesity. Fat mass is the strongest predictor of central arterial dysfunction, closely followed by leptin and BMI.

359. Usefulness of MRI for the Evaluation of Subclinical Atherosclerosis in Both Extracranial Carotid and Intracranial Cerebral Arteries

Ryuichi Kato, MD,[1] Yukihiko Momiyama, MD,[1] Hiroaki Taniguchi, MD,[1] Teruyoshi Kihara,[2] Akira Kameyama,[2] Masayoshi Nagata, MD,[2] Fumitaka Ohsuzu, MD.[1] [1]*First Department of Internal Medicine, National Defense Medical College, Saitama, Japan,* [2]*Iruma Heart Hospital, Saitama, Japan.*

Introduction: Recently, MRI became a useful tool for noninvasively detecting atherosclerotic plaques in carotid arteries. MRI evaluation of carotid plaques was shown to closely correlate with histopathology in patients undergoing carotid endarterectomy. However, the usefulness of MRI evaluation of subclinical carotid atherosclerosis in asymptomatic patients with atherosclerotic risk factors has not been elucidated. Duplex ultrasonography (DUS) is most commonly used to evaluate subclinical carotid atherosclerosis.

Purpose: To determine the accuracy of MRI evaluation of subclinical atherosclerosis in carotid arteries in comparison to DUS and to show the usefulness of MRI evaluation of both carotid and intracranial cerebral arteries in the same exam session.

Methods: Carotid plaque MRI was performed on GE Signa 1.5 T CV/i scanner in 45 patients (mean age 65 ± 7 years) who had some atherosclerotic risk factors but no history of cerebrovascular events or symptoms. Transverse T2-weighted and proton density-weighted images of carotid arteries were obtained using a black blood technique with a commercially available carotid phased-array coil (ScanMed) and fat suppression. Parameters were TR = 2 RR intervals, TE = 60 ms (T2 W), 10 ms (PDW), 10-cm FOV, 3-mm slice thickness, no interslice gap, 256 × 256 matrix, and 16 echo-train. Plaques were defined as focal or diffuse thickening, and plaque thickness was measured as the distance between intima and outer arterial wall boundary (probable intima-adventitia). Of the 45 patients, 26 also underwent carotid DUS, and plaques were defined as focal or diffuse thickening of intima-media layer of $\geq$ 1.3 mm on DUS. Carotid arteries were divided into 2 regions (common carotid-bulb and internal carotid), and the presence of plaques and the maximal plaque thickness in each region were evaluated by MRI and DUS. In addition to carotid plaque MRI, 3-dimensional TOF MRA of carotid and intracranial cerebral arteries as well as brain MRI (T1 W and T2 W images with 7-mm slice thickness) were also performed. Total examination time was 40 minutes.

Results: On DUS, carotid plaques were found in 21 of 26 patients and in 50 of 104 carotid regions. MRI correctly detected carotid plaques in 49 regions, but MRI did not detect one small plaque (2 mm in size). MRI misdiagnosed flow artifacts in 2 regions and intima-media thickening (1.1 mm) in 1 region to be plaques. As a result, the overall agreement

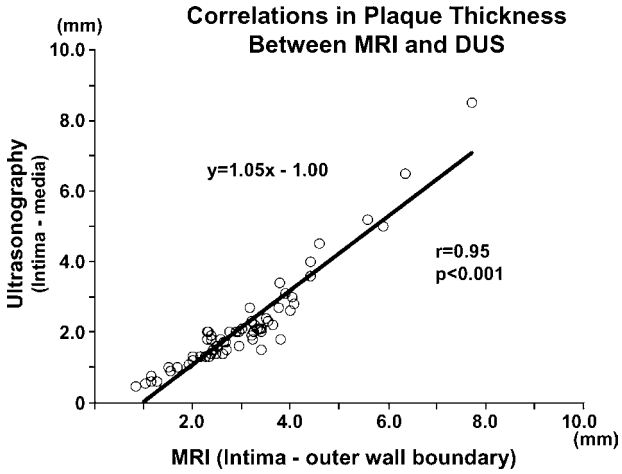

Figure 1.

for the detection of carotid plaques between MRI and DUS was 95% (kappa value = 0.90). Notably, the measurement of maximal plaque thickness in carotid arteries highly correlated between MRI and DUS ($r = 0.95$, $p < 0.001$), as shown in Figure 1. Of the 45 patients, 33 (73%) were found to have carotid plaques by MRI. However, brain MRI detected asymptomatic small infarcts in 17 patients (38%), of whom 13 also had carotid plaques but 4 did not have any carotid plaques. Moreover, MRA did not detect any stenosis in intracranial cerebral arteries but detected small aneurysm in 2 patients (4%).

Conclusions: MRI is useful for noninvasively evaluating subclinical atherosclerosis in carotid arteries in asymptomatic patients with atherosclerotic risk factors. The accuracy for the detection and measurement of carotid plaques by MRI seems to be compatible with that by DUS. Moreover, MRI can also evaluate some abnormalities in intracranial cerebral arteries in the same exam session, thereby making the evaluation of the cerebrovascular system more accurately.

360. Comparison of Magnetic Resonance Imaging Based Atherosclerotic Plaque Indices and Traditional Risk Factors in Patients With and Without Coronary Artery Disease

Venkatesh Mani, PhD,[1] Silvia H. Aguiar, MD,[1] Karen B. Weinshelbaum,[1] John E. Postley, MD,[2] Vitalii V. Itskovich, PhD,[1] Juan Gilberto S. Aguinaldo, MD,[1] Daniel D. Samber, PE,[1] Valentin Fuster, MD, PhD,[1] Zahi A. Fayad, PhD.[1] [1]*Imaging Sciences Laboratories, Mount Sinai School of Medicine, New York, NY, USA,* [2]*College of Physicians and Surgeons, Columbia University, New York, NY, USA.*

Introduction: Though traditional risk factors have predictive power for atherosclerosis, they are not always useful in determining which individual will have coronary artery disease CAD. The purpose of this study was to use a CMR

based atherosclerotic Plaque Index (PIN) to measure the burden of atherosclerotic disease (BAD) and correlate it with various traditional risk factors in terms of CAD.

Methods: 100 subjects at risk for atherosclerosis (67 men, 33 women; mean age 54.3 ± 20.5 years) were imaged using a 1.5 T scanner. 12–24 transverse images 3 mm thick centered on the carotid bifurcation and 32–48 transverse images 5 mm thick imaging the aorta from the aortic arch to the level of the iliac bifurcation were obtained using rapid extended coverage black blood turbo spin echo sequence (Mani et al., 2004). The total examination time was < 1 hour. The inner, outer vessel wall and the diameter of the lumen on two axes were measured (Figure 1). Average wall area of carotids (CWA) and aorta (AWA) and PIN (vessel wall area normalized to average lumen diameter) for aorta (PINA) and carotids (PINC) were calculated for all patients Framingham Score and 10-year risk was also calculated for all the patients.

Results: The demographics were as follows: 57% of the subjects had a family history for heart disease, 13% were smokers, 14% had a history of stroke, 20% were diabetic, 18% had CAD and 65% were on anti-cholesterol medication. Comparing patients without CAD and those with CAD, Framingham Scores (7.51 ± 4.20 for patients without CAD vs. 7.28 ± 4.07 for patients with CAD, $p = 0.447$, NS) and 10-year risks (0.117 ± 0.069 for patients with no CAD vs. 0.141 ± 0.089 for patients with CAD, $p = 0.216$, NS) were not significantly different in our cohort. However, CWA (28.15 ± 11.39 for patients without CAD vs. 33.46 ± 11.0 for patients with CAD, $p = 0.041$), PINC (4.83 ± 1.89 for patients without CAD vs. 5.74 ± 1.85 for patients with CAD, $p = 0.037$), AWA (132.7 ± 58.5 for patients without CAD vs. 190.2 ± 62.9 for patients with CAD, $p < 0.001$) and PINA (6.82 ± 1.98 for patients without CAD vs. 8.76 ± 2.67 for patients with CAD, $p < 0.001$) were all significantly higher in patients with CAD as compared to those without CAD.

Conclusions: MRI is a non-invasive technique to detect vascular pathology in high-risk patients. PIN may be used to screen patients especially at risk for CAD and its incorporation in cardiovascular assessment might be useful.

REFERENCES

Mani, V., Itskovich, V. V., Szimtenings, M., Aguinaldo, J. G. S., Samber, D. D., Mizsei, G., Fayad, Z. A. (2004). Rapid extended coverage (REX) simultaneous multislice black blood vessel wall imaging. *Radiology* 23:281–288.

361. Noninvasive Assessment of Coronary Artery Vasomotor Response to Cold Pressor Test Using CMR

Andressa Borges, MD, Yi Wang, DSc, William Schapiro, RT, Nathaniel Reichek, MD. *Research, St. Francis Hospital, Stony Brook University, Roslyn, NY, USA.*

Introduction: The assessment of endothelial dysfunction (ED) provides diagnostic and prognostic information in patients at risk for coronary artery disease and predicts cardiovascular event rates. Coronary artery ED impairs the increase in coronary arterial flow and lumen size produced by cold pressor testing (CPT). Alternatively, nitroglycerin (NTG) causes endothelial-independent vasorelaxation and an increase in coronary blood flow.

Hypotheses: We hypothesized that coronary imaging and phase-contrast CMR (PC-CMR) could be used to assess changes in coronary artery cross sectional area (CSA),

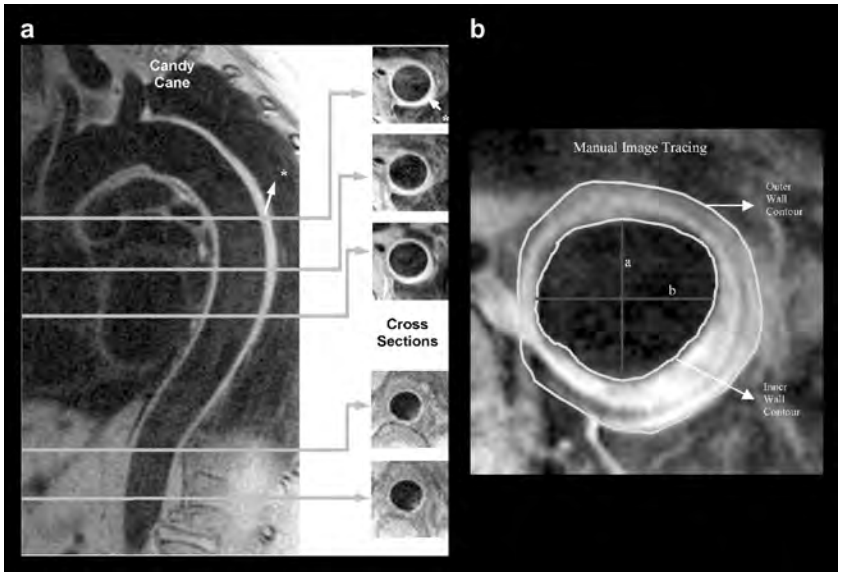

Figure 1.

coronary blood flow and flow velocity during CPT and following sublingual NTG in control subjects (Controls) and patients with risk factors associated with ED, such as hypertension, hyperlipidemia, diabetes, smoking (Risk).

Methods: Coronary CSA, mean diastolic coronary blood flow (CBF) and mean diastolic flow velocity (V) were measured at baseline and at 90 seconds of CPT, and before and serially after NTG 0.4 mg s.l. Breath-hold turbo spin echo CMR (FOV 195 × 240 cm matrix 125 × 256) and segmented phase contrast TurboFLASH CMR velocimetry were used to image a cross-section of the proximal left anterior descending coronary artery and CSA, CBF and V assessed. Findings were compared in Controls (n = 7, 4 women; age 52 ± 11 yrs) and Risk (n = 16, 14 men; age 64 ± 5 yrs).

Results: CBF increased during CPT in Controls but not in Risk. No change in CSA was detected in either group. At peak NTG effect, CBF increased in Controls and in Risk, while CSA increased in Controls, with a strong trend in Risk. Changes in V paralleled changes in CBF throughout.

Conclusions: PC-CMR identified an increase in CBF and V during CPT in control subjects, but not in patients with risk factors for CAD. CMR also depicted endothelium-independent vasodilation with increased CBF and V following NTG. Thus, CMR may permit direct noninvasive assessment of coronary vasomotion and endothelial dysfunction.

	CSA (cm2) CONT	CSA (cm2) RISK	CBF (ml/sec) CONT	CBF (ml/sec) RISK	V (cm/sec) CONT	V (cm/sec) RISK
Baseline 1	.12 ± .02	.15 ± .06	.21 ± .12	.39 ± .18	5.7 ± 2.6	8.7 ± 3.8
Cold Pressor	.12 ± .02	.14 ± .05	.47 ± .27*	.37 ± .15	8.0 ± 4.0*	8.7 ± 3.9
Baseline 2	.13 ± .04	.15 ± .06	.22 ± .12	.40 ± .18	6.0 ± 3.0	9.3 ± 3.9
NTG	.18 ± .02**	.19 ± .08#	.52 ± .24*	.74 ± .41***	9.3 ± 3.6#	12.1 ± 5.2*

*p < 05 **p < 005 ***p < 0005 #p = 07 vs. baseline

362. Long Term Fate of Left Atrial Thrombi and Incidence of Cerebral Embolism under Continuous Anticoagulation Therapy—A Prospective, Serial and Controlled Study using Cerebral Diffusion-Weighted Imaging and Transesophageal Echocardiography

Katharina A. Strach, MD, Matthias Hackenbroch, MD, Carsten Meyer, MD, Alexandra Schmiedel, MD, Heyder Omran, Hans H. Schild, MD, Torsten Sommer, MD. *Radiology, University Hospital Bonn, Bonn, Germany.*

Background: Patients (pts) with atrial fibrillation (AF) and atrial thrombi are known to have an increased risk for cerebral embolism. However, there is little known about the clinical course of atrial thrombi and the incidence of cerebral embolism in those patients during anticoagulation therapy. The high sensitivity of diffusion-weighted imaging (DWI) suggests that this technique could provide an improved estimate of cerebral ischemic events associated with the presence of left atrial thrombi.

Purpose: The aims of this prospective study were 1. to evaluate the incidence of clinically silent and apparent cerebral embolism in patients with newly diagnosed atrial fibrillation and atrial thrombi by using DWI, to assess 2. the long term fate of atrial thrombi under continued anticoagulation therapy and 3. the incidence of cerebral embolism during a follow-up period of 12 months with continuous anticoagulation therapy.

Methods: Study group inclusion criteria were: 1. newly diagnosed AF with evidence of left atrial thrombi detected by TEE and 2. new start of anticoagulation therapy [International Normalized Ratio (INR) 2.5–3.5]. The study group consisted of 32 pts (18 males, 14 females) with a mean age of 63 ± 10 years. 19 pts (12 males, 7 females; mean age 55 ± 12 years) with 1. newly diagnosed AF but no evidence of atrial thrombi and 2. equivalent anticoagulation regimen as in study group served as control group. The following procedures were performed in a serial and prospective manner at the beginning of the study, at 4 weeks, at 3 months and at 1 year in both groups: 1) Magnetic resonance imaging (MRI) studies of the brain including DWI [1.5 Tesla, diffusion gradient b-values of 0, 500, and 1000 s/mm^2, repetition time (TR) 4000 ms, echo time (TE/TEd) 120 ms/85 ms, slice thickness 6 mm, matrix 101 × 256)], 2) transesophageal echocardiographic studies (TEE) for detection of thrombi in left atrium (LA) or LA appendage, and assessment of thrombus echogenity, left ventricular ejection fraction, LA volume, and peak emptying velocities of the LA appendage and 3) clinical neurologic assessment.

Results: 11 out of 32 pts (34%) had bright diffusion lesions on the initial MR studies consistent with acute cerebral emboli; in 10/11 pts (91%) emboli were clinically silent. In 4 out of 32 pts (13%) DWI depicted new or additional cerebral emboli (n = 9) during the follow-up period despite continuous anticoagulation therapy. 2 (50%) of these patients had clinically apparent neurologic deficits. In the control group 1 out of 19 pts (5%) had evidence of cerebral embolism as assessed by DWI at the beginning of the study while no embolism occured during the 12 months follow-up. 16% (5/32) of left atrial thrombi in the study group resolved completely under anticoagulation therapy within 4 weeks, 53% (17/32) resolved within 12 months. Pts with cerebral embolism revealed by DWI had significantly larger thrombi (as assessed by TEE on the initial TEE: 3.2 ± 2.2 cm^2 vs. 1.0 ± 0.6 cm^2; p = 0.003) and lower thrombus echogenity (p = 0.04) compared to pts without embolism. No significant correlation existed between peak emptying velocities of the LA appendage, left ventricular ejection fraction and LA volume with cerebral embolism (p < 0.05).

Conclusion: 1) The incidence of clinically inapparent cerebral emboli in pts. with newly diagnosed AF and atrial thrombi is much higher than the incidence of clinically apparent emboli and has been underestimated in the past. 2) Only 53% of atrial thrombi disappear within 12 months under anticoagulation therapy. 3) New cerebral embolism may occur even with continued effective anticoagulation therapy in 13% of pts. 4) Larger thrombus size and low thrombus echogenity are associated with a significant ($p < 0.05$) higher risk of cerebral embolism.

363. Signal Intensity Change of Carotid Intraplaque Hemorrhage; A Long Term Follow Up In Vivo MRI Study

Norihide Takaya, MD,[1] Chun Yuan, PhD,[1] Baocheng Chu, MD,[1] Tobias Saam,[1] Nayak Polissar,[2] Carol Isaac,[3] Judith McDonough,[3] Marina Ferguson, MT,[1] Thomas Hatsukami, MD.[3] [1]*Department of Radiology, University of Washington, Seattle, WA, USA,* [2]*The Mountain-Whisper-Light Statistical Consulting, Seattle, WA, USA,* [3]*Department of Surgery, University of Washington, Seattle, WA, USA.*

Introduction: Prior studies of the MRI signal characteristics of intracerebral hemorrhage have defined the stages of hemorrhage as fresh (< 1 week), recent (1–6 weeks) and old (> 6 weeks). However no reports have shown the time course of MRI signal changes for intraplaque hemorrhage in advanced carotid atherosclerosis.

Purpose: The purpose of this study is to observed the signal intensity change of intraplaque hemorrhage by MRI.

Methods: Fourteen patients with MRI evidence of carotid intraplaque hemorrhage at baseline examination underwent follow-up scans 18 months later. A standardized protocol was used to obtain 4 different contrast-weighted images (T1, T2, proton density and 3D time of flight). The age of intraplaque hemorrhage was defined as fresh (stage I) and recent (stage II), based on previously published criteria. Stage I hemorrhage appears hyperintense signal on T1/TOF images and iso- to hypointense on T2/PD images, compared to the adjacent sternocleidomastoid muscle. Stage II hemorrhage appears hyperintense on all 4 contrast weightings.

Results: 142 MRI cross-sectional levels were available for analysis amongst the 14 patients. Intraplaque hemorrhage was identified in 80 MR slices (83 locations) at baseline examination. Stage I hemorrhage was present in 6 slices

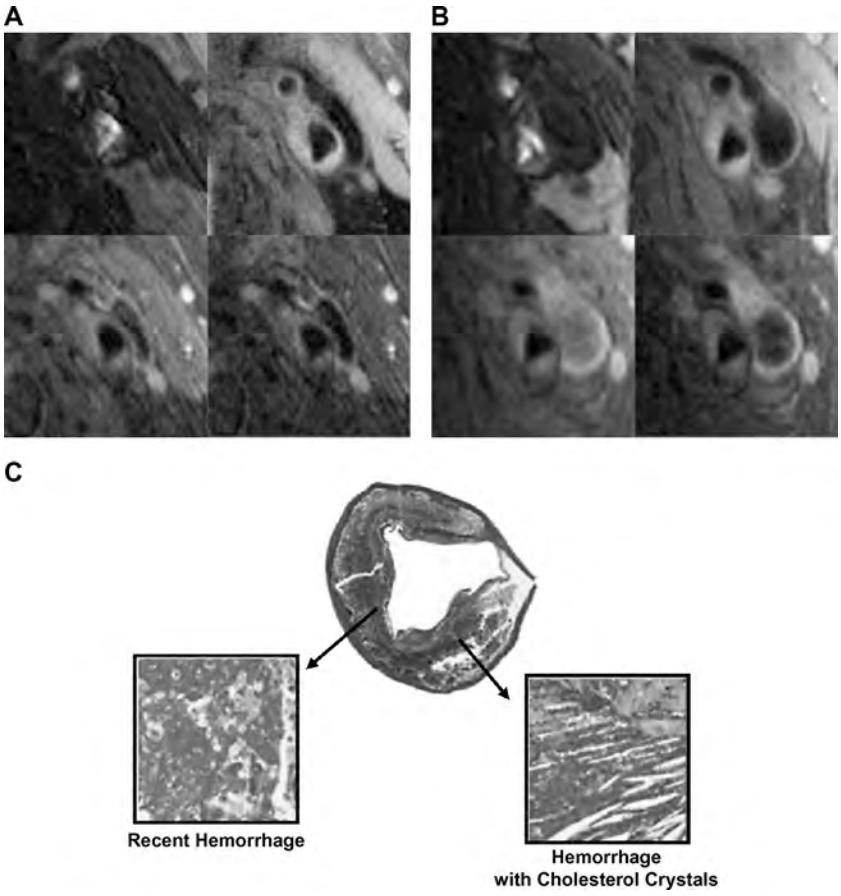

Figure 1.

(7.5%) and stage II hemorrhage was observed in 71 slices (88.8%). Three slices (3.8%) contained both stage I and stage II hemorrhages in the same slice level. At the 18 month follow-up examination, 78 locations (94.0%) demonstrated signal intensity indicating that the hemorrhage stage remained unchanged.

Conclusions: The MRI signal characteristics of intraplaque hemorrhage in advanced carotid atherosclerosis remains unchanged after 18 months in the overwhelming majority of cases. These findings suggest that plaque hemorrhage evolves more slowly compared to intracranial hemorrhage, or that plaques with hemorrhage are more prone to repeat hemorrhage events (Figure 1).

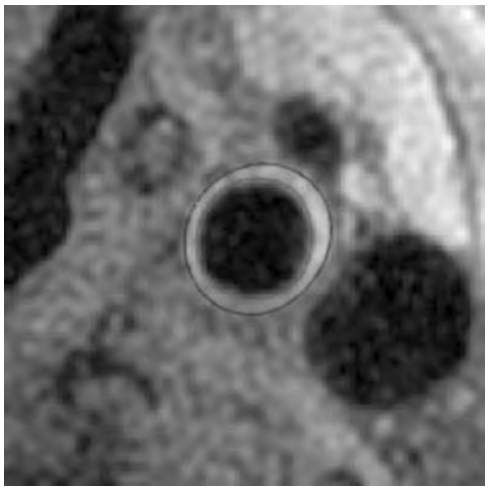

Figure 1.

364. Is Common Carotid Artery Mean Wall Thickness by MRI Comparable to Intima-Media Thickness by B-Mode US?

Hunter Underhill, MD,[1] William Kerwin, PhD,[1] Thomas Hatsukami, MD,[2] Chun Yuan, PhD.[1] [1]*Radiology, University of Washington, Seattle, WA, USA,* [2]*Surgery, University of Washington, Seattle, WA, USA.*

Introduction: High-resolution magnetic resonance imaging (MRI) has emerged as a powerful tool in the non-invasive evaluation of local atherosclerotic disease in the carotid artery. However, to obtain an indication of the patient's systemic atherosclerotic disease status, B-mode ultrasound (US) must currently be employed to measure common carotid artery intima-media thickness (IMT). Changes in plaque morphology and IMT are becoming central in outcome studies as both are emerging as separate viable end-points for evaluating the success of pharmaceutical intervention. Since both modalities cover a similar segment of the common carotid artery, the possibility of obtaining both plaque morphology and IMT using a single imaging modality must be considered. If viable, future progression studies would benefit from a reduction in cost, simplification of protocol design and minimization of patient time commitment.

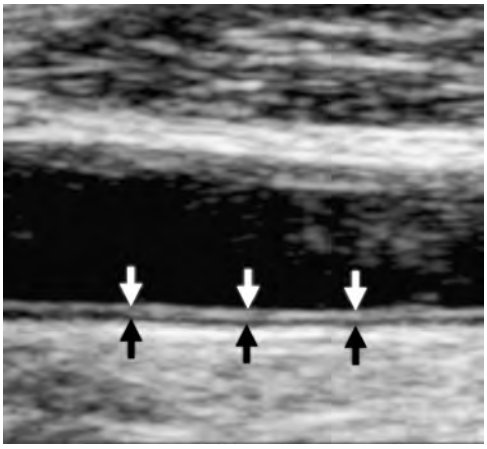

Figure 2.

Purpose: We sought to determine if measuring the thickness of the common carotid artery wall by cross-sectional, black-blood, T1 W MRI is equivalent to measuring common carotid artery IMT by B-mode US.

Methods: The carotid arteries of 17 subjects with 16–79% carotid stenosis by duplex US were examined by high-resolution MRI and B-mode US. The MRI examination included acquisition of black-blood, T1-weighted cross-sectional images. Acquisition parameters were: TR/TE = 800/9.3 ms, echo train length (ETL) = 8, field of view (FOV) = 16 cm, matrix size = 256 × 256, slice thickness 2 mm. Approximate acquisition time was 6 minutes. At a distance 0.8–1 cm proximal to the bifurcation, the lumen and outer wall boundaries of the common carotid artery were automatically detected via a novel technique that utilized a B-spline snake (Figure 1). The average thickness between these two boundaries was computed and declared as mean

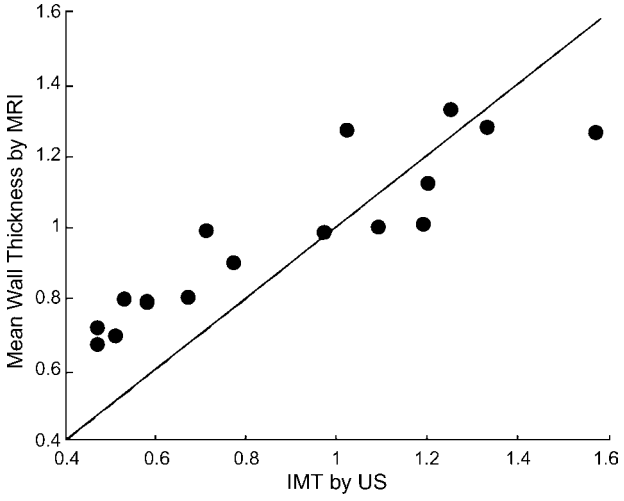

Figure 3.

wall thickness. B-mode US images were centered 1 cm proximal to the bifurcation and were acquired by an experienced, trained ultrasonographer following a standardized clinical trial imaging protocol. IMT was measured along the medial common carotid artery wall in the longitudinal plane (Figure 2) over a 10 mm length using an automated program provided by Q-Lab (Philips Medical Systems).

Results: Automated mean wall thickness by MRI was highly correlated with B-mode US IMT ($r = 0.91$) as seen in Figure 3. In general, an overestimation by MRI was apparent at the lower values, which may be due to the inclusion of the adventitia in the MRI measurement.

Conclusion: Amongst individuals with a 16–79% carotid stenosis, MRI measurement of common carotid wall thickness is highly correlated with ultrasound measurement of IMT. Although further evaluation is needed to determine the exact relationship between measurements and to assess their comparative reproducibility, automated mean wall thickness by MRI may serve as an alternative to IMT by B-mode US. In patients with black blood, T1 W, carotid MRI, it may be possible to obtain both local detail and systemic atherosclerotic information in a rapid fashion (<6 min).

365. Increased Central Pulse Wave Velocity in Uncomplicated Diabetes Type 2 Assessed by CMR

Rutger W. vd Meer, MD,[1] Michaela D. Diamant, MD, PhD,[2] Jeroen J. Bax, MD, PhD,[3] Theodorus A. M. Kaandorp, MD,[1] Jos J. M. Westenberg, PhD,[1] Albert de Roos, MD, PhD,[1] Hildo J. Lamb, MD, PhD.[1] [1]*Radiology, Leiden University Medical Center, Leiden, The Netherlands,* [2]*Endocrinology, VU University Medical Center, Amsterdam, The Netherlands,* [3]*Cardiology, Leiden University Medical Center, Leiden, The Netherlands.*

Introduction: Type 2 diabetes mellitus (DM2) has a rapidly increasing prevalence, which has been projected to rise to 5.4% by 2025. In addition, DM2 is associated with high morbidity and mortality. Arterial stiffness, as measured by studying pulse wave velocity (PWV), is considered to be highly predictive of cardiovascular mortality in subjects with DM2. Until now, PWV is usually measured using Doppler or applanation tonometry, showing increased PWV in patients with *established* DM2. Recently, CMR flow was introduced as an alternative method for assessment of PWV. CMR is highly reproducible, and is capable of accurately measuring pulse wave travel length, which is impossible when using other techniques. It is unknown whether pulse wave velocity is raised in *uncomplicated*, early-stage DM2.

Purpose: To determine central PWV in patients with uncomplicated DM2, using CMR flow.

Methods: Thirty subjects (14 patients with uncomplicated DM2, and 16 age-and gender matched healthy controls) were studied. MRI velocity mapping (retrospectively ECG-gated gradient-echo sequence, with a temporal resolution of 25 ms) was performed to measure bloodflow proximal in the descending aorta and just above the bifurcation of the abdominal aorta. PWV was calculated by dividing the aortic distance between those two points (see Fig. 1), by the time delay between the points-of-arrival at both imaging levels. To determine the point-of-arrival, straight lines were fitted through the flow data-points at baseline, and through the data-points during the acceleration phase of the flow curve. The intersection of these two fitted lines was determined, and the corresponding time-point was considered as the arrival time of the pulse wave. Thereafter, the time difference between the proximal and distal points along the aorta was calculated.

Results: Patients showed a significantly higher mean aortic PWV than controls (6.6 ± 1.4 vs. 5.6 ± 0.8, $P < 0.05$) and showed a significant positive correlation with diastolic blood pressure, systolic blood pressure, fasting plasma bloodglucose, and insulin levels, as well as with an insulin resistance index ($P < 0.05$). In addition, the association with plasma HDL levels and CRP tended to be significant. Intra-observer reproducibility was excellent, average difference was -0.05 ± 0.5 ($P > 0.05$). Limits of agreement were -1.04 to 0.94 for intra-observer variability. Correlation between both measurements by the same observer was statistically significant ($r = 0.93$, $p < 0.01$).

Conclusions: Patients with uncomplicated diabetes mellitus type 2 show an increased central pulse wave velocity as determined by CMR flow. In addition, the point-of-arrival analysis for PWV showed excellent reproducibility. Furthermore, a large prospective clinical trial is

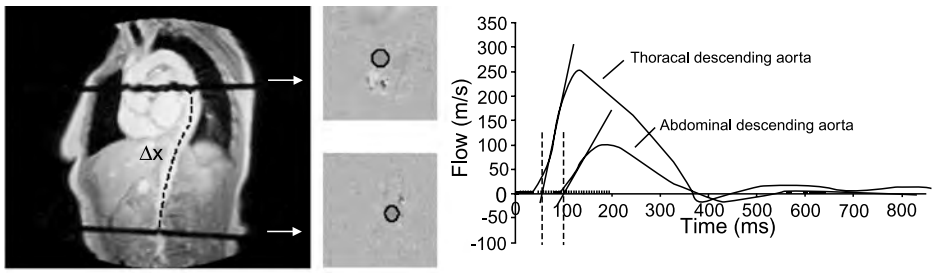

Figure 1.

needed for determining the clinical value of CMR determined PWV.

366. Luminal and High-Resolution 3D Vessel Wall Imaging of Carotid Artery Disease Using CMR and Compared With Histology

Anitha Varghese,[1] Lindsey A. Crowe,[1] Peter D. Gatehouse,[1] Guang-Zhong Yang,[2] Timothy Cannell,[1] David M. Nott,[3] David N. Butcher,[4] Mary N. Sheppard,[4] David N. Firmin.[1] Dudley J. Pennell,[1] Raad H. Mohiaddin.[1] [1]*Cardiovascular Magnetic Resonance, Royal Brompton Hospital, London, UK,* [2]*Royal Society/Wolfson Medical Image Computing Laboratory, Imperial College, London, UK,* [3]*General & Vascular Surgery, Chelsea & Westminster Hospital, London, UK,* [4]*Histopathology, Royal Brompton Hospital, London, UK.*

Introduction: Symptomatic atherosclerotic cardiovascular disease (CVD) is increasingly felt to be the result of factors additional to percentage of arterial luminal stenosis. Little et al showed that most myocardial infarctions result from occlusion at sites which had previously only demonstrated stenoses of less than 50% on angiography and such work has led to the concept of plaque vulnerability. Characteristic structural features of vulnerable plaques include greater positive remodelling and plaque areas and a large lipid core underlying a thin fibrous cap. Both luminal stenosis and interrogation of plaque constituents can be evaluated non-invasively with cardiovascular magnetic resonance (CMR). Currently, CMR at the carotid arteries is readily performed and disease at this site can be used to evaluate the risk of both cerebral and coronary events.

Purpose: To develop a protocol for the evaluation of carotid artery atherosclerotic disease encompassing assessment of luminal stenosis, arterial remodelling, and plaque constituents.

Methods: Five subjects scheduled for carotid endarterectomy were imaged using a Siemens Magnetom Sonata 1.5 T (Tesla) scanner, Siemens phased-array neck coil, a purpose-built two element phased-array surface carotid coil(s) and a specially designed head and neck cushion. Subjects had severe carotid artery stenoses (> 70%) and were symptomatic ($n = 2$) or asymptomatic ($n = 3$). CMR was performed according to the protocol detailed in Figure 1. The protocol comprised localisation of the lesion for surgical removal, high-resolution imaging of this plaque, contrast-enhanced magnetic resonance angiography (CE-MRA) of the carotid and subclavian arteries, and repeat high-resolution imaging following gadolinium contrast. High-resolution imaging was performed using a three dimensional (3D) volume selective fast spin echo (FSE) technique. The T1-weighted sequence used the following parameters: matrix size = 256; 0.47 × 0.47 mm pixels; 28 slices of 2 mm thickness; field-of-view [FOV] = 120 × 24 mm approximately; time to echo [TE] = 11 ms; repetition time [TR] according to a single multiple of the subject's R-R interval (1 × RR); echo train length [ETL] = 11; fat suppression; and 650 ms inversion time following double inversion preparation pulse. The T2-weighted parameters were similar excepting a TE of 53 ms and a TR = 2 × RR. The region chosen for measurement was centered 56 mm around the relevant carotid plaque. Data was

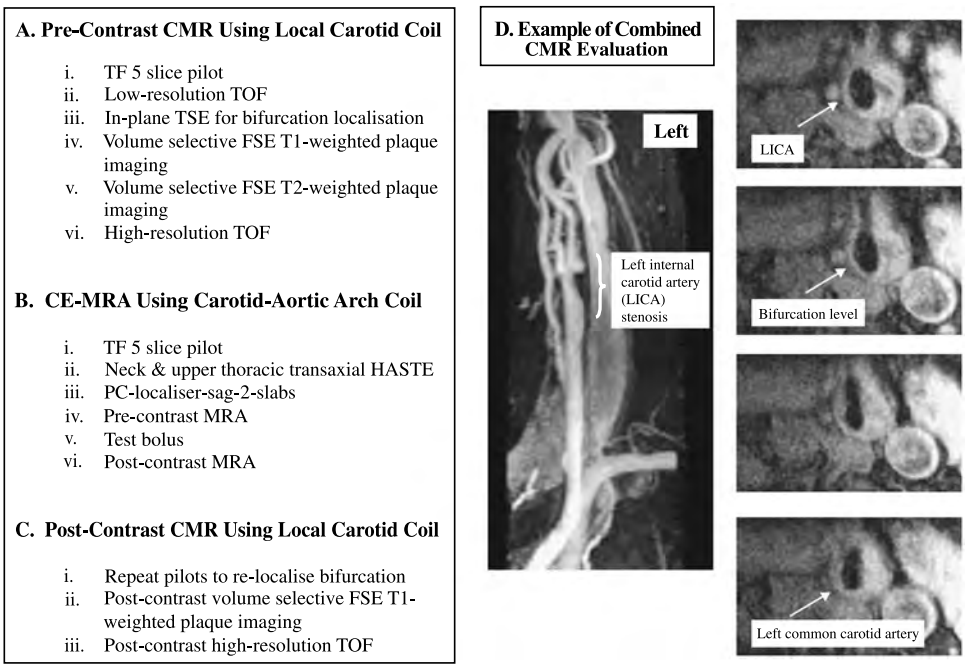

Figure 1. Protocol for CMR Assessment of Subjects Prior to Carotid Endarterectomy.

collected in the form of multispectral cross-sectional CMR images from which registration with histological sections was made.

Results: Luminal stenosis as assessed by CE-MRA and Doppler ultrasonography were well correlated with stenosis severity exceeding 80% in all 5 subjects. There was evidence of significant remodelling in both asymptomatic and symptomatic subjects with the lumen area:plaque area ranging from 0.01 to 0.31. Minimum carotid arterial lumen area was 0.7 mm^3 with a plaque area of 62 mm^3 in that individual at the same level. Qualitative analysis of plaque constituents by high-resolution 3D volume selective FSE CMR and histology had good agreement with both demonstrating the 3 asymptomatic subjects to have more predominantly fibrotic plaques while the symptomatic subjects had predominantly lipid on histology.

Conclusions: A combined protocol using CE-MRA with high-resolution 3D volume selective FSE CMR can establish stenosis severity, arterial remodelling and plaque constituents at carotid atherosclerotic disease. This can be used to provide additional information in the noninvasive risk stratification of patients under consideration for surgical or medical therapy of CVD as well their safe follow-up following appropriate intervention.

367. Feasibility of In Vivo, Multi-Contrast Weighted MR Imaging of Carotid Atherosclerosis for Multi-Center Studies

Baocheng Chu, MD, PhD,[1] Xue-Qiao Zhao, MD,[2] Tobias Saam, MD,[1] Vasily L. Yarynkh, PhD,[1] William S. Kerwin, PhD,[1] Kelly D. Flemming, MD,[3] John Huston, III, MD,[4] William Insull, Jr., MD,[5] Joel D. Morrisett, PhD,[5] Scott D. Rand, MD, PhD,[6] Kevin J. DeMarco, MD,[7] Nayak L. Polissar, PhD,[8] Jianming Cai, MD, PhD,[1] Annette Kampschulte, MD,[1] Thomas S. Hatsukami, MD,[9] Chun Yuan, PhD.[1] [1]*Radiology, University of Washington, Seattle, WA, USA,* [2]*Medicine, University of Washington, Seattle, WA, USA,* [3]*Neurology, Mayo Clinic, Rochester, MN, USA,* [4]*Radiology, Mayo Clinic, Rochester, MN, USA,* [5]*Medicine, Baylor College of Medicine, Houston, TX, USA,* [6]*Radiology, Medical College of Wisconsin, Milwaukee, WI, USA,* [7]*Radiology, Laurie Imaging Center, New Brunswick, NJ, USA,* [8]*The Mountain-Whisper-Light Statistical Consulting, Seattle, WA, USA,* [9]*Surgery, University of Washington, Seattle, WA, USA.*

Introduction and Purpose: Previous studies demonstrated that MRI is capable of characterizing the morphology and composition of human carotid atherosclerotic plaques. This study is to test whether carotid MRI can be performed at multiple centers with similar image quality (ImQ) and consistent inter-scan coverage.

Methods: Thirty-nine subjects from 5 clinical sites (site 1 = 11, site 2 = 16, site 3 = 2, site 4 = 3, site 5 = 7) were imaged on GE 1.5 T scanners using a standardized carotid imaging protocol with 5 weightings [T1, proton density (PD), T2, TOF, and contrast-enhanced (CE) T1]. MR technologists from the 5 sites received comprehensive protocol training. A maximum coverage of 24 mm (12 slices) was designed for each of 4 scans (baseline, 4, 8, 13 weeks). The adequacy of coverage was calculated as the percent of arteries with at least 6 slices matched across all four scans. ImQ was evaluated using a 5-point scale for each image. ImQ ≥ 3 was acceptable for image analysis (Figure 1).

Results: Across 5 sites, mean ImQ was 3.4–4.2 for T1 W; 3.6–4.4 for CE-T1 W; 3.4–4.2 for PDW; 3.3–4.2 for T2 W;

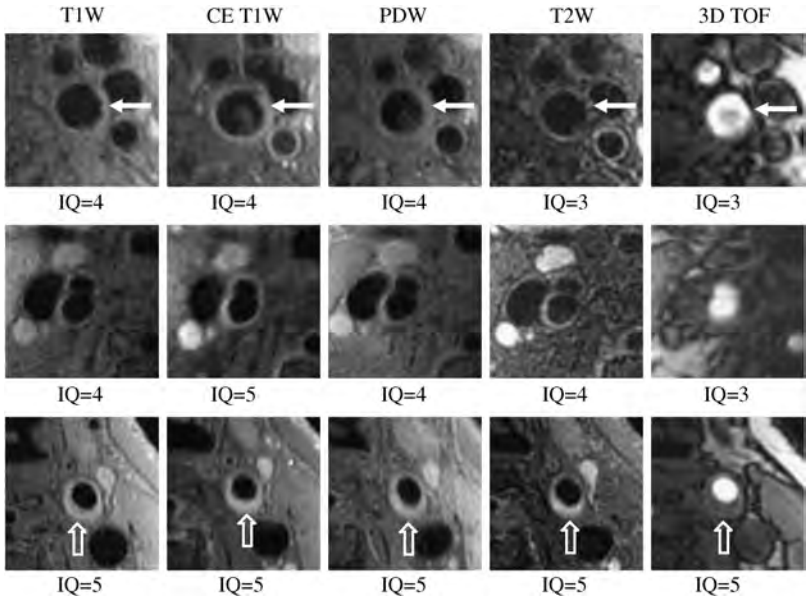

Figure 1. Overall mean ImQ was obtained by averaging 5 matched weigthings.

Table 1. Consistent coverage of carotid arteries across 4 MR scans among 5 sites

		Site 1	Site 2	Site 3	Site 4	Site 5
Index side	Number of arteries	11	16	2	3	7
	Mean coverage	9.1	8.7	8.5	8.0	8.3
	Adequacy of coverage*	100%	100%	100%	100%	100%
Non-index side	Number of arteries	10**	15**	2	2**	7
	Mean coverage	8.9	8.1	8.5	7.0	7.6
	Adequacy of coverage*	100%	93%	100%	50%	100%

*Adequacy of coverage at each site was calculated as the percent of arteries with at least six slices matched across all 4 MR scans.
**One carotid artery was not analyzed because carotid bifurcation of this study was not within the coverage.

and 3.4–4.0 for TOF. Overall mean ImQ was 3.5–4.2. All sites had at least six-slice coverage (mean 8.0–9.1) for all index carotid arteries (Table 1).

Conclusions: Using a standardized carotid imaging protocol, image quality and coverage was comparable among sites. Carotid MRI is technically feasible for use in multi-center studies.

368. Influence of Aortic Distensibility on the Functional Behavior of the Left Ventricle in Patients With Aortic Valve Regurgitation

Ana G. Almeida, MD, PhD, Eduardo I. Oliveira, MD, Pedro N. Marques, MD, Claudio David, MD, Arminda Veiga, MD, Monica M. Pedro, MD, Conceiçao A. Coutinho, MD, PhD, Joao C. Cunha, MD. *Cardiology, University Hospital Santa Maria, Lisbon, Portugal.*

Introduction: Magnetic resonance imaging (MRI) allows accurate estimation of aortic and cardiac dimensions and valvular function. Previous works have found that aortic distensibility (AD) is determinant on the pathophysiology of hypertension, coronary artery disease, aortic disease of Marfan, left ventricle failure.

Purpose: In this study we aimed to assess if, in patients with aortic aneurysm and aortic valve regurgitation (AR), AD had any influence on left ventricle (LV) dimensions and function, as assessed by MRI.

Methods: We studied 29 consecutive patients (aged 45 ± 11 years-old, range 32–64; 22 men) with ascending aortic aneurysm and severe AR (regurgitation fraction > 55%), known since 7 ± 4 years. Seven patients complained of fatigue and the remaining were asymptomatic. Exclusion criteria: non-sinusal rhythm, saccular aneurysm of ascending aorta, previous history of hypertension. All patients were submitted to MRI after 24 hours of suspension of medications, using sequences of high resolution cine-MRI for all measurements. The following calculations were obtained: 1) Maximal dimension of ascending aorta (mm); 2) AD of ascending aorta, calculated as: (Variation between end-systolic and end-diastolic area (cm2)/end-diastolic area (cm2))/pulse pressure (dynes cm^{-1}; 1 mmHg = 1,332 dynes cm^{-1}); 3. LV function: a) end-diastolic and end-systolic volumes (mL) and mass (grams), by Simpson's method; b) ejection fraction (%).

Results: AD varied from 0.05–2.4 dynes cm^{-1} (0.68 ± 0.50). There was no correlation between ascending aortic distensibility and age, as well as with the ascending aorta maximal diameter (47 ± 4 mm). There was no correlation between age, maximal ascending aorta diameter or known duration of AR and LV volumes, ejection fraction or mass. We found, however, a significant inverse correlation between aortic distensibility and LV end-diastolic volume ($r = -0.58$, $p = 0.002$), end-systolic volume ($r = -0.65$, $p = 0.001$) and LV mass ($r = -0.53$, $p = 0.002$).

Conclusions: In patients with ascending aortic aneurysm and AR, aortic distensibility, as assessed by MRI, may play role on the LV pathophysiology. This may have prognostic and therapeutic implications, namely on the timing for surgical intervention.

369. A Novel Method of Measuring Pulsatile Hemodynamics Using Invasive Pressure Measurements and MR Flow Data

Vivek muthurangu, David Atkinson, PhD, Marc Eric Miquel, PhD, Derek Hill, PhD, Reza Razavi, MD MRCPCH. *Imaging, Kings College London, London, UK.*

Introduction: Pulmonary hypertension is assessed by invasive measurement of pulmonary vascular resistance (PVR). We have set up a programme of MR guided diagnostic cardiac catheterisation, and demonstrated the advantages of simultaneous acquisition of invasive pressures and MR flow data for calculation of PVR. However, in the pulsatile cardiovascular system total arterial compliance also contributes to ventricular load; therefore assessment should be based on measurement of both PVR and compliance. Using MR flow data and invasive pressure measurements compliance can be calculated by parameter optimization of the 2 element Windkessel model. Thus MR guided cardiac catheterisation can be used to measure PVR and compliance, providing full assessment of pulsatile hemodynamics in these patients.

Purpose: To demonstrate the feasibility of using a combination of invasive pressure and MR flow measurements to calculate PVR and compliance.

Methods: 11 patients underwent cardiac catheterization, in an MR interventional suite (1 · 5 T Intera I/T MRI scanner, Philips, The Netherlands) with x-ray back-up (BV Pulsera

cardiac x-ray unit, Philips, Best, The Netherlands). Invasive pressure and MR flow was acquired at baseline (condition 1) and at 20 ppm nitric oxide (condition 2). Vascular resistance was the mean pulmonary artery pressure divided by the mean pulmonary artery flow. MR flow data and vascular resistance were inputted into a 2 element Windkessel model. Parameter optimization of the Windkessel model using systolic and diastolic pressure allowed calculation of compliance. PVR and compliance were calculated using this method at condition 1 and 2. A two-tailed t-test was used to compare the hemodynamic responses to NO. Correlation coefficients were used study the relationship between resistance and compliance. A p value of < 0.05 was taken as statistically significant. Statistical analysis was performed using Matlab (Mathworks, USA).

Results: MR guided cardiac catheterisation with simultaneous acquisition of MR flow data and invasive pressure data was performed on all patients. In response to 20 ppm of NO, there was a statistically significant fall in systolic pressure (53.8 ± 23.6 to 50.4 ± 24.1 mmHg, $p = 0.002$) and pulse pressure (33.1 ± 12.5 to 30.5 ± 12.8 mmHg, $p = 0.007$). This was associated with a significant fall in resistance (0.94 ± 0.61 to 0.87 ± 0.6 mmHg.mL^{-1}.s, $p = 0.01$) and a significant increase in total arterial compliance (0.56 ± 0.55 to 0.66 ± 0.62 mL/mmHg, $p = 0.02$). There was a moderate/good correlation between resistance and 1/compliance ($r = 0.75$, $p < 0.0001$, regression coefficients, m = 2.21 and c = 0.96 for all data sets; $r = 0.72$, $p < 0.0001$ at condition 1; $r = 0.77$, $p < 0.0001$ at condition 2). In 5/11 patients, resistance decreased by $\geq 10\%$ in response to NO. In 4/5 of these patients the fall in resistance was associated with a significant increase in compliance.

Conclusion: We have demonstrated the feasibility of quantifying both resistance total arterial compliance using simultaneously acquired invasive pressure measurements and MR flow data. In our facility cardiac catheterisation was accomplished by MR guidance with x-ray back up. Pulmonary artery catheterisation can be accomplished without imaging prior to MR scanning, thus in the future potentially allowing this technique to be used in a conventional cardiac MR scanner. Using this technique we have demonstrated a relationship between resistance and compliance. We have also demonstrated an increase in total arterial compliance in response to NO. In conclusion, we believe that measurement of both pulmonary artery compliance and resistance will give new insights into the pathophysiology of pulmonary hypertension and may be important in assessing suitability for long term medical therapy.

370. MRI Signs of Carotid Plaque Inflammation in Patients with Unstable Angina

Luigi Natale,[1] Agostino Meduri,[1] Antonella Lombardo,[2] Antonio Bernardini,[1] Alessandra Porcelli,[1] Carlo Liguori,[1] Lorenzo Bonomo.[1] [1]*Radiology, Catholic University of Sacred Heart, Rome, Italy,* [2]*Cardiology, Catholic University of Sacred Heart, Rome, Italy.*

Introduction: Inflammation may contribute to destabilize vulnerable plaques in acute coronary syndromes by promoting rupture and erosion. This premise led to the hypothesis that systemic inflammatory factors could be related with widespread plaque activity in many vascular districts and to the development of a variety of techniques for detection of vulnerable plaques.

Purpose: To evaluate with contrast enhanced-MRI (CE-MRI) plaque inflammation signs in carotid arteries of pts with unstable angina (UA) and to relate them to serum levels of C-reactive protein (CRP), used as a marker of systemic inflammation.

Methods: 27 pts with carotid plaques, 16 with UA (mean age: 64) and 11 with stable angina (mean age: 68) underwent carotid arteries MRI (1.5 T GE scanner), with SE, FSE and black blood FSE sequences, before and 10 to 15 minutes after Gadolinium-DTPA (Gd) iv. administration (0.2 mmol/Kg). We considered 3 markers: 1) wall thickening, index of arterial wall edema or infiltration; 2) increased T2 or FSE-STIR signal intensity (SI), index of arterial wall or plaque edema; 3) arterial wall or plaque enhancement, index of increased capillary permeability. Totally 37 plaques were evaluated (17 patients with monolateral and 10 with bilateral stenosis). CRP levels were determined with the ELISA essay.

Results: 19 plaques showed wall thickening and/or increased T2 and/or FSE-STIR SI and Gd enhancement, 5 plaques showed only contrast enhancement, whereas 13 plaques had no inflammation signs. CRP levels of patients with enhanced plaques were significantly higher than those of patients without enhancement (median values: 12.5 vs 3.3, $p < 0.05$).

Conclusions: Pts with UA showed plaque inflammation signs more frequently than controls; patients with UA and inflammation signs showed higher CRP levels than pts with UA and no inflammation signs. Our results suggest a

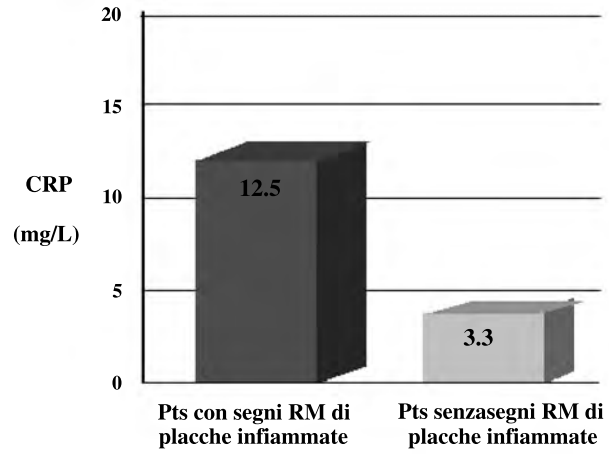

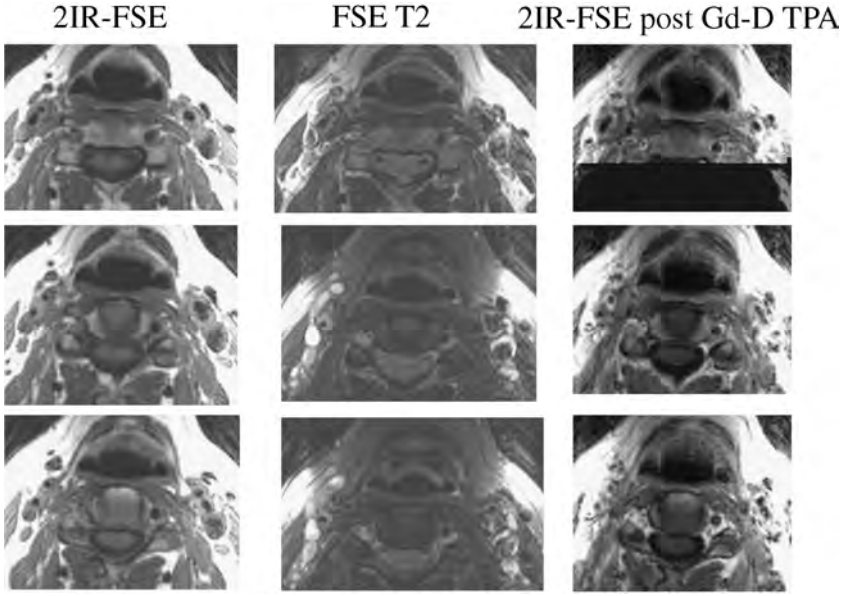

widespread plaque activity, possibly mediated by systemic inflammation, in acute coronary syndromes.

371. Carotid Plaque MRI Pattern is Independent from Degree of Stenosis

Ralf Wassmuth, MD, Steffen Bohl, MD, Heike Olthoff, MD, Matthias G. Friedrich, MD, Rainer Dietz, MD, Jeanette Schulz-Menger, MD. *Franz-Volhard-Clinic, CharitÃ© University Medicine Berlin, Berlin, Germany.*

Introduction: Beside the degree of stenosis plaque composition determines the risk of plaque rupture. In experimental settings magnetic resonance imaging (MRI) visualized carotid plaque components with high spatial resolution.

Purpose: We evaluated plaque composition with in-vivo MRI in relation to ultrasound-derived degree of luminal stenosis.

Methods: We scanned 53 patients (48–89 years) with carotid stenosis as defined by ultrasound in a 1.5 T MRI scanner with a bilateral phased array coil. Mean degree of stenosis based on ultrasound velocity measurements was 79 ± 12%. We acquired axial 3 mm slices starting in the common carotid artery just below the bifurcation with an in-plane resolution of 0.3 mm/pixel. Cardiac gated double inversion fast spin echo images were obtained in proton-density-, T1- and T2-weighting. Scan parameters were TR = 2 RR for PDW and T2, TR = 1 RR for T1; matrix size 256 × 256, FOV 130 mm, bandwidth 20 kHz, number of acquisitions = 2. Two independent readers evaluated plaque signal and composition. Heterogeneity was defined as presence of a hypointense core in T2 or a hyperintense focus in all contrast weightings. The relation of heterogeneity and degree of stenosis was analyzed with a Mann–Whitney U test.

Results: Image quality was sufficient for evaluation in 46 patients (87%). In MRI 22 plaques (48%) appeared homogeneous whereas 24 appeared heterogeneous (52%). Homogeneous and heterogeneous plaques did not differ in degree of stenosis (81 ± 13% vs. 79 ± 9%, $p = 0.3$). Among the homogeneous plaques 17 were predominantly isointense in PDW and T1 (77%), 11 were isointense in all contrast weightings (50%) suggesting fibrous tissue.

Conclusion: In a large group of patients with stenotic carotid atheroma, only 52% displayed complex plaque morphology on MRI implicating increased risk of plaque rupture. Plaque heterogeneity did not relate to degree of luminal stenosis.

372. The Differential Effects of Bosentan and Sildenafil on Pulmonary Arterial Pulsatility in Severe Pulmonary Arterial Hypertension

Julian W. Strange,[1] Mark A. Westwood,[1] Gideon Paul,[2] Martin R. Wilkins,[2] J Simon R. Gibbs,[3] Raad H. Mohiaddin.[1] [1]*CMR Unit, Royal Brompton Hospital, London, UK,* [2]*Experimental Medicine, Imperial College, London, UK,* [3]*Cardiology, Imperial College, London, UK.*

Introduction: Pulmonary arterial hypertension (PAH) is associated with raised pulmonary arterial (PA) resistance and reduced compliance. This results in right ventricular dilatation and hypertrophy leading to ultimate failure and death. While effective therapies for idiopathic PAH have been previously shown to reduce PA resistance, their effect on the PA wall has only been shown in a single acute

study where PA pulsatility was measured using intravascular ultrasound (IVUS) during an infusion of epoprostenol (prostacyclin). Pulsatility is assessed by calculating the change in luminal cross sectional area from systole (LAs) to diastole (LAd) and is expressed as a percentage (Pulsatility = LAs-LAd/LAs × 100). Whereas the invasive nature of IVUS limits its use in serial studies, CMR can safely assess the cross sectional area of both the pulmonary trunk and aorta throughout the cardiac cycle and hence pulsatility determined.

Purpose: To compare the effect of two new oral agents for PAH, Sildenafil and Bosentan, on the pulmonary vasculature using a CMR based assessment of pulmonary pulsatility.

Methods: In a randomised double blind trial, 25 Patients with idiopathic PAH (WHO functional class III) were treated with oral Sildenafil (50 mg tds) or Bosentan (125 mg bd) for 16 weeks. A 6 minute walk test and a CMR scan (Siemens Sonata 1.5 T) were performed at baseline and at 16 weeks of therapy. Left ventricular (LV) and right ventricular (RV) volumes and function were assessed using the previously validated method of contiguous short axis slices. Pulmonary trunk and aortic root pulsatility were also assessed using True FISP prospectively gated cines. Pulsatility was determined by measuring the cross sectional area of the pulmonary or aortic trunk in both systole and diastole and determining the percentage change between the two.

Results: There was a significant change from baseline in pulsatility of both the aortic root (mean change 3.20% 95% CI 0.51% to 5.90%, mean $p < 0.03$) and the pulmonary trunk (mean change 2.21%, 95% CI 0.02% to 4.41%, $p < 0.05$) for all therapies. This was associated with a significant increase in cardiac output (mean change 0.46 l/min, 95% CI 0.24 l/min to 0.69 l/min, $p < 0.0002$). There was also a significant difference in the change in pulmonary trunk pulsatility (mean difference 4.66%, 95% CI 0.59% to 8.73% $p < 0.03$) but not the change in aortic root pulsatility (mean difference 0.60%, 95% CI − 4.92% to 6.13%, $p = 0.82$) at 16 weeks in the Sildenafil group compared to the Bosentan group. There was associated with greater exercise capacity as assessed by 6 minute walk test (mean difference 55 m, 95% CI 2 m to 108 m, $p < 0.05$) at 16 weeks in the Sildenafil group compared to the Bosentan treated population. A significant reduction in RV mass compared to baseline only occurred in the Sildenafil treated patients (mean reduction 8.8 g, 95% CI 2 g to 16 g, $p < 0.05$). There was no significant difference in change in cardiac output between the therapies.

Conclusions: Pulmonary and aortic pulsatility increases in association with increased cardiac output. We have also demonstrated that Sildenafil has an additional effect on pulmonary trunk pulsatility which cannot solely be attributed to increased cardiac output. This was associated with a significant reduction in RV mass and might have import implications for improving right ventricular function and could be a marker of clinical haemodynamic improvement.

373. Comparing MRI and Echocardiographic Assessment of Right Ventricular Function: The True "Gold" Standard

Michael D. Puchalski, Shala M. Smith, RDS, Lloyd Y. Tani, MD. *Pediatric Cardiology, University of Utah, Salt Lake City, UT, USA.*

Background: The assessment of right ventricular (RV) size and function is important in the management of many patients (pts) with heart disease. Although many consider MRI the gold standard for the assessment of the RV, echo is the modality most often used. To date, there have been no studies comparing subjective assessment of RV size and function by echo with quantitative MRI assessment.

Methods: Pts with right-sided congenital heart disease who underwent echo within 6 months of the MRI formed the study group. Four experienced echocardiographers blinded to the MRI results independently reviewed the echoes for RV dilatation and function (graded as normal, mild, moderate, or severe). The associations of subjective echo estimates of RV size and function with volumes and EFs calculated from MRI were assessed using Spearmans rank correlation coefficients. Moderate RV dilation was defined as 3 SD and moderately decreased EF 40% by MRI. Sensitivity and specificity for moderate disease were calculated. Interobserver variability was also reviewed.

Results: The study group consisted of 22 pts aged 16.6 7.1 years, with interval between MRI and echo of 49 54 days. Correlation coefficients between subjective assessment of RV size and MRI indexed volume were similar for the 4 echocardiographers, ranging from 0.62 to 0.74 ($p < 0.05$). The best reviewer had a specificity of 100% but described only 9/15 pts with moderate dilation (sensitivity 60%). Correlation coefficients between subjective assessment of RV function and MRI RVEF were more variable, ranging from − 0.24 to 0.63, with only one reviewers assessment significantly correlated with MRI. This reviewer had 100% specificity but described only 1/7 pts with moderately decreased function (sensitivity 14%). Subjective assessment of RV size and function differed between observers by at least 2 grades in 7/22 cases.

Conclusion: Subjective assessment of a dilated RV with decreased function by echo in pts with right heart disease is poor compared to the measured end-diastolic volume and EF by MRI. In addition, there is a significant variation between observers reviewing individual pts.

374. Towards Safer Cardiac Intervention: A Novel Approach that Combines X-Ray and Magnetic Resonance Imaging for Guidance of Aortic Stent Implantation

Sanjeet Hegde, MBBS, MRCPCH,[1] Marc Miquel, PhD,[2] Kawal Rhode, PhD,[2] Vivek Muthurangu, MBBS, MRCPCH,[1] Derek Hill, PhD,[2] Shakeel Qureshi, MBBS, MRCP,[3] Reza Razavi, MBBS, MRCP, MD.[1] [1]*Imaging Sciences/Pediatric*

Cardiology, King's College London, London, UK, [2]Imaging Sciences, King's College London, London, UK, [3]Pediatric Cardiology, Guy's Hospital, London, UK.

Introduction and Hypothesis: X-ray and MR interventional suites (XMR) are facilities that incorporate both MR and x-ray imaging and using a registration technique it is possible to integrate the superior structural information of MR images with conventional x-ray images allowing for safer cardiac catheter intervention.

Methods:

Phantom experiments: In order to optimise stent imaging we used a 'vascular coarctation' phantom (cellulose dialysis tubing & rubber tubing) with inflow tube from a pulsatile blood pump (model 1423, Harvard Apparatus, MA, USA) and an outflow tube connected to a five litre reservoir of water doped with manganese chloride (20 mg/L) to simulate the relaxation properties of blood (T1 $\sim$ 1000 ms, T2 $\sim$ 120 ms). Stroke volumes of 60 mls and a heart rate of 70 beats/min were used. We successfully deployed under MR guidance a 16 mm CP (Chetham Platinium, NuMed, Inc, Hopkinton, USA) stent into the region of narrowing in the tubing. We acquired multi slice 'black blood' turbo spin echo (TR 833 ms, TE 80 ms, slice thickness 6 mm) images and through plane phase contrast (TR 6.9 ms, TE 3.8 ms, flip angle 15, slice thickness 7 mm) images of the stent.

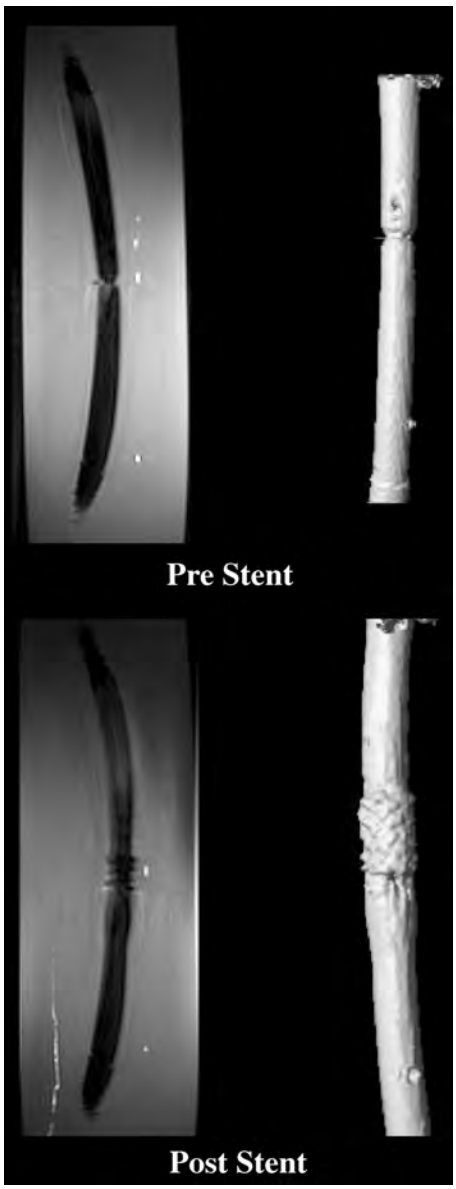

Figure 1.

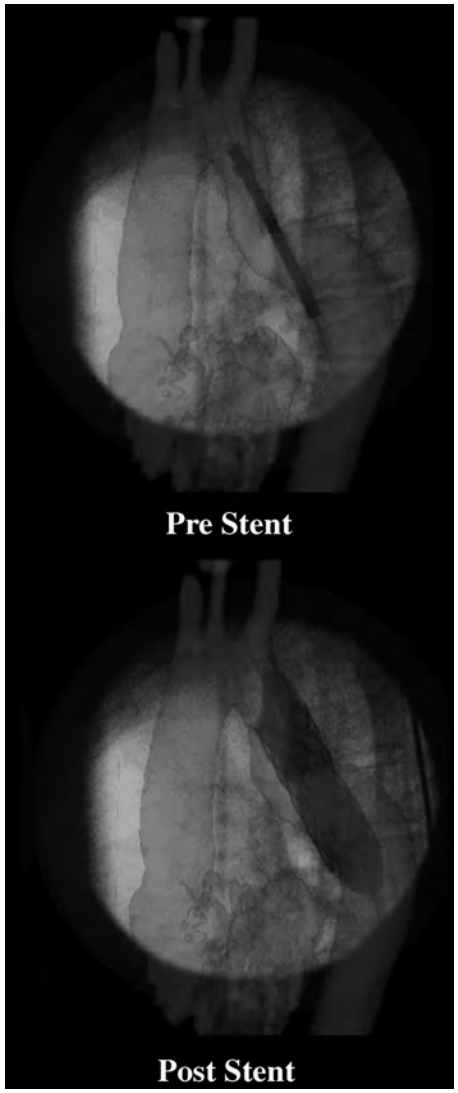

Figure 2.

Patient study: This is a prospective study looking at stent implantation in a series of patients with coarctation using XMR guidance. In the first patient three-dimensional magnetic resonance angiography (MRA) images of the aorta were obtained to produce a volume rendering.

Following MR acquisition the patient was moved to the x-ray end of the suite where optical tracking was used to determine the transformation matrices relating MR and x-ray image coordinates thus allowing real-time fusion. Registration errors were previously shown to be clinically acceptable. Stent implantation was performed using the XMR technique at the x-ray end of the suite under general anaesthesia. MR phase contrast flow and invasive pressure measurements were also performed pre and post stent implantation providing valuable physiological information.

Results: We were able to identify the region of narrowing in the tubing and also volume render the stent after deployment, from the multi slice turbo spin echo images (Fig. 1). By optimising the imaging sequences it was possible to minimise susceptibility and radiofrequency artefacts. Using the XMR technique the interventionalist was able to guide the catheter in the patient and found the MR images very useful for accurate deployment of the stent and for selecting optimal radiographic views without administration of any additional x-ray dose (Fig. 2). The pressure gradient (post isoprenaline) across the coarctation reduced from 52 mm Hg to 16 mm Hg following stent implantation.

Conclusion: We have demonstrated that our technique can be successfully used to guide cardiac interventions. The excellent three-dimensional structural information of MR images, superimposed on the x-ray images, can be made available to the interventionalist in real time. This bridges the gap between the two modalities and offers an exciting new way to guide cardiac interventions. Further work is being carried out to optimise imaging sequences, improve image registration and possibly reduce the x-ray dose for such a procedure.

375. Evaluation of Aortic Compliance in Adolescents After Coarctation Repair Using Magnetic Resonance Imaging: Functional Aortic Wall Properties Correlate Better to Hypertension than the Percentage of Aortic Restenosis

Joachim G. Eichhorn, MD,[1] Christian Fink, MD,[2] Ivan Zuna, PhD,[2] Raoul Arnold, MD,[1] Herbert E. Ulmer, MD,[1] Hans-Ulrich Kauczor, MD.[2] [1]*Pediatric Cardiology, University Children's Hospital, Heidelberg, Germany,* [2]*Radiology, Deutsches Krebsforschungszentrum, Heidelberg, Germany.*

Introduction: While often considered to be cured, patients with repaired coarctation of the aorta (CoA) frequently have premature morbidity and even mortality. "Repair" may not be synonymous with "cure" of a cardiovascular abnormality. The pathophysiology of hypertension after CoA repair is not fully understood. Restenosis or residual stenosis accounts for only a minority of cases of postoperative hypertension. Hypertension may be associated with anatomical and functional changes in the arterial vasculature. It was hypothesised that intrinsic abnormalities of the aortic wall may impair aortic wall properties (e.g. elasticity). This idea suggests that the defect may not be limited to the small area of CoA but may be a widespread vascular anomaly. The elasticity is usually quantified by compliance measurements. Therefore, the relative temporal change in the vessel cross-sectional area throughout the cardiac cycle has to be determined. The possibility of non-invasive monitoring of changes in compliance could be an important application for the follow-up of patients after CoA repair.

Purpose: In this work we determined the compliance using a magnetic resonance (MR) method in patients with clinically suspected relevant restenosis after CoA repair.

Methods: 32 patients (mean, median age [range]: 15, 16 [9–25] years) were examined on a clinical 1.5 T whole-body MR scanner (Magnetom Vision/Symphony, Siemens, Erlangen, Germany) using a standard body phased-array coil. In addition to a contrast-enhanced 3D-MR angiography (FLASH 3D, TE/TR = 1.8/4.6 ms, matrix: 215 × 512, slice = 1.25 mm, $\alpha = 50°$, 0.2 mmol/kg Gd-DTPA) the MR protocol included 2D CINE MR measurements for the assessment of aortic compliance (FLASH; TE/TR = 4/18 ms, matrix: 192 × 256; slice = 6 mm, $\alpha = 40°$). All measurements were positioned perpendicular to the descending aorta at the level of the diaphragm. The data analysis included the calculation of the compliance C [10^{-5} Pa^{-1}] which is defined by the relative change in the vessel cross-sectional area ΔA divided by the difference between systolic and diastolic blood pressure Δp.

Results: A significant restenosis (>40% of aortic diameter at diaphragm level) was found in 18/32 patients, only half of them ($n = 9$) showed systemic hypertension (>97. percentile of age correlated normative value). In the group ($n = 14$) without significant restenosis 10 patients (71%) showed high systemic blood pressure. There was no correlation of the percentage of stenosis (34 ± 23%; range 0–80%) to the presence of hypertension (e.g. a patient with 80%-restenosis showed normotension) or to the compliance (C = 5.38 ± 1.71). But the aortic compliance was significantly reduced (Duncan's multiple range test: $\alpha < 0.05$) in the patients with hypertension ($n = 19$; C = 3.82 ± 1.30) in

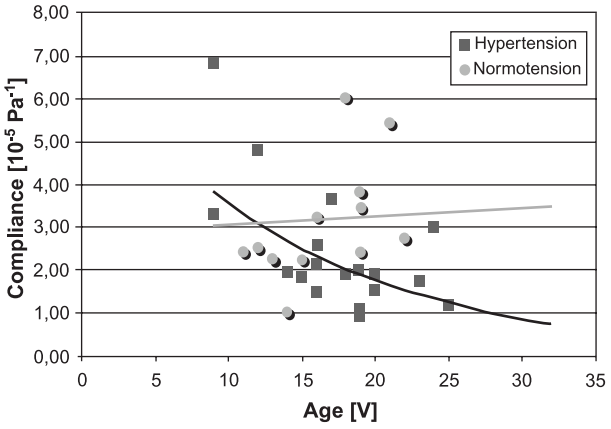

relation to the patients without hypertension (n = 13; C = 5.89 ± 3,17). 3 of 9 patients with hypertension and restenosis showed a normal compliance (3.–97. percentile of age correlated normative value).

Conclusions: Inconspicuous morphology may not exclude residual hypertension. Vascular morphology is only one possible reason for hemodynamic changes. The results of signifant decreased aortic compliance in the group of hypertension (the influence of higher Δp has to be considered carefully) might confirm the hypothesis of intrinsic abnormalities of aortic wall properties as an important cause of systemic hypertension. The findings may potentionally contribute to the decision for surgical or interventional approach in patients with restenosis and hypertension: MR compliance measurements might help to identify patients with restenosis but without fixed intrinsic abnormalities of the aortic wall and which therefore would have the biggest benefit of surgical or interventional therapy such as normalisation of their systemic blood pressure. For that purpose further studies examining the potential value of compliance measurements for the follow-up and to guide therapy indications are warranted.

376. MRI Guided Dilatation of Aortic Coarctation and Stent Placement: Feasibility and Comparison to X-Ray Guided Catheter Techniques

Carsten Rickers, MD,[1] Michael Jerosch-Herold, PhD,[2] Xudong Hu, MD,[3] Naveen Murthy, MD,[3] Myra Urness, BsC,[3] Jochen Weil, MD,[1] Norbert Wilke, MD.[4] [1]*Pediatric Cardiology, University Hospital Eppendorf, Hamburg, Germany,* [2]*Cardiology, University of Oregon, Portland, OR, USA,* [3]*Radiology, University of Minnesota, Minneapolis, MN, USA,* [4]*Radiology, University of Florida, Jacksonville, FL, USA.*

Purpose: The aim of the study was to assess the feasibility of MRI guided dilatation of artificially created coarctation of the aorta (CoA) and stent placement using intravascular miniature antenna guidewires in a porcine model. The results where directly compared to conventional x-ray guided catheter interventions.

Methods: In 12 healthy farm pigs (19 to 55 kg), a coarctation of the aorta was created by operative banding of the aorta at the site of the ductus arteriosus (60 to 90% stenosis). After 2–8 weeks all animals underwent an MRI study and conventional x-ray guided catheterization for a complete hemodynamic and anatomical evaluation of the CoA. The pigs were randomized for x-ray or MR-guided balloon dilatation. Anatomical and hemodynamic MR imaging was performed and compared to x-ray. For improved catheter tracking and high resolution intravascular imaging, MRI guidewires (Surgi-Vision) were used. Various stent designs in conjunction with or without loopless antenna wires were tested. Real-time MRI was performed with a steady-state free precession pulse sequence ("true FISP"; TR = 1.4 ms, TE = 1.15 ms, flip angle = 40°, 50–60 phase-encodings, 128 by 128 image matrix, 7–15 frames/sec, 1400 Hz/pixel, 35 mm slice thickness). All studies were performed in a dedicated cardiac MR-scanner. The severity of the stenosis was assessed with true fisp cine and velocity encoded MRI. With the real-time pulse sequence running under interactive user-control a customized delivery sheath (AGA medical) was tracked towards the stenosis. A self-exspanding stent was delivered and a balloon dilatation was performed. Following the procedure both MR and x-ray measurements were compared to intraoperative measurements and pathology.

Results: We confirmed the feasibility of using real-time MRI to follow the position of an antenna guiding catheter within the aorta and its branches. Successful deployment of the stent and balloon dilatation of the CoA could be monitored in all cases. For improved visualisation nitinol stents in conjunction with a loopless antenna were superior to other stent designs. The correlation of high resolution intravascular MR measurements of the diameters of the stenosis to intraoperative measurements was (MRI: $y = 1.01 \times - 0.24$, $r = 0.96$) and (X-ray: $y = 0.90 \times + 0.24$, $r = 0.62$) for x-ray measurements. There was no significant difference in gradient measurements (MRI: 52 ± 23 vs x-ray: 51 ± 18 mm Hg; $p = 0.13$). Procedure time was significantly shorter using x-ray (23 ± 12 vs. 35±28 minutes; $p<0.05$) due to a learning curve with MRI.

Conclusions: These data demonstrate that real time MR-guided balloon-dilatation and stent placement is feasible in aortic coarctation. Compared to x-ray MRI has advantages with respect to radiation exposure and sizing of the stenosis imaging but at the cost of longer procedure times. A nitinol stent design in conjunction with a loopless antenna enhances MRI visualisation.

377. Aortic Coarctation Stent Repair Performed with Real-Time MRI guidance is Safe and Feasible in a Swine Model

Amish N. Raval, MD,[1] James D. Telep, MD,[1] Michael A. Guttman, MSc,[2] Cengizhan Ozturk, PhD,[1] Michael Jones, MD,[1] Richard B. Thompson, PhD,[2] Ranil DeSilva, MD, PhD,[1] Ronnier J. Aviles, MD,[1] Venkatesh K. Raman, MD,[1] Elliot R. McVeigh, PhD,[2] Michael C. Slack, MD,[1] Robert J. Lederman, MD.[1] [1]*Cardiovascular Branch, National Heart Lung and Blood Institute/National Institutes of Health, Bethesda, MD, USA,* [2]*Laboratory of Cardiac Energetics, National Heart Lung and Blood Institute/National Institutes of Health, Bethesda, MD, USA.*

Introduction: Real-time MR imaging (rtMRI) can now guide transcatheter treatment of cardiovascular disease in large animal models. Compared with X-ray, rtMRI offers superior tissue imaging in any arbitrary plane without ionizing radiation. Human therapeutic procedures guided by rtMRI

have been limited by the unavailability of clinical-grade catheter devices.

Purpose: To demonstrate preclinical safety and feasibility study of rtMRI guided stenting in a porcine surgical model of aortic coarctation entirely using commercially available catheter devices.

Methods: Surgical aortic coarctation was created in 9 healthy swine (23–38 kg). Percutaneous coarctation stenting was performed 4–6 weeeks later using commercially available catheter devices in a combined X-ray/MRI (XMR) laboratory. Commercially available active (Intercept guidewire, Surgi-Vision), and passive (BIB balloon and Cheatham Z-stent, NuMed) were used for the procedure. 5 mM Gd-DPTA was used to enhance balloon inflation visualization. Real-time SSFP (TruFISP) imaging was displayed in-room with multi-slice, and 3D rendering capability using a custom-designed low latency, interface on an external workstation. Pre and post stent deployment double inversion recovery FSE/SSFP/contrast enhanced MRA and subsequent xray angiography with digital subtraction was performed. Pre and post catheter derrived pressure hemodynamics and phase contrast MRI was performed for gradient assessment across the stenosis.

Results: MRI permitted procedure planning, device navigation, tracking, deployment, hemodynamic measurements, and assessment of stent apposition. Following sheath insertion, and baseline xray angiography smooth transfer between imaging systems with uninterrupted hemodynamic monitoring was performed. Stent delivery balloons (mean caliber 13.6 ± 0.9 mm) became visible when ''dumbbells'' were created around the stent. ''Active'' antenna coil guidewires substantially shortened procedure time compared with ''passive'' nitinol guidewires by improving device visualization. was performed to assess for stent apposition and complications. Baseline rest peak-to-peak catheter/after isoproteronol stress/peak instantaneous PCMRI gradient was 16.6 ± 7.7/33.8 ± 18.1/24.4 ± 6.7 mmHg respectively. After stenting the rest peak-to-peak/peak instantaneous PCMRI gradient was reduced to 3.6 ± 2.7/7.8 ± 6.5 mmHg (both $p < 0.01$ compared with baseline, respectively). Follow-up catheterization and necropsy showed durable gradient reduction and appropriate neointima formation.

Conclusions: We have demonstrated the preclinical safety and feasibility of stent delivery for aortic coarctation entirely using rtMRI and commercially-available catheter devices.

378. Abnormalities of the Great Vessels in Bicuspid Aortic Valve Disease: Insights from Cardiovascular Magnetic Resonance

Anita R. Bhandiwad, MD,[1] Connie W. Tsao, MD,[2] Peter G. Danias, MD, PhD,[2] Warren J. Manning, MD,[2] Candice K. Silversides, MD, MPH.[2] [1]*Cardiology, Emory Crawford Long Hospital, Atlanta, GA, USA,* [2]*Cardiology, Beth Israel Deaconess Medical Center, Harvard Medical School, Boston, MA, USA.*

Background: Abnormalities in the walls of the great vessels are common in patients with a bicuspid aortic valve (BAV). Using cardiovascular magnetic resonance (CMR), we sought to explore differences in great vessel anatomy and compliance among subjects with BAV and trileaflet aortic valves (TAV).

Methods: A case control study design was used with thirty-two subjects [16 subjects with BAV and 16 age-and gender-matched subjects with TAV]. The ascending aorta diameter, descending thoracic aorta diameter and main pulmonary artery diameter were measured on T1-weighted black-blood fast spin-echo CMR images acquired on a 1.5 T Philips CMR scanner and normalized for body surface area. Blood pressure was noninvasively monitored and compliance of the ascending and descending thoracic aorta was calculated in a subset of 18 subjects [Compliance = π[Systolic aortic diameter^2 − Diastolic aortic diameter^2]/{4[Systolic blood pressure − Diastolic blood pressure]}.] Comparisons between groups were performed using the Wilcoxon signed ranks test.

Results: The study included 30 males and 2 females (mean age 44 ± 13 years). Subjects with BAV had a larger ascending aorta diameter (19.4 ± 3.0 vs. 16.7 ± 2.5 mm/m^2, $p = 0.01$), but there was no difference in descending aorta

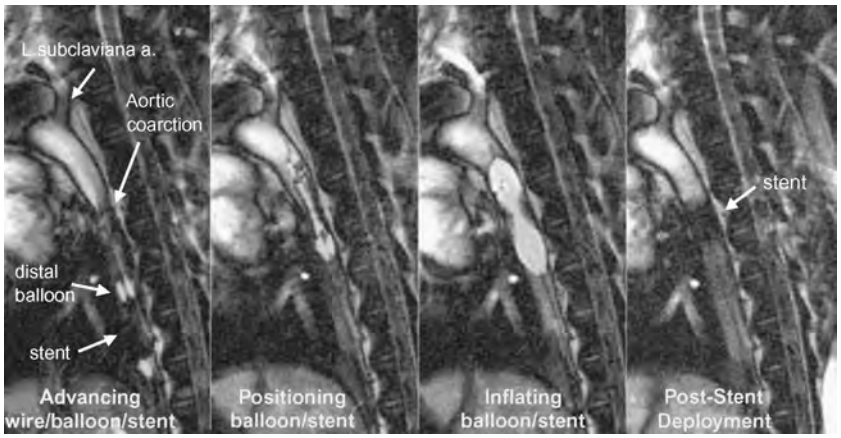

diameter ($p = 0.9$) or main pulmonary artery diameter ($p = 0.16$) compared to TAV subjects. In BAV subjects, ascending aorta diameter and main pulmonary artery diameter were linearly related ($r = 0.7$, $p < 0.01$), while no significant correlation was present in TAV subjects ($r = 0.5$, $p = 0.06$). Compliance in the descending thoracic aorta was decreased in BAV subjects compared to TAV subjects (0.0017 ± 0.0008 vs. 0.0026 ± 0.0011 mm^2/kPa/mm, $p = 0.05$). For both BAV and TAV subjects, the compliance of the descending aorta was not significantly related to age, ascending aorta diameter or descending aorta diameter. There was no difference in ascending aortic compliance ($p = 0.8$).

Conclusion: The ascending aorta is dilated in BAV subjects; however, in this series other major vessels do not seem to develop pathologic dilation. BAV is associated with decreased compliance of the descending thoracic aorta, the etiology of which merits further study.

379. The Role of Contrast Enhanced MR Angiography in Infants with Complex Congenital Heart Disease in the First Months of Life

Richard E. Slaughter, MBBS FRACR,[1] Wendy E. Strugnell, BSc,[1] Robyn A. Riley, DipAppSc,[1] Christopher Moysey Whight, MBBS FRACP,[2] Lora Medoro, MBBS.[1] [1]*Cardiovascular MRI Research Centre, Prince Charles Hospital, Brisbane, Australia,* [2]*Department of Cardiology, Prince Charles Hospital, Brisbane, Australia.*

Introduction: Echocardiography is a powerful tool in the assessment of infants with complex congenital heart disease in the first months of life. Echocardiography is well suited to the evaluation of the infant heart but has limitations in the assessment of structures outside the cardiac mass. A percentage of young infants therefore proceed to catheter angiography to evaluate complex anatomy involving the aortic arch, pulmonary arteries and veins and aorto-pulmonary collaterals. The primary requirement for management of the young infant is accurate anatomical information as intracardiac pressures and pulmonary resistance is either obtainable by Doppler ultrasound or is not relevant. Furthermore, cardiac catheterisation involves a radiation burden and a significant risk of morbidity. MRI has the potential to provide the important anatomical information required to manage these patients and to allow delay or avoidance of catheter angiography.

Purpose: To evaluate the role of contrast enhanced MRA in infants (0–4 months of age) with complex congenital heart disease in whom echocardiography was inconclusive, and to determine if catheter angiography could be avoided.

Method: We reviewed 18 studies on 12 patients (6 preoperative, 6 postoperative) referred for MRI. Of the 6 postoperative patients, 3 had serial examinations for progressive complications. MR imaging was performed on a 1.5 Tesla Signa Twinspeed system with either a 4-element cardiac phased array coil or 8-element head coil depending on patient size. All patients were examined under general anaesthesia. MRA was performed using a 3D TOF FSPGR acquisition following a Gd-DTPA injection of 0.2 mmol/kg into a peripheral vein. Using real-time imaging (Fluoro-trigger) the imaging acquisition was commenced immediately on visualisation of contrast in the cardiac chambers. A second image acquisition was obtained immediately following the first to demonstrate the whole of the vascular anatomy. Respiration was suspended at end-expiration with total time of breath-hold approximately 40 s (10 s for real-time, 10–15 s per image acquisition). Total examination time was 5 to 10 minutes.

Results: All studies provided excellent anatomical detail, defining complexities of the aortic arch, pulmonary arteries, pulmonary veins and aorto-pulmonary collaterals. This was particularly valuable in the demonstration of progressive post operative changes in pulmonary and systemic venous anatomy. Information obtained with MRA was sufficient to avert the need for subsequent or repeated catheterisation in overall patient management.

Conclusion: MRA in infants with complex congenital heart disease in the first months of life may provide important information to assist with the management of these patients. When echocardiography provides incomplete or equivocal information, the use of MRA may allow catheter angiography to be avoided. This is an important consideration for this difficult patient group where serial assessment post-operatively with catherisation is otherwise required.

380. Bright Blood Cine Magnetic Resonance Imaging Evaluates Aortic and Mitral Valve Morphology in Pediatric Congenital Heart Disease

Susan Ghods, MD,[1] Matthew A. Harris, MD,[2] Paul M. Weinberg, MD,[2] Mark A. Fogel, MD.[2] [1]*Pediatric Radiology, Children's Hospital of Philadelphia, Philadelphia, PA, USA,* [2]*Pediatric Cardiology, Children's Hospital of Philadelphia, Philadelphia, PA, USA.*

Introduction: Echocardiography is the most widely used imaging technique to diagnose valvular morphology in children. The purpose of this study is to determine the diagnostic value of cine magnetic resonance (MR) imaging in the evaluation of aortic and mitral valve architecture in pediatric congenital heart disease.

Methods: Cine-MR data were reviewed retrospectively in 47 patients with congenital heart disease (mean age 9 yrs, range 3 months-19 yrs). Cine imaging of the aortic valve using FLASH ($n = 27$) or True-FISP ($n = 12$) sequences, and cine imaging of the mitral valve using FLASH ($n = 10$) were used to determine valve architecture.

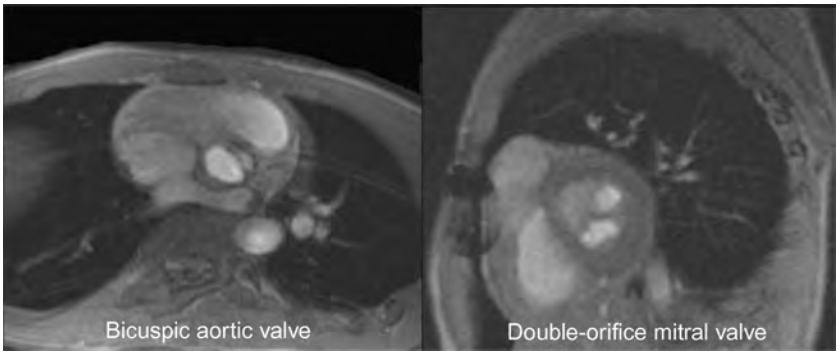

Results: Aortic valve leaflets and commisures were visualized in all 39 subjects. Normal trileaflet (n = 20), bicuspid (n = 16) and unicuspid (n = 1) aortic valves were identified. Leaflet fusion was observed involving the right and left cusps in 14 bicuspid valves and right and non-coronary cusps in 2. Two patients with truncus arteriosus had quadracuspid truncal valves. Aortic valve architecture was better visualized with FLASH, with a high flip angle to accentuate the contrast of inflowing blood, than with True-FISP. Normal mitral valve orifice architecture was identified in 9 patients and a double orifice valve with nearly equal sized orifices in 1. All bicuspid and unicuspid aortic valves, as well as double orifice mitral valve were confirmed by echocardiography.

Conclusions: Bright blood cine MR is a useful modality for evaluating aortic and mitral valve morphology in children with congenital heart disease.

381. Interstudy Reproducibility of Right and Left Ventricular Volume and Mass Measurements by Cardiovascular Magnetic Resonance in Repaired Tetralogy of Fallot Patients

Sonya V. Babu-Narayan,[1] Beatriz Bouzas,[1] Craig S. Broberg,[2] Philip J. Kilner.[1] [1]*Cardiovascular Magnetic Resonance Unit, Royal Brompton Hospital, London, UK,* [2]*Adult Congenital Heart Unit, Royal Brompton Hospital, London, UK.*

Introduction: Reproducibility of cardiovascular magnetic resonance (CMR) has been published in the normal heart and in both heart failure and hypertrophic cardiomyopathy for both the left and right ventricle. We sought to determine both intra-observer and inter-observer reproducibility of ventricular volumes and mass measurements in the growing population of repaired tetralogy of Fallot patients, in whom, ventricular morphology is more intricate and both right and left ventricular function has prognostic importance.

Methods: 20 acquisitions were made in 10 adult repaired tetralogy of Fallot patients (6 male, 4 female) who underwent two separate CMR scans on the same day. SSFP cines were acquired in planes including vertical long axis, basal short axis scout, four chamber, and short axis stack. The basal slice was aligned to contain myocardium in the end diastolic frame in both VLA and four chamber view. Cines were then acquired at 10 mm intervals (7 mm slice thickness, 3 mm gap) until the apex was covered (usually 10–12 cines).

Analysis and Measurement: Biventricular volume, mass and function was quantified on all 20 scan acquisitions by two independent experienced observers blind to one another and any previous analysis of the same patient. Manual contours for right ventricular (RV) and left ventricular (LV) epicardium and endocardium were drawn in end diastole and endocardial planimetry in end systole. Simpson's rule was then used to derive volumes and mass. Systolic volume was subtracted from diastolic volume to obtain ejection fraction. Trabeculations were included in the ventricular mass.

Results: Coefficient of Variability (%) for intraobserver 1/intraobserver 2 and interobserver is expressed in the table.

	Right ventricle			Left ventricle		
	IntraScan		Interobserver	IntraScan		Interobserver
CoV (%) Variable	Observer1	Observer2	Obs1 vs. Obs2	Observer1	Observer2	Obs1 vs. Obs2
EDV	4.91	2.89	5.65	4.80	4.73	7.86
ESV	3.69	4.15	6.82	6.27	5.77	11.31
SV	5.53	6.22	4.68	4.99	5.46	3.46
EF	1.46	3.10	4.92	2.07	2.37	2.69
Mass	4.49	5.27	7.91	3.12	5.86	4.44

EDV = end diastolic volume, ESV = end systolic volume, SV = stroke volume, EF = ejection fraction.

Conclusion: Overall interobserver interscan variability showed that CMR had good reproducibility for RV and LV volumes, mass and systolic function. Inter-observer variability in RV measurements was relatively good as compared with published data for the normal RV (using segmented FLASH cine imaging). Our data show that intraobserver variability and interscan variability were relatively small. Experienced single observers making all measurements where possible will increase reproducibility, particularly with more challenging ventricular morphologies.

382. Effects of Metallic Implants on MRI Evaluation of Fontan Palliation

Ruchira Garg, MD,[1] Andrew J. Powell, MD,[1] Laureen Sena, MD,[2] Audrey C. Marshall, MD,[1] Tal Geva, MD.[1] [1]*Cardiology, Children's Hospital Boston, Boston, MA, USA,* [2]*Radiology, Children's Hospital Boston, Boston, MA, USA.*

Background: Cardiovascular MRI (CMR) is increasingly used in patients after Fontan palliation for anatomic and functional imaging. Multiple surgical procedures and transcatheter interventions in this population frequently involve metallic implants which can compromise CMR image quality. This study examined the effect of implants on CMR quality in patients with Fontan palliation.

Methods: Image quality for anatomical and functional analysis was evaluated for 120 CMR studies performed in 101 consecutive patients with Fontan palliation using a 5-level scoring system. Image quality was determined for ventricular function, and for the following 13 anatomic segments: Inferior vena cava; superior vena cava; veno-pulmonary (Fontan) pathway; right and left pulmonary veins; proximal and distal left pulmonary artery; proximal and distal right pulmonary artery; ascending aorta; transverse arch; aortic isthmus; descending aorta. Segments were considered "well-visualized" if they scored ≥ 4. Interobserver agreement was determined for 20 randomly selected studies.. The type and location of implanted devices were determined by review of the patients' medical records.

Results: Of the 101 patients studied, 46% ($n = 45$) had no metallic implants, and no reduction in image quality: 100% of anatomic segments were adequately visualized and the median image quality for ventricular function assessment was 5/5. The presence of any implant (54% of studies) reduced the proportion of adequately imaged anatomy to 77% ($p < 0.001$), and reduced the median image quality grade for ventricular function assessment to 3/5 ($p < 0.001$). Regardless of implant type, image quality for anatomy segments and function was significantly reduced when compared with patients with no metallic implants: Vascular coils, 69% of anatomic segments and 3/5 image quality for ventricular function ($p < 0.001$); stents, 81% and 3/5 ($p < 0.001$); and occluding devices, 77% and 3/5 ($p < 0.001$). Of the 14 patients with occluding devices alone, 5 had implantation of nickel-titanium alloy devices after 1997. In none of these 5 patients was imaging quality reduced (well-visualized segments 100%, function score 5/5). This was statistically significant compared with anatomical and function scores in the 9 patients with older generation devices (well-visualized segments 85%, function score 2), $p \leq 0.002$. The presence of metallic implants precluded quantitative analysis of ventricular volumes and function in 24 studies (20%). In 21 studies in which a complete image dataset of ventricular volumes and function could not be achieved using a steady-state free precession imaging sequence, data acquisition was repeated with a segmented k-space fast spoiled gradient echo sequence. In 13 of these 21 studies the repeated acquisition resulted in a diagnostic-quality complete image dataset. Interobserver agreement was excellent for both anatomy and function with a median difference of 0 (range-2 to 2), ($p = 0.24$).

Conclusion: The experience with this cohort highlights the importance of selecting devices for implantation that produce minimal or no artifacts on MRI during transcatheter interventions. Adjustment of imaging sequences can reduce the artifact due to metallic implants, as was the case for ventricular function analysis. Finally, the manufacturers of these devices should continue to expand the range of

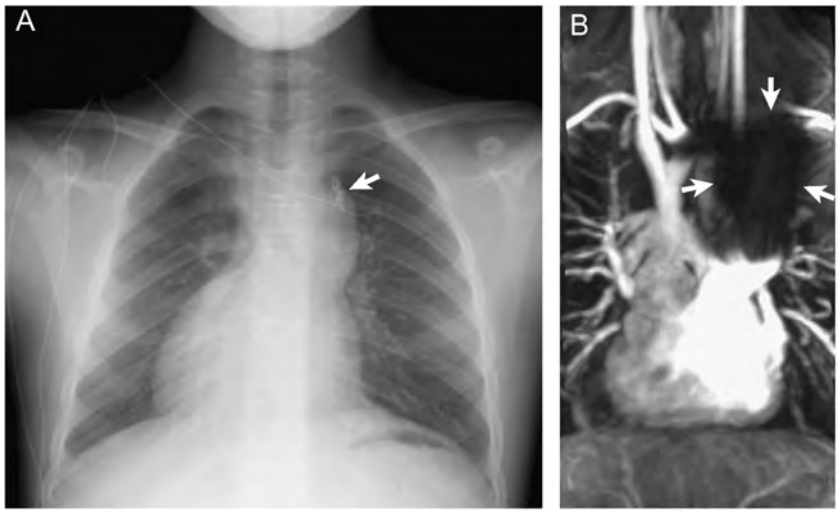

Figure 1. A. Chest radiogram in a patient with heterotaxy syndrome and dextrocardia who underwent a Fontan operation. A stainless steel coil was placed in his left internal mammary artery before the Fontan operation (arrow). B. A large image artifact produced by the coil is seen on the gadolinium-enhanced 3D magnetic resonance angiogram.

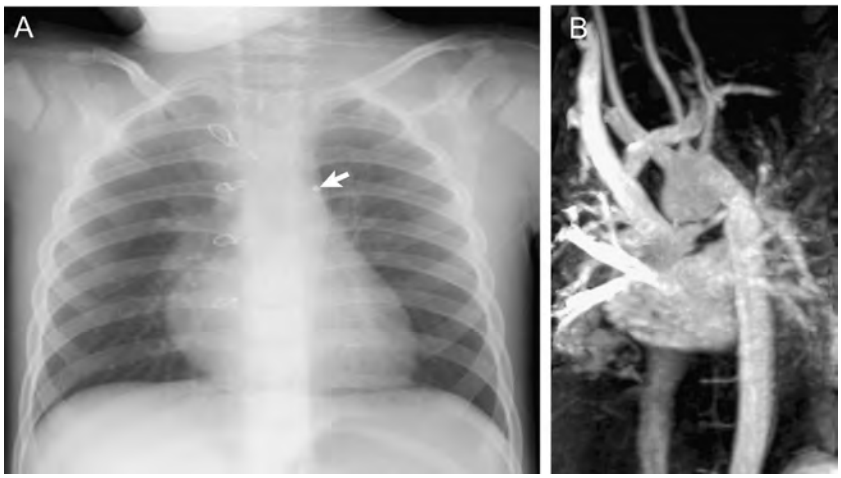

Figure 2. A. Chest radiogram in a patient with hypoplastic left heart syndrome, status post Fontan operation. A platinum coil was placed in his left internal mammary artery before the Fontan operation (arrow). B. No image artifact is seen on the gadolinium-enhanced 3D magnetic resonance angiogram.

products with minimal or no ferromagnetic materials suitable for transcatheter therapy in infants and children (Figs. 1 and 2).

Effects of metallic implants on MRI evaluation of cardiac anatomy and function after Fontan

	Percentage of studies	Percent of anatomic segments with image quality score ≥ 4	Comparison with "No implants" group	Median image quality score for ventricular function assessment
No implants	46	100 (77–100)		5 (2–5)
Any implant	54	77 (0–100)	$p < 0.001$	3 (1–5)
Coils	36	69 (0–100)	$p < 0.001$	3 (1–5)
without additional implants	20	77 (15–100)		3 (1–5)
Occluding devices	26	77 (0–100)	$p < 0.001$	3 (1–5)
without additional implants	12	92 (62–100)		3 (2–5)
Stents	11	81 (0–100)	$p < 0.001$	3 (3–5)
without additional implants	5	100 (77–100)		4 (4–5)

383. Assessment of Right Ventricular Function in Congenital Heart Disease Using Interactive Real-Time Radial Steady State Free Precession Imaging

Susan Ghods, MD[1], Matthew A. Harris, MD[2], Heiko Meyer, PhD[1], Mark A. Fogel, MD[2]. [1]*Radiology, Children's Hospital of Philadelphia, Philadelphia, PA, USA,* [2]*Cardiology, Children's Hospital of Philadelphia, Philadelphia, PA, USA.*

Introduction: Right ventricular (RV) function is particularly important to determine in patients with congenital heart disease. Segmented steady-state free precession (True-FISP) MR imaging has become an excellent method for evaluation of the RV volume and ejection fraction (EF). The images are acquired either during multiple 10–20 second breath-holds, or nonbreath-hold with multiple acquisitions. Patients with diminished ventricular function may not tolerate multiple breath-holds or prolonged acquisition time. Interactive real-time True-FISP allows real time imaging without cardiac gating or breath-holding in a very short scan time.

Purpose: To determine the accuracy of RV volume measurements using interactive real-time radial True-FISP in children with congenital heart disease.

Methods: 9 patients referred for assessment of RV function (4 with tetralogy of Fallot; 3 with hypoplastic left heart syndrome; 1 with double outlet right ventricle; 1 with congenital pulmonary stenosis) were included. Both non-breath-hold, segmented True-FISP and interactive real-time

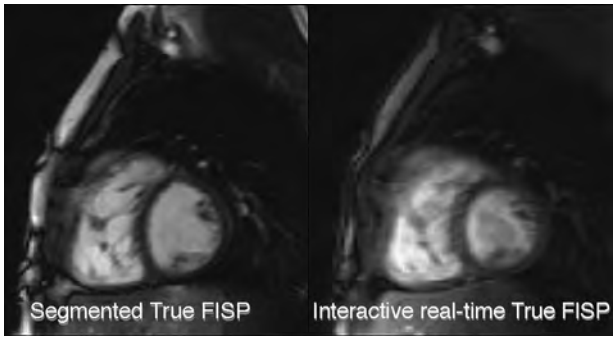

True-FISP were performed in short-axis plane. RV end-diastolic volume (RVEDV), RV end-systolic volume (RVESV), stroke volume (SV), and ejection fraction (EF) were calculated.

Results: The total acquisition time for interactive real-time True-FISP was considerably shorter than for segmented True-FISP (1 min versus 10 min). The image quality of real-time True-Fisp was sufficient for RV volume measurements in all 9 subjects. RVEDV and RVESV were not statistically different between two techniques (129 ± 102 ml versus 130 ± 90 ml for RVEDV, and 51 ± 44 ml versus 52 ± 37 ml for RVESV). SV was 78 ± 58 ml versus 78 ± 54 ml, and EF was 63 ± 8 versus 60 ± 7. The P values were not statistically significant.

Conclusions: Interactive real-time True-FISP provides accurate quantitative assessment of RV volume and EF in pediatric congenital heart disease.

384. Aortic Autograft Dilatation and Impaired Distensibility in Ross Patients, Assessed with MRI

Heynric B. Grotenhuis, MD, Jos J. M. Westenberg, PhD, Joost Doornbos, PhD, Jaap Ottenkamp, PhD, MD, Johan H. C. Reiber, PhD, Albert de Roos, PhD, MD. *Radiology, Leiden University Medical Center, Leiden, The Netherlands.*

Introduction: A pulmonary autograft to replace a dysfunctioning aortic valve (Ross procedure) is widely used because of low numbers of reoperation, the lack of need for anticoagulation, and potential for growth of the autograft. However, recent reports indicate that dilatation of the autograft frequently occurs during follow-up. Therefore, we investigated the degree of dilatation and its effect on aortic root distensibility in 10 Ross patients with MRI, and compared the results to those of age and gender matched volunteers.

Purpose: Investigation of diameters and distensibility of the aortic root in Ross patients with MRI, compared with matched volunteers.

Methods: Ten Ross patients and 7 volunteers (matched for age and gender, mean (SD) age 18.1 (4.2) years; mean (SD) follow-up for Ross patients 7.8 (1) years) underwent a MR-imaging protocol on a 1.5 Tesla scanner (Philips Gyroscan Intera). Diameters of the aortic root at the level of the annulus (ANN), sinus of Valvalva (SOV), sino-tubular junction (STJ) and the ascending aorta (AA) at the level of the pulmonary trunk were assessed, while distensibility measurements were performed at the level of the STJ. Distensibility is defined as:Dist ($mmHg^{-1}$) = ($A_{max} - A_{min}$)/A_{min} × ($P_{max} - P_{min}$)(with A_{max} and A_{min}fsmaximal and minimal cross-sectional lumen area (mm^2) respectively, and P_{max} and P_{min} systolic and diastolic blood pressure (mmHg) respectively.)Two orthogonal scout images of the aortic root were obtained for planning of the acquisition planes. Minimal lumen area was expected early in the cardiac cycle during the iso-volumetric contraction phase, while the maximal area was expected when the peak of aortic flow was passing through the AA. Therefore, first the flow was measured at the level of the AA with a phase-contrast sequence, to determine the optimal delay between the R-wave and timing of the acquisition of the cross-sectional minimal and maximal area measurements. The acquisition plane positions were manually adjusted for both measurements, thus correcting for through-plane motion of the aortic root during contraction (Figure 1). Distensibility was assessed using an SSFP-type sequence (B-TFE). Scan parameters included: FOV 220 mm, scan matrix 176 × 176, voxel size 1.25 mm × 1.25 mm × 6 mm, TR 3.2 ms, TE 1.23 ms. Temporal resolution of the phase-contrast study ranged between 4 and 7 ms. The high temporal

Table 1. Mean distensibility (SD) (in $mmHg^{-1}$) and mean (SD) diameters (in mm) for ross patients and healthy volunteers

	Ross patients mean (SD)	*p*-value Mann–Whitney U-test	Volunteers mean (SD)
Distensibility	1.94 (1.28)	$p < 0.01$	6.60 (3.99)
Diameter ANN	34.0 (7.8)	$p < 0.01$	26.4 (2.6)
Diameter SOV	43.5 (5.0)	$p < 0.01$	30.0 (2.6)
Diameter STJ	34.8 (7.3)	$p = 0.01$	26.5 (7.3)
Diameter AA	31.1 (6.6)	$p = 0.02$	25.3 (2.9)

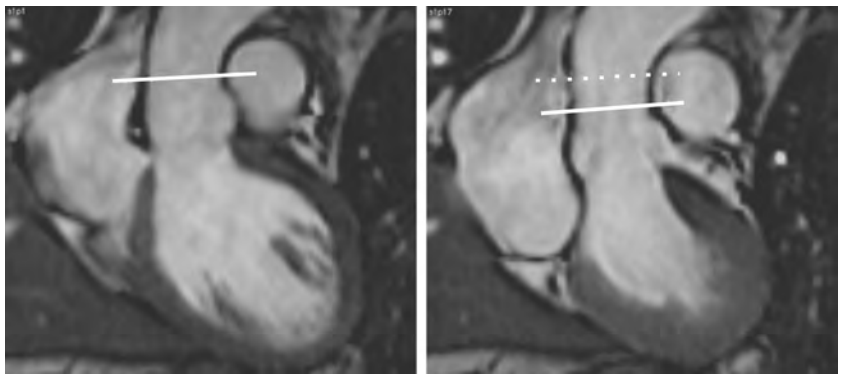

Figure 1.

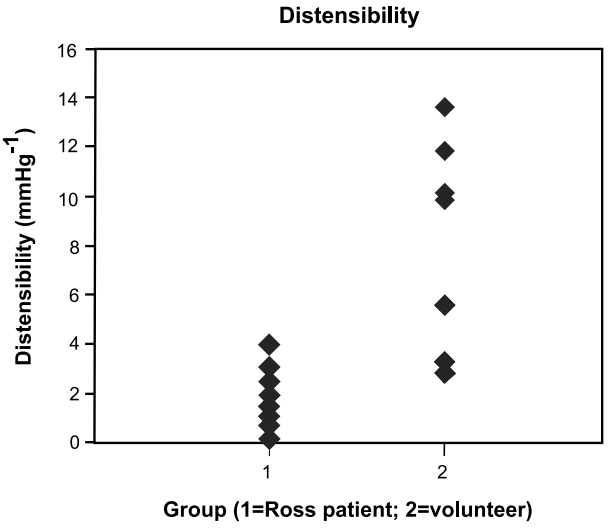

Figure 2.

resolution of this flow measurement enabled optimal timing of the acquisition of the maximal and minimal cross-sectional areas. Total examination time did not exceed 25 minutes.

Results: The results are summarized in Table 1. A significantly decreased mean distensibility was observed in the Ross patient group compared to healthy volunteers (Mann–Whitney U-test $p < 0.01$) (Figure 2). Also, the diameters at all levels were significantly larger in Ross patients (Mann–Whitney U-test $p < 0.05$ for all 4 levels).

Conclusion: The Ross patient group showed a significantly decreased mean distensibility of the aortic root as well as a significantly increased lumen diameter compared to healthy volunteers. MRI allowed for fast and accurate assessment of these clinically relevant parameters. We believe that, despite the overall good results of the Ross procedure reported in literature, both dilatation and decreased distensibility of the aortic autograft might pose an increased risk for reoperation in the future.

385. Magnetic Resonance Delayed Enhancement for the Detection of Fibrous Tissue in Postoperative Pediatric Patients with Various Forms of Congenital Heart Disease

Matthew A. Harris, MD, Susan Ghoads, MD, Paul M. Weinberg, MD, Mark A. Fogel, MD. *Pediatric Cardiology and Radiology, The Children's Hospital of Philadelphia, Philadelphia, PA, USA.*

Background: Because endothelialization occurs on conduits and patches, we hypothesized that delayed enhancement MRI should identify these areas as well as other fibrous tissue such as valve leaflets and their annuli.

Methods: We retrospectively reviewed myocardial viability studies. Ages ranged from 4 months to 19 years. Studies were reviewed for the presence of delayed enhancement involving conduits, ventricular septal defect (VSD) patches, valve leaflets and their annuli. Group 1 ($n = 14$) diagnoses included tetralogy of Fallot, transposition with VSD, double-outlet right ventricle, truncus arteriosus, and atrioventricular canal. Group 2 patients who had never undergone surgery involving placement of conduits or VSD patches were used as controls ($n = 12$).

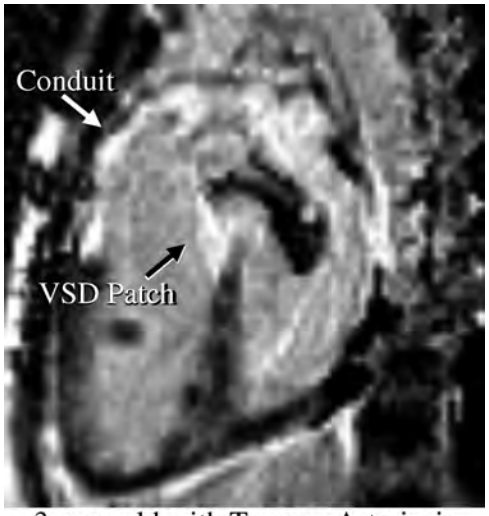

3-year-old with Truncus Arteriosis

Results: In Group 1, delayed enhancement of the conduit occurred in 11/14 pts (79%), VSD patch in 7/14 pts (50%), and involvement of the valve leaflets or annuli in 11/14 pts (79%). 2/14 patients (14%) did not have any delayed enhancement. In Group 2 there was no evidence of delayed enhancement in the region of the outflow tracts, and 3/12 (25%) pts experienced delayed enhancement involving the tricuspid valve.

Conclusion: Magnetic Resonance delayed enhancement can identify regions of fibrous tissue formation on conduits and VSD patches in postoperative pediatric patients with various forms of congenital heart disease. This information may be helpful for understanding and tracking the development of fibrous tissue in surgically reconstructed hearts.

386. Quantitative Evaluation of Right Ventricular Volume Curves Obtained with Steady State Free Precession MRI in Pediatric Patients after Tetralogy of Fallot Repair

Michael D. Taylor, MD, PhD,[1] Taylor Chung, MD,[2] Rajesh Krishnamurthy, MD,[2] John P. Kovalchin, MD,[1] G. Wesley Vick, III, MD, PhD.[1] [1]*Pediatric Cardiology, Baylor College of Medicine, Houston, TX, USA,* [2]*Pediatric Radiology, Baylor College of Medicine, Houston, TX, USA.*

Introduction: Patients with Tetralogy of Fallot (TOF) have persistent right ventricular hemodynamic abnormalities after surgical repair. The right ventricular dysfunction is secondary to a combination of factors including chronic volume

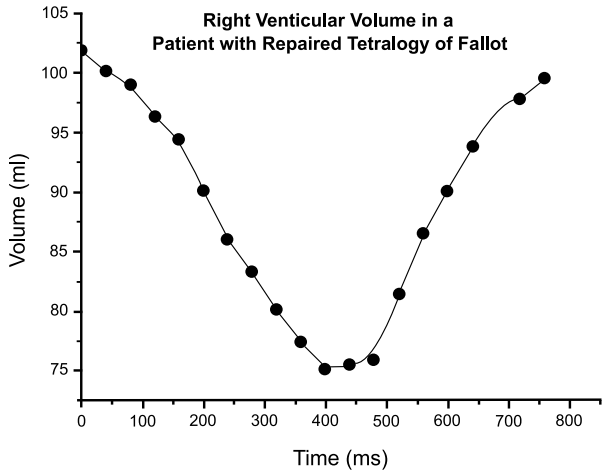

overload from pulmonary regurgitation, electromechanical disruption, and outflow tract and/or branch pulmonary artery stenoses. The ability to accurately assess early subtle degradation in right ventricular function would allow for more accurate timing of pulmonary valve replacement. Cardiovascular magnetic resonance imaging (CV MRI) has been used successfully to evaluate the right ventricular mass, end-diastolic volume, and ejection fraction in patients with Tetralogy of Fallot. However, there is little data describing the right ventricular volumetric dynamics in these patients.

Purpose: The primary objective of this work was to develop new CV MRI parameters to describe right ventricular dynamics in post-operative patients with Tetralogy of Fallot.

Methods: Fourteen patients (ages 2–17 years) with Tetralogy of Fallot were assessed. The patients had undergone either transannular patch, non-transannular patch, or RV-to-pulmonary artery conduit repair. Each patient underwent a complete CV MR evaluation including anatomical, functional, and phase contrast flow encoded imaging. All images were acquired on a Philips 1.5 T magnet equipped with high field gradients. The right ventricular function was assessed with a cine balanced fast field echo [bFFE, a steady state free precession (SSFP)] sequence acquired in the short axis orientation. Typically, 12 images were acquired from the apex to the base of the heart. The temporal resolution was 30–40 ms per image acquisition. After image reconstruction, the right ventricular volumes were determined by observer directed automated contour detection. The right ventricular volume versus time curves were used for analysis. The parameters calculated for each patient were the standard volumetric measurements including ejection fraction and end-diastolic volume. In addition, the dynamic parameters calculated were the maximum dV/dt, dV/dt_{norm} (normalized to the end-diastolic volume), delta t (the time to the maximum dV/dt), and delta t/cycle length ratio.

Results: Reproducible right ventricular volume curves were generated for all the patients. All images were of sufficient quality for analysis. The average ejection fraction was 38 ± 12%. The average end-diastolic volume in the RV normalized to body surface area was 75 ± 22 ml/m^2. The dV/dt parameter varied widely amongst the patient population and was strongly dependent on the end-diastolic volume. Consequently the dV/dt was normalized to the body-surface indexed RV end-diastolic volume. The average value for this parameter was 1.19 ± 0.3 ml*m^2/ml*s. The time to maximum slope had a wide range, but when taken as a fraction of the total cycle length was 0.31 ± 0.05.

Conclusions: Cine CV MR has become a popular method for assessing right ventricular function in post-operative Tetralogy of Fallot patients. The current generation of SSFP sequences provide improved blood to endocardial border contrast which allows efficient semi-automated ventricular curve generation. Consequently, we have shown that it is feasible to generate curves describing the dynamic function of the right ventricle. Using new time dependent metrics in addition to volumetric data will be helpful in monitoring right ventricular function, especially in determining the indications for and timing of pulmonary valve placement.

387. Disparity Between Size and Differential Blood Flow in Pulmonary Arteries in Postoperative Congenital Heart Disease Using MRI

Karen G. Ordovas, Christofer Tan, MD, Gautham P. Reddy, MD, MPH, Oliver M. Weber, PhD, Charles B. Higgins, MD.
Radiology, UCSF, San Francisco, CA, USA.

Introduction: Pulmonary artery stenoses may remain after surgery for congenital heart disease. Documentation of the hemodynamic significance of stenoses is necessary to determine the need for further intervention (Haramati et al., 2002). It is likely that morphology alone provides incomplete assessment for this purpose (Helbing and de Roos, 2000); therefore there is a necessity for functional evaluation (Kang et al., 2003). Phase-contrast cine MR imaging (VEC MRI) has been shown to be an accurate technique for measuring

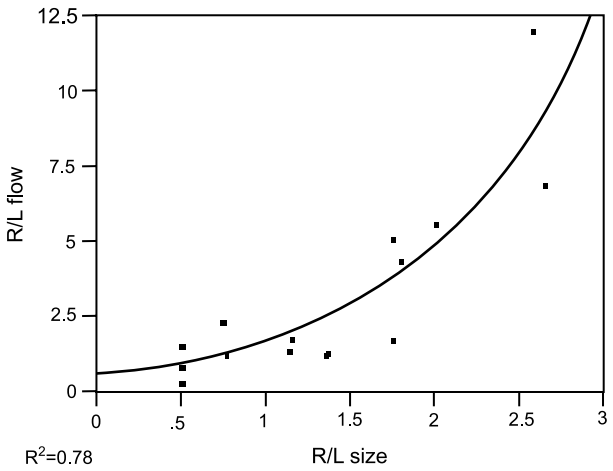

Figure 1.

flow in the right and left pulmonary arteries (Caputo et al., 1991; Kang et al., 2003). Accordingly, the purpose of the current study was to compare severity of stenoses (size) and blood flow in right and left pulmonary arteries in patients with branch pulmonary arterial stenoses after surgery for congenital heart diseases (CHD) throught MRI.

Patients and Methods: Fifteen patients with surgically repaired congenital heart disease underwent MRI studies for the assessment of branch pulmonary arterial stenoses. Spin-echo images were used to assess morphology of stenoses while velocity-encoded cine MRI was used to measure flow in the right and left pulmonary arteries. Magnitude and phase images were obtained in planes perpendicular to the long axis of the right and left pulmonary arteries just before their first branches, with a slice thickness of 5 to 10 mm. The encoding velocity selected was 200 cm/s or higher if aliasing phenomenon was detected. The ratios of the narrowest diameter of right to left pulmonary arteries (R/L size) and the blood flow (R/L flow) were calculated. This proportion attempted to control for between patient biological variations (body size). The correlation between the two ratios was assessed via Spearman's correlation. An exponential regression was applied to use R/L size to predict R/L flow. The significances of the regression coefficients were assessed by the F test. The predictive residuals were calculated in order to evaluate the clinical utility of estimating the R/L flow based on R/L size and assess its difference from the measured R/L flow.

Results: R/L size varied from 0.5 to 2.66, while R/L flow varied from 0.36 to 12.02. There was an exponential correlation between R/L size and R/L flow, considering the latter as the dependent variable, with $r^2 = 0.78$ and $p = 0.001$ (Figure 1). Predictive residuals ranged from −136% to 54% of the true R/L flow. There was no linear correlation.

Conclusion: This study demonstrated that morphological evaluation of the pulmonary arteries does not predict accurately differential right and left pulmonary artery blood flow in patients with pulmonary stenoses, signifying that measurement of pulmonary artery diameter is not clinically useful for this purpose. Therefore blood flow measurements are essential when considering the need for further interventional procedures. Velocity-encoded cine MRI is a noninvasive method for simultaneous morphologic and functional evaluation of pulmonary artery stenoses in patients with congenital heart diseases.

REFERENCES

Caputo, G. R., Kondo, C., Masui, T., et al. (1991). Right and left lung perfusion: in vitro and in vivo validation with oblique-angle, velocity-encoded cine MR imaging. *Radiology* 180:693–698.

Haramati, L. B., Glickstein, J. S., Issenberg, H. F., Haramati, N., Crooke, G. A. (2002). MR imaging and CT of vascular anomalies and connections in patients with congenital heart disease: significance in surgical planning. *Radiographics* 22:337–349.

Helbing, W. A., de Roos, A. (2000). Clinical applications of cardiac magnetic resonance imaging after repair of Tetralogy of Fallot. *Pediatr. Cardiol.* 21:70–79.

Kang, I., Redington, A. N., Benson, L. N., et al. (2003). Differential regurgitation in branch pulmonary arteries after repair of Tetralogy of Fallot. A phase-contrast cine magnetic resonance study. *Circulation* 17:2938–2943.

388. In Vitro Quantification of Cells Labeled with Magnetic Nanoparticles Using Off-resonance Sequence

Takayasu Arai,[1] Charles H. Cunningham, PhD,[2] Michael V. McConnell, MD,[1] Steven M. Conolly, PhD,[2] Phillip C. Yang, MD.[1] [1]*Department of Medicine, Division of Cardiovascular Medicine, Stanford University, School of Medicine, Stanford, CA, USA,* [2]*Department of Electrical Engineering, Stanford University, Stanford, CA, USA.*

Introduction: Cell transplantation may provide a therapeutic alternative to protracted diseases such as end-stage heart failure. However, in vivo evaluation of cell-based therapy has not been possible. One of the critical assessments is to quantify the volume of the transplanted cells at the site of transplantation. Using super-paramagnetic iron oxide (SPIO) labeling, conventional MR gradient recalled echo (GRE) imaging allows us to detect $T2^*$ dephasing signal from SPIO-labeled cells. However, negative contrast techniques suffer from partial volume effects, which can make quantitation difficult. We have developed a new pulse sequence exploiting off-resonance spin echo (OR) characteristics of the magnetic dipole to generate positive MR signal from SPIO labeled cells. In this study, we tested the ability of OR sequence to quantify in vitro the proliferation of SPIO-labeled mouse embryonic stem cells (mESC).

Methods: Cell labeling solution was prepared by incubating 0.05 mg/ml of ferumoxides (Feridex, Berlex Lab, Wayne, NJ) with 1 microgram/ml of poly-l-lysine as a transfection agent for 60 minutes. The mESC were cultured with mESC medium with 10^3 units/ml leukemia inhibitory factor (ESGRO, Chemicon International, Temecula, CA) to suppress differentiation. The labeling solution was incubated with approximately 5×10^5 mESC for 24 hours. The labeling solution was removed, and four samples of the labeled mESC were allowed to divide with mESC medium for 4 days. Cells were counted using a hemocytometer. At days 1, 2, and 4, mESC suspended in the vials were inserted into agar gel for susceptibility matching. Four vials filled with 0.9% saline were allowed to settle to the bottom. The vials were filled with 0.05 mg/ml of ferumoxides solution as positive control. GRE (100 ms TR, 7.2 ms TE and 30 flip angle) and OR imaging (200 ms TR, 14 ms TE, matrix 256×256 over a 12 cm FOV and 16 NEX) were performed using a conventional 1.5 T Signa MRI scanner (GE, Milwaukee, WI). Signal area was measured by computing the number of pixels 5 standard deviations above the mean

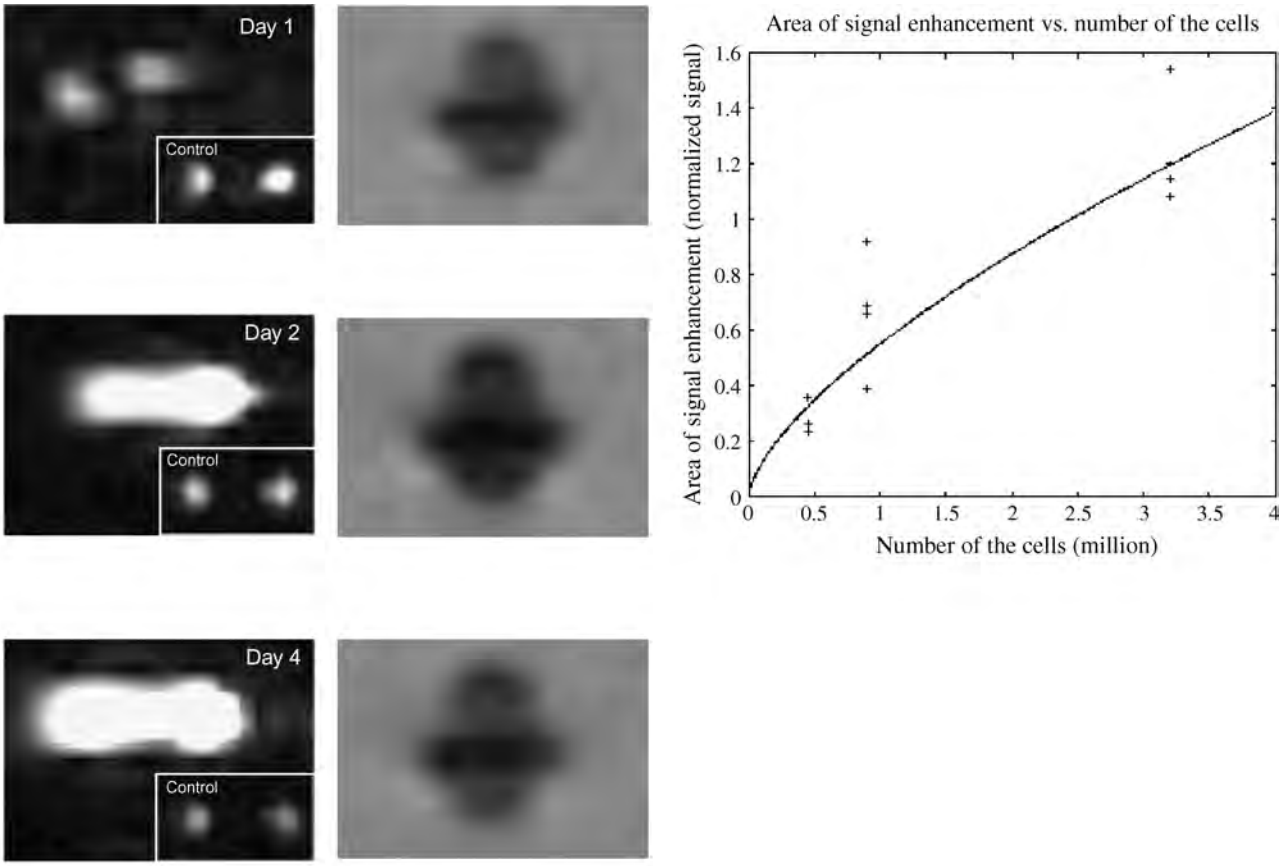

Figure 1. (A) OR (left) and GRE (right) images 1 day after labeling (number of the cells: 0.45 million). (B) OR (left) and GRE (right) images 2 days after labeling (number of the cells: 0.9 million). (C) OR (left) GRE (right) images 4 days after labeling (number of the cells: 3.2 million). (D) Relationship between the area of signal enhancement and the number of the labeled cells.

noise magnitude. In theory, we would expect that the area enclosed between enhancement regions should vary with two-thirds power of the volume of the labeled cells.

Results: As shown in Figure 1A–C, conventional GRE image shows negative signal from SPIO-labeled cells, however, the area of positive signal measured from OR images increased as the population of labeled cells increased, though the total amount of ferumoxides particles in each cell population is presumably constant. Figure 1D demonstrates the relationship between the area of signal enhancement and the number of the labeled cells. The solid line represents a fit of the data to the expected functional form, area of signal enhancement = k (volume)^2/3.

Conclusions: This study demonstrates the OR sequence's promise for estimating both location and volume of labeled cells in vivo. This may be more robust than GRE methods, which suffer from typical negative contrast drawbacks, including partial volume artifacts. Volume estimates over time should allow for viability studies, even while the magnetic tag is diluting during each generation. The relationship between the volume of the labeled cells and the area of signal enhancement was monotonic, and qualitatively follows the expected two-thirds power law. Further research is needed to properly compare this method to GRE and other positive contrast methods.

389. Dynamic Changes of Cardiac Fiber and Sheet Architecture during Cardiac Contraction Quantified with Diffusion Tensor MRI

Junjie Chen, MS, Wei Liu, ScD, Xiaoxia Yang, BS, Huiying Zhang, MS, Liz Lacy, BS, Samuel A. Wickline, MD, Xin Yu, ScD. *Cardiovascular MR Laboratories, Washington University, Saint Louis, MO, USA.*

Introduction: Myocardial fiber structure is a key determinent of ventricular function. Previous studies from our lab and others have established diffusion tensor MRI (DTMRI) as a reliable method to characterize baseline fiber structure in both normal and diseased hearts. However, changes of fiber structure in cardiac cycle have not been definitively resolved.

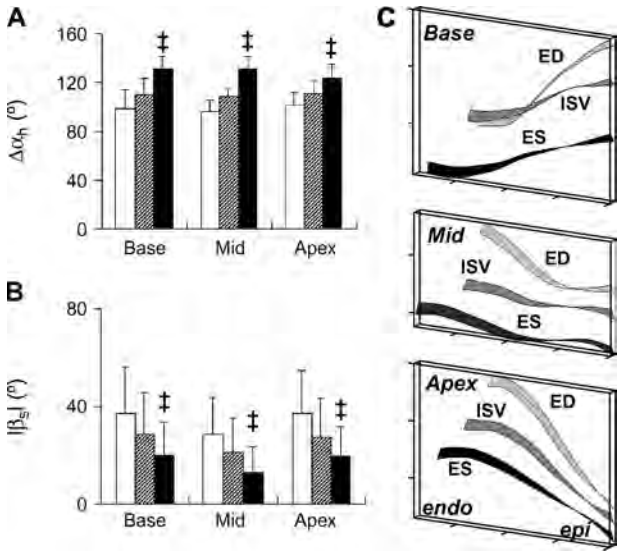

Figure 1.

In the current study, we characterized myocardial fiber and sheet structure from diastole through systole with DTMRI.

Methods: Hearts of 2–4 month old Sprague-Dawley rats (n = 21) were excised for retrograde perfusion in a working heart Langendorff preparation. A water filled latex ballooon was inserted through mitral valve into left ventricle to record left ventricular developed pressure (LVDP) and the heart rate (HR). The rate-pressure-product (RPp = HR × LVDP) was calculated as an index of cardiac work. Three physiological states of contraction were studied: 1) end-diastole (ED), 2) isovolumic contraction (ISV), and 3) end-systole (ES). Hearts were first arrested at ED with KCl for DTMRI. Subsequently, the hearts were perfused with Krebs-Henseleit buffer to resume heart work. Finally, systolic contracture was induced with $BaCl_2$ perfusion. At the end of the experiment, the hearts were quickly fixed at either ISV (n = 10) or ES (n = 11) for DTMRI. Diffusion-weighted MR images were acquired on a Varian 4.7 T scanner at each physiological state. A multi-slice spin-echo sequence with diffusion sensitizing bipolar gradient was used. Imaging parameters were: TE, 36 msec; Δ, 20 ms; δ, 6 ms; b-value, 948 s/mm^2; image voxel size, 156 μm × 156 μm × 1 mm. The apparent diffusion tensor was calculated from diffusion-weighted images as described previously (Chen et al., 2003). Diffusion anisotropy was characterized with the use of fractional anisotropy (FA). Lateral myocardial fiber architecture was quantified in 20° sectors at base, midventricle (Mid), and apex. Specifically, the 1st eigenvector of diffusion tensor was used to define myofiber orientation, and the 2nd eigenvector defined the sheet orientation (Tseng et al., 2003).

Results: Cardiac function of the isolated perfused heart was well maintained during the experiment. RPP before and after KCl arrest was 43,711 ± 10,890 bpm × mmHg and 41,368 ± 10,496 bpm × mmHg respectively (p = N.S.). FA in ED, ISV and ES hearts were 0.36 ± 0.03, 0.32 ± 0.05 and 0.30 ± 0.04 ($p < 0.001$ compared to ED) respectively, indicating preserved diffusion anisotropy. Transmural differences of myofiber helix angle ($\Delta\alpha_h$) increased slightly from ED to ISV (p = N.S. for ISV versus ED), and further increased significantly by ES (Figure 1A, $p < 0.001$ for ES versus ED). In contrast, the magnitude of myocardial sheet angle ($|\beta_s|$) decreased progressively from ED to ISV and ES (Figure 1B, $p < 0.001$ for ES versus ED). The three-dimensional lateral sheet architectures at ED, ISV and ES were reconstructed from the DTMRI data (Figure 1C).

Conclusion: Dynamic changes of cardiac fiber structure atdifferent phases of cardiac cycle were quantified using DTMRI. The present study validated previous observations by Streeter and colleagues regarding changes of fiber orientation in systole. Specifically, the myofiber orientation changed minimally from end-diastole to isovolumic contraction. However, myofibers become more longitudinally orientated by end-systole. In addition, DTMRI revealed that sheet slope in the wall continuously decreased from end-diastole to end-systole. We conclude from these data that the dynamic changes of fiber and sheet structure will contribute up to 12% of circumferential shortening and 40% of wall thickening during cardiac contraction. This contribution of myocardial sheets to local wall thickening confirms a profound newly observed effect of myocardial architecture on local mechanics that cannot be recorded in any other way than DTMRI.

REFERENCES

Chen, J., et al. (2003). *Am. J. Physiol.* 285:H946–H954.
Tseng, W. Y., et al. (2003). *J. Magn. Reson. Imaging* 17:31–42.

390. Interactive Real-Time Adjustment of Shim Currents and Transmit Frequency in SSFP and GCFP Sequences

Wolfgang G. Rehwald, PhD,[1] Burkhard Sievers, MD,[2] Raymond J. Kim, MD,[2] Robert M. Judd, PhD.[2] [1]*Siemens Medical Solutions and Duke Cardiovascular MR Center, Durham, NC, USA,* [2]*Duke Cardiovascular MR Center, Durham, NC, USA.*

Introduction: Steady state free precession (SSFP) pulse sequences such as true FISP (true Fast Imaging with Steady Precession) and a new free precession sequence, GCFP (Global Coherent Free Precession), are susceptible to off-resonance transmitter frequencies and poor shimming. Specifically, inappropriate frequency and shim settings cause flow and banding artifacts (stop bands) in SSFP sequences and loss of signal in GCFP. Manual correction of these errors is inconvenient, however, because the effect of each change can typically only be visualized through side-by-side comparison from images acquired during consecutive breath holds. We hypothesized that real-time control of frequency and shim,

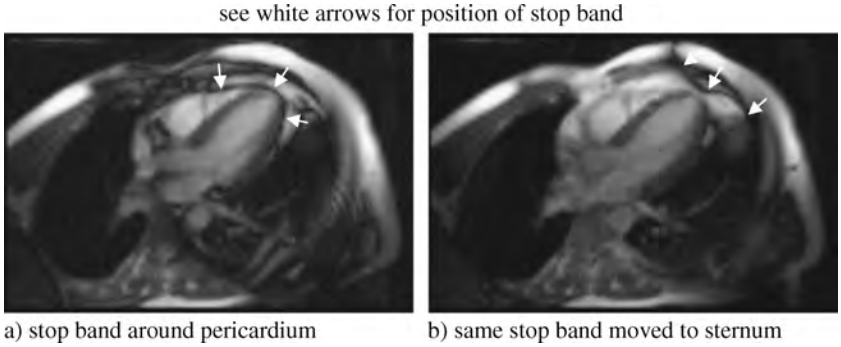

Figure 1. Moving banding artifacts by changing the transmit frequency in True FISP.

combined with real-time scanning, would allow the scanner operator to interactively optimize SSFP and GCFP image quality in a few seconds.

Purpose: To provide interactive real-time control of transmitter frequency and magnetic field shims for optimization of SSFP and GCFP image quality.

Materials and Methods: We modified the low level scanner software in order to allow real-time control of transmit frequency and first order shims while continuously imaging at 6 up to 16 frames/second on a clinical MR scanner (Magnetom Sonata, Siemens, Erlangen, Germany). While running an interactive real-time MRI scan, first order shims are entered in logical coordinates (phase, frequency, slice) in uT/m. They are converted into physical coordinate values (x, y, z). Tune-up shim values can be loaded with the push of a button at any time. When shim values are changed, the sequence stops for 100 ms during which the new values are sent to the gradient hardware. Gradient coil currents are changed accordingly and the sequence resumes. Frequency changes are implemented as phase increment per TR. All effects are immediately visible in the image following the adjustment providing instant feedback to the operator. Typical parameters for True FISP were TR 2.35 ms, flip angle 50 degrees, fov 360 mm, temporal resolution 155 ms, matrix size 128 × 66, slice thickness 8 mm, bandwidth = 1347 Hz/pixel, and phase fov 68.8%. For GCFP we used TR 3.28 ms, flip angle 30 degrees, fov 300 mm, temporal resolution 65 ms, matrix size 128 × 20, excitation slice thickness 5 mm, bandwidth 2298 Hz/pixel, and phase fov 15.6%.

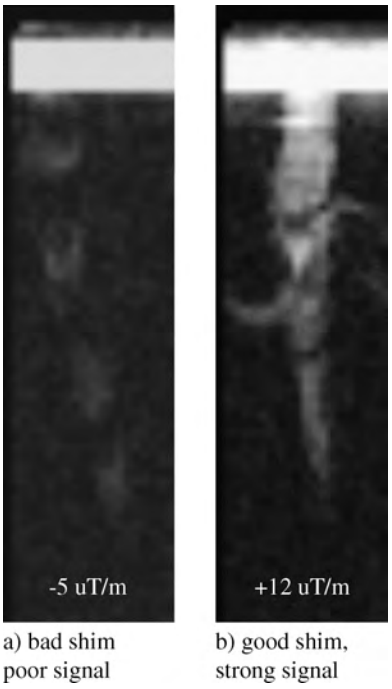

Figure 2. a) Signal decay and b) Persistence due to bad and good shim in GCFP, respectively.

Results: Shim and frequency adjustment of the True FISP sequence were studied in volunteers and a phantom. Severe flow artifacts in the aortic outflow tract were caused by deliberately creating a bad shim and then removed by adjusting the transmit frequency. Banding artifacts due to bad shim were moved away from the myocardium in a four-chamber view of the heart by either modifying the frequency, see Fig 1, or by adjusting the shim. In GCFP imaging, the shim in slice direction was varied between −5 uT/m and + 12 uT/m destructing or yielding signal in the abdominal aorta and renal arteries, see Fig 2.

Conclusions: Adjustment of shim and transmit frequency in real-time is a graphic and visually traceable tool for image quality improvement. It affords shift or removal of artifacts in True FISP MR images improving their clinical utility. In GCFP, it is a required tool that enables the operator to improve phase coherence of flowing spins and to preserve their signal. Furthermore, the described sequence is a useful research tool for comprehensive artifact examination and understanding.

391. Advantages of Parallel Acquisition in Cardiac MR Perfusion Imaging

Yiu-Cho Chung, PhD, Orlando P. Simonetti, PhD. *Cardiovascular MR R&D, Siemens Medical Solutions USA, Inc., Chicago, IL, USA.*

Table 1. Protocols evaluated in the phantom experiments

Resolution (readout)	128			192		
Parallel imaging	No	Yes		No	Yes	
Bandwidth (Hz/pixel)	850	850	400	840	840	400
T1 (msec)	100	128	100	100	127	100
Acq. window (msec)	147	93	148	148	94	147
TR (msec)	1.9	1.9	3.1	1.9	1.9	3.1
Phase encode (PE) lines	78	48	48	76	48	48
Effective PE lines	78	78	78	76	78	78
Pixel size (mm2)		3.8 × 2.8			3.6 × 1.9	
Protocol	1	2	3	4	5	6

Introduction: First-pass MR perfusion imaging can be used to detect myocardial ischemia (Wike et al., 0000). Fast imaging techniques are commonly used to provide adequate spatial coverage of the heart. Recently, the time-savings offered by parallel acquisition techniques (PAT) has been used to increase spatial resolution (Luk et al., 0000; Plein et al., 0000). Cardiac perfusion images typically have low signal-to-noise ratios (SNR); using PAT (which reduces SNR by at least $\sqrt{}$ p, p = acceleration factor) to acquire higher resolution images is counter-intuitive. The effect of PAT on the T1-weighting of turboFLASH is also unknown. Understanding the effect of PAT on the SNR/CNR of turboFLASH perfusion imaging would facilitate imaging protocol optimization. We shall show here through phantom experiments how PAT, when used with an appropriate choice of imaging parameters, can maintain image SNR and improve T1 weighting.

Purpose: To evaluate the effect of PAT and image resolution on the SNR/CNR of a turboFLASH based cardiac perfusion pulse sequence using a phantom with different T1 compartments.

Methods: The phantom used has 5 compartments doped with different amounts of $MnCl_2.4H_2O$ to provide T1 values of approximately 1.24 s, 812 ms, 483 ms, 300 ms and 177 ms (values similar to those of heart tissue before and after contrast agent injection). Six protocols were tested, using saturation recovery turboFLASH (SR-TFL) with or without PAT to evaluate the strategies of: a) reduced acquisition time with increased saturation delay time (TI) for better T1 recovery; b) improved SNR through reduced receiver bandwidth. See Table 1.

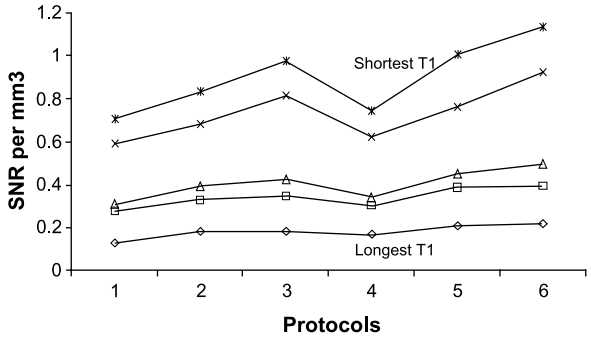

Figure 1. The SNR/mm^3 from the 5 phantom compartments for the six protocols.

The experiment was performed on a Siemens MAGNETOM Sonata. Common protocol parameters were: time per slice = 174 ms; 8° flip angle; 8 mm slice thickness; GRAPPA (Griswold et al., 0000) with p = 2, 8 additional lines for coil sensitivity maps; 8-channel array coil used for signal reception; 40 measurements, ECG triggered with simulated RR interval of 800 ms; 4 slices per RR. For each compartment, SNR at the 20th measurement was calculated and CNR were measured relative to the compartment with the longest T1.

Results: Despite the 50% difference in voxel size, SNRs from protocol 1 and 6 are practically the same before voxel size normalization. For comparison purpose, Figure 1 shows the SNR/mm^3 for the 5 compartments using the six protocols.

Table 2 shows the SNR and CNR per mm^3 for two compartments selected to simulate enhanced (T1 = 300 msec) and un-enhanced (T1 = 812 msec) myocardium. The results showed that: 1) there is a significant SNR/mm^3 advantage using PAT; 2) with PAT, greater SNR/mm^3 improvement is obtained by lowering bandwidth than by extending TI; 3) The SNR/mm^3 gain with PAT for 192 matrix resolution was greater than for 128 matrix resolution.

Discussions: An unexpected gain in SNR/mm^3 with PAT was found in the SR-TFL sequence used for first-pass myocardial perfusion imaging. Keeping bandwidth constant, PAT saves time that allows for longer TI and hence more T1 recovery of signal. Trading the time-savings of PAT for lower

Table 2. SNR and CNR per mm^3 for two compartments selected to stimulate enhanced (T1 = 300 msec) and un-enhanced (T1 = 812 msec) myocardium

Protocol	1	2	3	4	5	6
SNR@ T1 = 812 ms	0.28	0.33	0.34	0.30	0.39	0.39
SNR@ T1 = 300ms	0.59	0.68	0.81	0.62	0.76	0.92
CNR	0.31	0.35	0.47	0.32	0.38	0.53

receiver bandwidth, the resulting TR increase improves both SNR and T1 contrast. This effect is more pronounced in tissues with short T1 s. PAT also reduces the number of RF pulses applied by almost half, reducing spin saturation. All these interactions give rise to a net SNR/mm^3 improvement.

Conclusions: This study shows experimentally that PAT improves the SNR/mm^3 and may be used in SR-TFL based cardiac perfusion imaging to reduce scan time per slice and obtain higher resolution images. This can help reduce motion artifacts and improve image quality.

REFERENCES

Chung, et al. *Proc. 10th ISMRM* 219.
Griswold, M. A., et al. *MRM* 47(6):1202–1210.
Luk, et al. *JCMR* 6(1):383–384.
Plein, et al. *JCMR* 5(1):92–93.
Wilke, et al. *Radiology* 204(2):373–384.

392. Mapping Regional Contractile Function: The Effect of Using Large Pixels to Map Strain

Anthony H. Aletras, Marilena Lekoudis, BS, Gauri S. Tilak, Andrew E. Arai, MD. *Laboratory of Cardiac Energetics, National Institutes of Health, Bethesda, MD, USA.*

Introduction: Although there are at least three competing methods for imaging myocardial strain with CMR (Tagging, HARP, DENSE), there are fundamental differences in the intrinsic resolution of each of these techniques. For example, tagging is limited by tag spacing, which generally has been large enough to preclude accurate intramural measurements of wall thickening. HARP, as a post-processing technique to analyze tagged images, is limited by the same constraints (Parthasarathy et al., 2004). By suppressing unwanted k-space spectral harmonics (Aletras and Arai, 2004; Epstein and Gilson, 2003), DENSE can acquire and analyze intramyocardial strain at a higher resolution.

Purpose: Lower image resolution will result in degradation of intramural myocardial strain estimations compared with a high resolution methodology.

Methods: Sixteen beagles were imaged at 1.5 T after a 90 minute occlusion followed by reperfusion. DENSE images were acquired along short axis views at pixel sizes of 1.1×1.1 mm^2, 1.4×1.4 mm^2, 2.2×2.2 mm^2, and 4.4×4.4 mm^2. The number of acquisitions was adjusted to yield theoretical relative SNR's of 100%, 94%, 141%, and 1130%, respectively. Note that the pixel size of 4.4×4.4 mm^2 was chosen to approximate HARP processing of tagged-images so that direct comparisons can be made. Average circumferential shortening (CS) and radial thickening (RT) were measured according to a 16-sector model. CS and RT values for each pixel size were compared by Bland-Altman analysis. Therefore, in all plots the x-axis has the average strain while the y-axis has the error between the pixels being compared.

Results: All the Bland Altman plots use the 1.1×1.1 mm^2 resolution strain maps as the reference for comparison. On a scale where normal myocardial strain is approximately 25 to 30%, all acquisitions done at a resolution of 2.2×2.2 mm^2 or better showed no significant bias

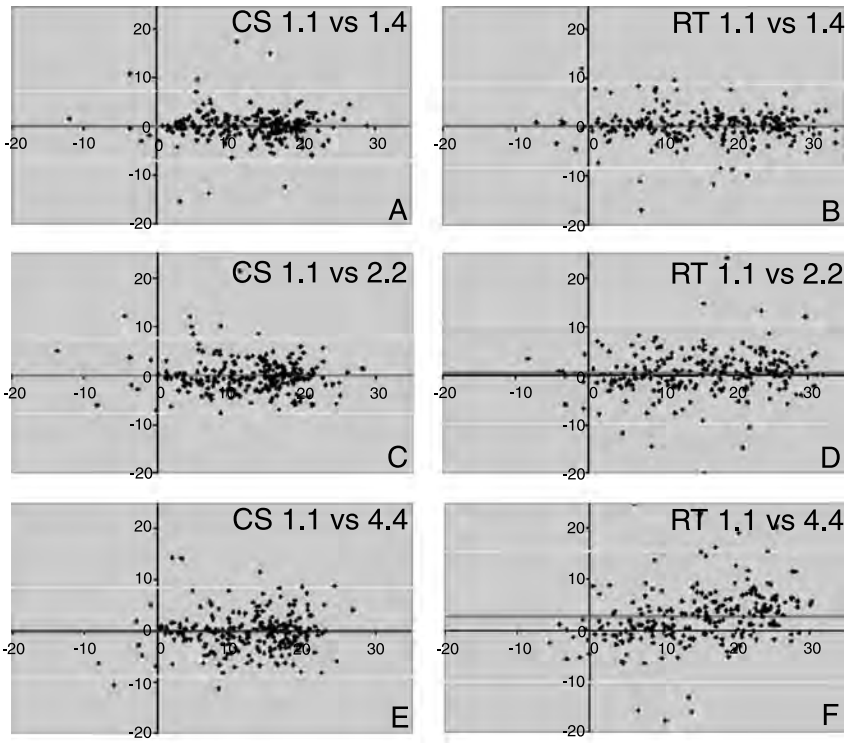

(< 0.5% strain). At a resolution comparable to tagging and HARP (4.4 × 4.4 mm^2), the bias was approximately 5 times higher. The limits of agreement as assessed by two standard deviations showed a step-wise increase in scatter as image pixel size increased. Comparing the 1.4 × 1.4 mm^2 resolution strain maps with the reference standard, the standard deviation of the error was 4%. For the 4.4 × 4.4 mm^2 image resolution, the limits of agreement were 52% worse as shown by the wider separation in the limits of agreement (panel F). Finally, the limits of agreement in the radial direction across the LV myocardium were substantially worse than the circumferential direction, particularly as pixel size increases.

Conclusions: Although it is not surprising that lower resolution strain acquisitions result in measurements that do not agree with a high resolution reference standard, it is important to recognize that the pixel size of strain maps derived from current tagging methods and HARP analysis studies is large enough to distort radial strain estimates.

REFERENCES

Aletras, A. H., Arai, A. E. (2004). *J. Magn. Reson.* 169(2):246–249.
Epstein, F. H., Gilson, W. D. (2003). *Proc. Int. Soc. Magn. Reson. Med.* 11:1566.
Parthasarathy, V., et al. (2004). *Proc. Int. Soc. Magn. Reson. Med.* 11:1797.

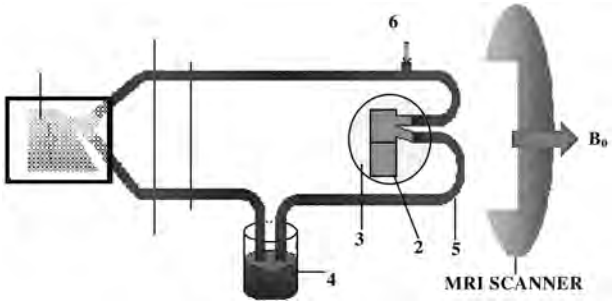

Figure 5. 1. Pump (model 1423, Harvard apparatus, MA, USA) 2. Heart phanton 3. Acrylic box with gelatin 4. Reservoir(5L) with manganese chloride (20 mg/l) 5. Out fow tube 6. Portal for catheter insertion.

393. Passive Catheter Tracking Techniques and Imaging Strategies for Endovascular Intervention—The Best Approach?

Sanjeet Hegde, MBBS, MRCPCH,[1] Marc E. Miquel, PhD,[2] Sebastian Kozerke, PhD,[3] Redha Boubertakh, PhD,[1] David Gilderdale, PhD,[4] Andrew Taylor, MBBS, MD, FRCR,[5] Stephen Keevil, PhD,[1] Derek Hill, PhD,[1] Reza Razavi, MBBS, MRCP, MD[1]. [1]*Imaging Sciences/Pediatric Cardiology, King's College London, London, UK,* [2]*Imaging Sciences, King's College London, London, UK,* [3]*Institute*

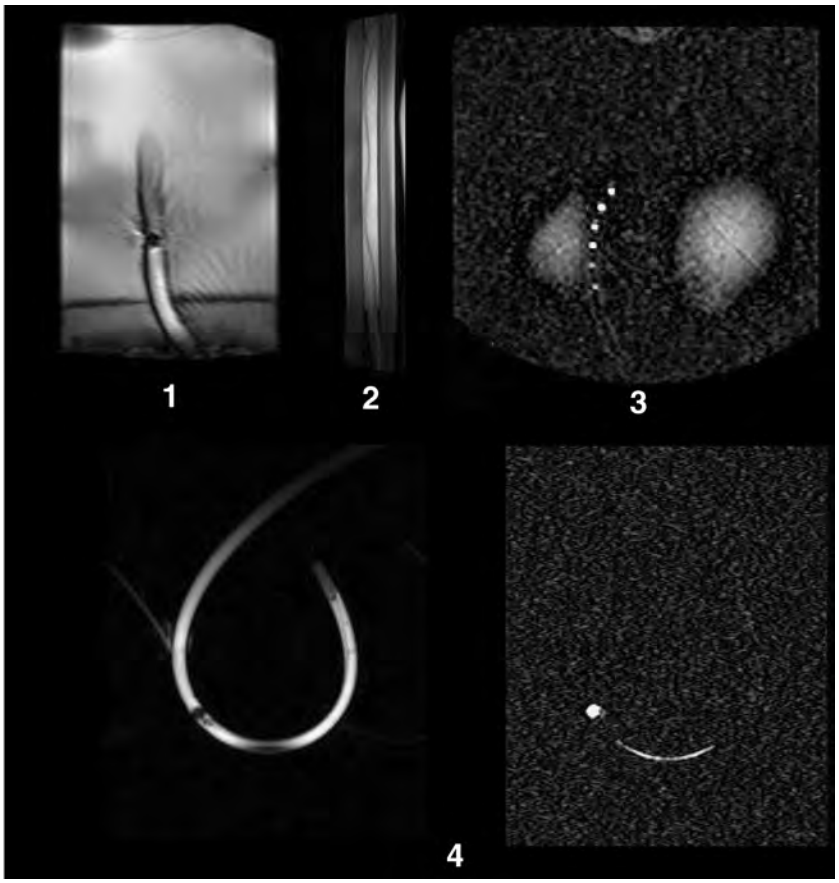

Table 1. Problems associated with each of the catheters

	Artefacts	Heating	Bio-safety problems	Hardware/ software changes
CO_2 balloon catheter	+	–	+	–
Dysprosium catheter	+ +	–	+ +	–
Tuned fiducial marker catheter	+ +	–	+ +	+
Fluorine catheter	+	–	+	+ + +

[(–) Not significant, (+) Minor, (+ +) Significant, (+ + +) Major].

for Biomedical Engineering, ETH and University Zurich, Zurich, Switzerland, [4]Imperial College, London, UK, [5]Departmentt of Clinical Radiology, Great Ormond Street Hospital for Children, London, UK.

Introduction: Magnetic resonance (MR) guided cardiac catheterisation has been successfully carried out in patients which has brought a few issues related to this technique to the fore. The lack of suitable catheters that are safe enough to use in the MR environment is a glaring weakness of this method of catheterisation. We chose to study passive catheter tracking techniques and have compared four different types of catheters in our set-up.

Methods: Imaging: The study was performed in an interventional XMR suite equipped with a 1.5 T Philips Intera MR scanner with a ^{19}F channel and Pulsera cardiac x-ray unit (Philips Medical Systems, Best, the Netherlands). We used a SENSE cardiac coil and a small transmit-receive fluorine surface coil. We used a real time SSFP sequence with a typical TE of 1 ms, scan percentage of 100, a 96 × 96 matrix reconstructed to 128 × 128 and a flip angle of 50°and a SSFP sequence used in interactive mode and with a typical TE of 1.4 ms, image matrix of 128 × 128, a flip angle of 50° and a 75% scan percentage. To image the tuned fiducial marker catheter we modified sequences so that flip angles gradually increased and decreased or low and high flip angles were interleaved and for the fluorine catheter we interleaved proton and fluorine imaging. *Phantom:* We used a 'non-flow' and a 'flow' phantom to simulate endovascular intervention (Fig. 1). *Catheter preparation:* We compared tracking of four different types of catheters so as to evaluate their suitability for endovascular intervention.

1. CO_2 catheter: standard 5Fr Berman balloon angiographic catheter (Arrow International, Reading, PA, USA), filled with 0.8 ml of CO_2.
2. Dysprosium catheter: catheter tubing extruded with dysprosium oxide (prototype provided by NuMed, Inc, Hopkinton, New York, USA).
3. Tuned fiducial marker catheter: six pre-wound fiducial markers mounted onto a 5Fr balloon angiographic catheter (Arrow, Reading, PA) 17 mm apart and aligned 45° to the long axis of the catheter.
4. Fluorine catheter: standard 5Fr Berman balloon angiographic catheter (Arrow International, Reading, PA, USA) with perfluorooctylbromide (Exfluor Research Corp., Texas, USA).

Results: The CO_2 filled balloon tip (Fig. 2) catheter can be safely used to track catheters but lack of visualisation of the length of the catheter is a significant disadvantage. The catheter extruded with dysprosium oxide (Fig. 3) along its length overcomes this disadvantage of the CO_2 balloon catheter but the reliance on orientation of the catheter within the magnetic field for optimum susceptibility artefact is a drawback. In addition the bio-safety of catheters extruded with dysprosium is yet to be explored. The tuned fiducial marker catheter (Fig. 4) offers a reliable solution to tracking and with improved pulse sequences we were able to show excellent tracking of the catheter tip and length. However, design of small enough markers that can be safely integrated into a catheter is a major hurdle. The fluorine catheter (Fig. 5) offers as yet the best option for catheter tracking in that we were able to image both the tip and along the length of the catheter reliably and safely (Table 1).

Conclusion: An essential requirement for magnetic resonance guided catheterisation in patients is the availability of a safe, reliable and reproducible catheter tracking method. Among the four catheters studied the 'fluorine catheter' allows for a safe, reliable and reproducible tracking method. However, a lot more work needs to be carried out into the optimum coil design and the hardware and software changes required to a conventional MR scanner.

394. Automated Calculation of Myocardial Mass and Infarct Size in Mice Using a Monte Carlo Markov Chain Active Contour

Robert Janiczek,[1] Nilanjan Ray, PhD,[1] Scott T. Acton, PhD,[1] R. Jack Roy,[2] Brent A. French, PhD,[3] Frederick H. Epstein, PhD.[2] [1]*Electrical Engineering, University of Virginia, Charlotesville, VA, USA,* [2]*Radiology, University of Virginia, Charlotesville, VA, USA,* [3]*Biomedical Engineering, University of Virginia, Charlotesville, VA, USA.*

Introduction: Cardiac MR studies in genetically engineered mice have already elucidated the roles of numerous genes in the pathophysiology of ischemic heart disease (Yang et al., 2002). While image acquisition time can limit throughput in these studies, data analysis is perhaps an even greater limiting factor. Therefore, in addition to faster imaging, there is a need for fast and automatic data analysis. Furthermore, automatic data analysis has the potential to reduce intra-and inter-observer variability.

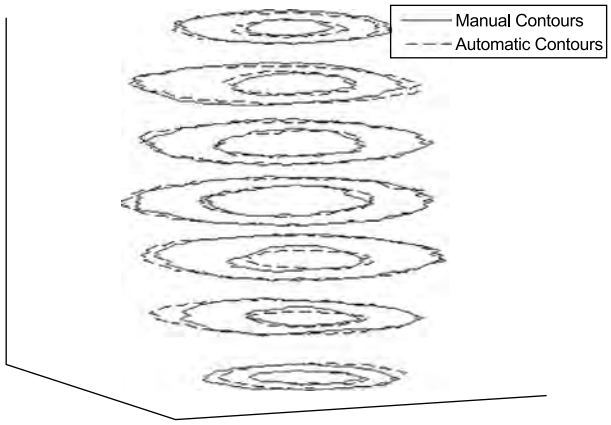

Figure 1. Example endocardial and epicacardial borders for one mouse heart.

Purpose: The purpose of this project was to develop an automated technique to segment the myocardial borders from cine MR images and infarct regions in gadolinium enhanced MR images of the murine heart. From these contours, myocardial mass and infarct size were computed.

Methods: Black-blood cine images and contrast-enhanced inversion recovery images covering the whole heart of 5 post-infarct mice were acquired using a 4.7 T MR scanner. For automatic segmentation, we fit two thin contours (snakes) to the epi-and the endocardial borders via Bayesian Markov chain Monte Carlo (MCMC) computation. The points $[(X_j,Y_j)]_{j=1\ldots N}$ on a snake are estimated through the maximization of the posterior probability: $p[(X_j,Y_j)]_{j=1\ldots N})$ is proportional to $p(G|[(X_j,Y_j)]_{j=1\ldots N})p([(X_j,Y_j)]_{j=1\ldots N})$, where G is a statistic, called the gradient inverse coefficient of variation (GICOV). The GICOV is defined as the ratio of the mean and the normalized standard deviation of image intensity derivatives computed in the outward normal direction over a snake $[(X_j,Y_j)]_{j=1\ldots N}$. The likelihood $p(G|[(X_j,Y_j)]_{j=1\ldots N})$ is non-central t-distributed when the snake is on a ramp edge corrupted with white Gaussian noise (Dong et al., 2004). G is maximal (minimal) when a contour lies along a strong, constant transition from bright to dark (dark to bright). From among a library of ellipses, the two ellipses with the maximum and the minimum G values are chosen as the initial contours representing the epi-and endocardial borders respectively. The prior distribution $p([(X_j,Y_j)]_{j=1\ldots N})$ is realized as a Markov Random Field (MRF) smoothness prior involving a first order neighborhood system (Li, 2001). The MRF prior constrains the snake to be smooth and be located near the initial ellipse. Next, Hastings' MCMC algorithm (Li, 2001) maximizes the posterior distribution estimating the epi-and endocardial borders. Fuzzy C-Means classification (Bezdek et al., 1999) was then used to classify pixels within the myocardium as infarcted and non-infarcted.

Results: An expert manually contoured the myocardial borders and infarcted regions of five murine hearts at end-sytole. The image pixel size in millimeters was $0.2 \times 0.2 \times 1$ for the cine images and $0.23 \times 0.23 \times 1$ for the gadolinium images. The proposed algorithm was then applied and compared to the manually-derived results. Figure 1 displays the manually-derived and automatically generated contours for one murine heart. The algorithm's average root mean squared error (RMSE) was 0.23 mm for the endocardial and epicardial borders. The average myocardial mass calculated by the algorithm was 105.4 ± 16.4 mg and had an average percent error of 3.8% compared to the manually-contoured result. The average automatically-calculated infarct size as a percent of myocardial mass was 34.7% ± 8.1% of left ventricular mass and the average error from the manually-contoured infarct size was 4.4%.

Conclusions: In this paper we demonstrated the feasibility of automating the calculation of myocardial mass and infarct size as a percent of myocardial mass. Future work will aim to further improve detection of the infarcted region in mice. Automatic analysis may significantly improve throughput in murine CMR studies.

REFERENCES

Bezdek, J. C., et al. (1999). Fuzzy models and algorithms for pattern recognition and image processing.

Dong, G., et al. (2004). *Automated Leukocyte Detection In Vivo. Asilomar Conference*.

Li, S. Z. (2001). *Markov Random Field Modeling in Image Analysis*.

Yang, Z., et al. (2002). *Circulation* 106:106–111.

395. Discrimination of Acute Myocardial Infarction from Scar Tissue Using the Blood Pool MR Contrast Medium Vistarem

Maythem Saeed, DVM, PhD,[1] Oliver Weber, PhD,[1] Randal Lee, MD, PhD,[2] Alastair Martin, PhD,[3] Loi Do, BS,[1] Philippe Robert, MS,[4] Claire Corot, PhD,[4] David Saloner, PhD,[1] Charles B. Higgins, MD.[1] [1]*Radiology, University of California San Francisco, San Francisco, CA, USA,* [2]*Medicine, University of California San Francisco, San Francisco, CA, USA,* [3]*Clinical Science, Philips Medical System, San Francisco, CA, USA,* [4]*MR imaging, Guerbet Group, Paris, France.*

Introduction: Extracellular MR contrast media provides excellent enhancement of acutely infarcted myocardium and scar tissue and the distinct enhancement is independent of infarct age (Kim et al., 1999; Fieno et al., 2000) despite the cellular and microvascular differences between acute and chronic (scar tissue) infarctions. Thus, new strategies are needed to discriminate acute infarction from scar tissue.

Purpose: The potential of the blood pool MR contrast medium Vistarem in discriminating acute myocardial infarction from scar tissue was tested in a swine model.

Methods: A midsternal thoracotomy was performed in 6 pigs. The LAD was occluded for 2 hrs/reperfusion. Animals

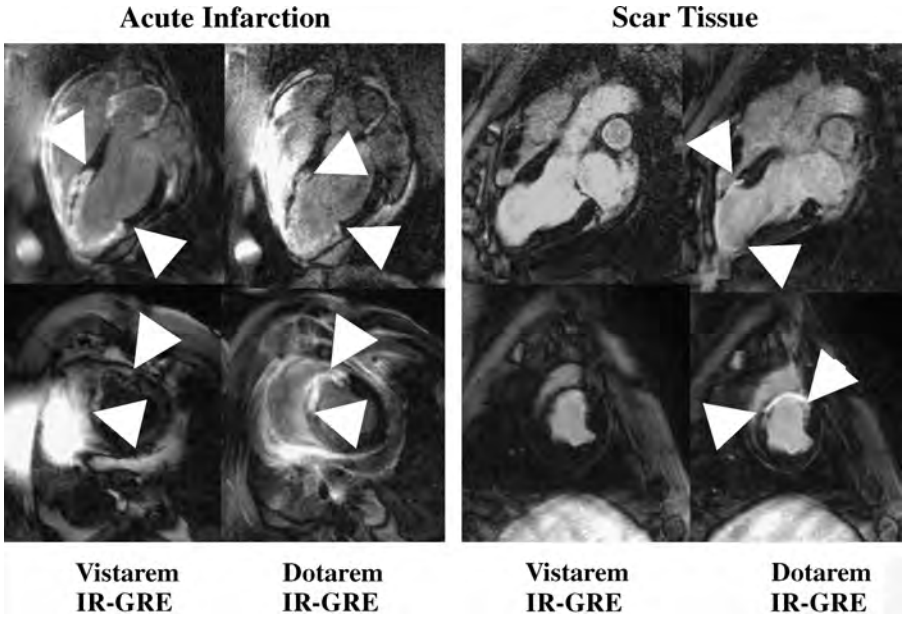

Figure 1.

were imaged at 3 days and 8 weeks after surgery using 1.5 T Intera scanner (Philips Medical Systems). In both sessions, images were acquired at baseline and after administration of 0.026 mmol/kg Vistarem and 0.1 mmol/kg Dotarem (Gd-DOTA; extracellular contrast medium, Guerbet Group, France). Inversion recovery gradient echo (IR-GRE), T1-weighted (T1-SE) and T2 (T2-SE) turbo-spin echo sequences were used to characterize the status of myocardium. Regional signal intensities were measured at baseline and every 10 min for 40 min post-Vistarem and for 20 min post-Dotarem. After the second imaging session, animals were euthanized and the hearts were stained with TTC to measure true infarction size. TTC-infarction size was compared to the spatial extent of enhancement on a slice-by-slice basis. All results were expressed as a mean ± SEM. A Student paired t-test was used for statistical analysis.

Results: SI ratio between infarcted and remote myocardium was 1.04 ± 0.05 on T1-SE on baseline images. On T2-SE, infarcted myocardium was visible as a bright region (SI ratio = 1.5 ± 0.1), but the borders were not defined. Vistarem and Dotarem provided clear delineation of infarcted myocardium (Figures 1 and 2). Peak enhancement was observed at 40 min post-Vistarem and at 20 min post-Dotarem, suggesting that accumulation of Vistarem in reperfused infarction is relatively slow. At 40 min post-Vistarem, SI ratio was 4.7 ± 0.7 on IR-GRE and 1.5 ± 0.1 on T1-SE. On IR-GRE, Dotarem provided greater enhancement (SI ratio = 7.9 ± 1.8, $p = 0.001$) than Vistarem, which can be attributed to larger fractional distribution volume and homogeneous distribution of Dotarem in infarction. The behavior of Vistarem in enhancing the scar tissue (8 weeks old) was different than in acute infarction. Vistarem did not enhance scar tissue (SI ratio = 1.1 ± 0.1 on IR-GRE and 1.1 ± 0.1 on T1-SE), which can be attributed to 1) poor vascularization and/or small blood volume, 2) impairment of microvascular permeability, 3) absence of interstitial edema and 4) the unique features of Vistarem. In contrast, Dotarem provided superb enhancement of the scar tissue on IR-GRE (7.2 ± 1.2) and moderate enhancement on T1-SE (1.5 ± 0.1) (Figures 1 and 2). The size of the enhanced regions in the acute phase was nearly

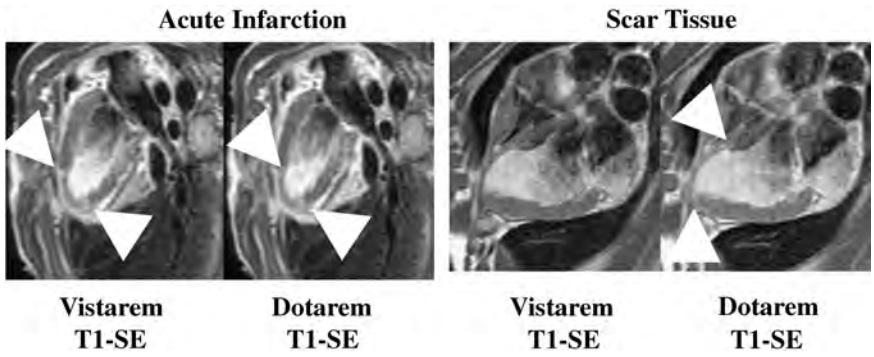

Figure 2.

identical after Vistarem (17.8 ± 2.1% of LV) and Dotarem (14.5 ± 3.1%, p = ns). During the 8 weeks evolution, the size of Dotarem-enhanced region on IR-GRE was smaller (12.1 ± 1.6%, $p = 0.01$) compared to the acute phase, but comparable to the true scar tissue size on TTC (12.2 ± 2.3%, p = ns). The reduction in size of Dotarem-enhanced region is related to the absence of peri-infarction zone, edema, hemorrhage, inflammation and replacement of myocardium by scar tissue. Vistarem did not provide differential enhancement, thus the size of scar tissue was not measured.

Conclusion:

1. Vistarem discriminates acute myocardial infarction from scar tissue and
2. Dotarem does not discriminate acutely infarcted myocardium from scar tissue, but it documents the presence of infarction. Thus, the combination of the two classes of MR contrast media can be used to characterize scarred myocardium and thereby more accurately direct the site for multi-potential stem cell delivery for the treatment of ischemic heart failure.

ACKNOWLEDGMENTS

This study was supported by grants from NIH (RO1HL07295) and Guerbet Group, France.

REFERENCES

Fieno, D. S., et al. (2000). *JACC*.
Kim, R. J., et al. (1999). *Circulation*.

396. In Vivo Cardiovascular Magnetic Resonance (CMR) Imaging to Detect Atherosclerosis with Macrophage-specific Gadolinium-containing Immunomicelles and Micelles

Vardan Amirbekian, Michael J. Lipinski, Juan C. Frias, Juan Gilberto S. Aguinaldo, Venkatesh Mani, Zahi A. Fayad.

Imaging Science Laboratories, Departments of Radiology and Medicine (Cardiology), The Mount Sinai School of Medicine—The Zena and Michael A. Wiener Cardiovascular Institute, New York, NY, USA.

Background: The ability to detect the uptake of gadolinium (Gd)-containing compounds in macrophage cells with cardiovascular magnetic resonance imaging (CMR) may enable non-invasive detection of atherosclerotic plaque. Immunomicelles and micelles have been shown to improve in vitro and ex vivo assessment of macrophages using MRI. The goals of this ongoing study are to evaluate the in vivo uptake of immunomicelles (micelles containing an antibody), micelles, and standard contrast agents in the murine aorta using in vivo CMR and to determine whether immunomicelles and micelles improve in vivo imaging of atherosclerotic plaque in apolipoprotein E knockout (ApoE KO) mice using CMR.

Methods: In previous experiments micelles, immunomicelles, and standard (i.e., Gd-DTPA) paramagnetic contrast agents were tested in the murine RAW 264.7 macrophage cell line. Cells were incubated for 2 hours with different concentrations of Gd-DTPA, micelles, and immunomicelles in culture flasks. The cells were centrifuged into cell pellets and imaged using a 1.5 T MR system with an inversion recovery spin echo sequence to determine the T1 of each cell pellet. Ex vivo analysis was performed using a 9.4 T MR system with a high-spatial resolution sequence (70 μm^3). In the current ongoing in vivo study micelles, immunomicelles, and standard (i.e., Gd-DTPA) paramagnetic contrast agents were tested in ApoE KO mice. Mice were imaged at baseline with a 9.4 T MR system with a high-spatial resolution sequence (CMR). The mice were then imaged at intervals following a tail injection of either micelles, immunomicelles, or standard (i.e., Gd-DTPA) paramagnetic contrast agents.

Results: Previous experiments showed that pellets of micelle-treated cells had a decreased T1 vs. Gd-DTPA-treated cells ($p < 0.0001$). Incubation with immunomicelles decreased T1 vs. micelles ($p < 0.05$). Confocal microscopy

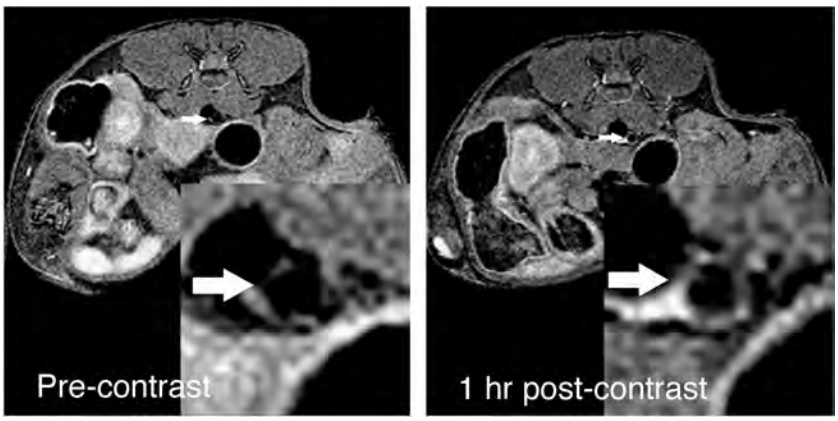

Figure 1.

demonstrated uptake of fluorescently-labeled immunomicelles and micelles. Ex vivo analysis demonstrated a 59% signal intensity increase in aortas incubated with immunomicelles vs. control and a 19% increase in signal for micelles vs. control. In previous in vivo work enhancement of atherosclerotic plaque was noted following injection of immunomicelle contrast agent (Please see Figure 1). In the current ongoing in vivo study enhancement of atherosclerotic plaque was noted in the murine aortas following injection of immunomicelles and micelles.

Conclusion: Immunomicelles and micelles improve in vitro and ex vivo assessment of macrophages using MRI. The current ongoing in vivo study shows promising results in the detection of atherosclerotic vascular disease using CMR. Immunomicelles may prove useful in the detection of high-macrophage density typical of high-risk plaques.

397. Direct Imaging of Regional Myocardial Function Using Strain ENCoded (SENC) MRI at 3 Tesla

Li Pan, MSE,[1] Matthias Stuber, PhD,[2] Nael F. Osman, PhD.[2]
[1]*Department of Biomedical Engineering, Johns Hopkins School of Medicine, Baltimore, MD, USA,* [2]*Department of Radiology, Johns Hopkins School of Medicine, Baltimore, MD, USA.*

Introduction: High field ($\geq$ 3.0 T) magnetic resonance imaging (MRI) systems have been demonstrated to produce better signal-to-noise-ratio (SNR) than that of 1.5 Tesla system. Due to the need for high temporal and spatial resolution, cardiac imaging will considerably benefit from the improvement in SNR at high field strength (Nayak, 2004). However, cardiac imaging at 3 T remains challenging because of several impediments at high field, such as increased B_0 inhomogeneity, reduced T_2^*, increased chemical shift and power deposition limitations. SENC (Osman, 2001) has been proposed as a technique which can direct image the cardiac contractility by producing cine functional images. In this study, we verify the ability of 3 T system to image the regional myocardial function using SENC. A spiral imaging sequence in combination with SENC was implemented. The acquired images were compared with those obtained on 1.5 T system.

Purpose: To direct image the regional myocardial function using SENC at 3 Tesla.

Methods: Image Acquisition: MR imaging was performed on clinical 1.5 T and 3 T MR whole body systems (Gyroscan Intera, Philips Medical System, Best, The Netherlands). The images were acquired on two normal human subjects with informed written consent. To reduce the acquisition time, the low-and high-tuning (required for SENC imaging) were applied alternating throughout the cardiac cycle. SENC images were acquired in one breath-hold of 12 heartbeats. A water selective spectral spatial excitation (1-3-3-1 binomial pulse) was used for fat suppression. The imaging parameters were: slice thickness = 10 mm, FOV = 350 mm, matrix size = 176 $\times$ 176, spiral interleaves = 12, spiral acquisition window = 12 ms, flip angle = 40. The temporal resolutions for 1.5 T and 3 T were 22.4 ms and 17.9 ms, respectively. SENC functional images were generated offline using a custom-built software written in MATLAB (Mathworks, Inc., Natick, MA).

SNR Evaluation: SNR measurements for the SENC imaging were computed from the anatomical images, generated by the summation of the low-and high-tuning images of the same cardiac phase. Two user-defined region of interests (ROIs) of signal were placed in the septal and the lateral wall of the left ventricle and the ROI of noise was defined anterior to the chest wall. To eliminate the DC-biased signal offset in the magnitude images, the SNR was computed by (Stissue- Snoise)/SDnoise, where Stissue was the mean intensity of the defined ROI of signal, Snoise was the mean intensity of the noise, and SDnoise was the standard deviation of the noise. (Bornert, 2001)

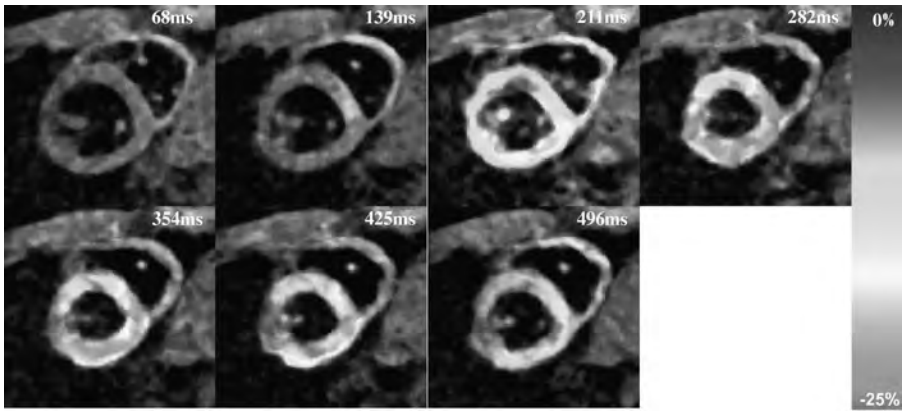

Figure 1. SENC functional image sequence (7 out of 30 timeframes, covering 70% of the cardiac cycle) in short-axis view acquired on 3T system. The color bar shows the scale of the Eulerian longitudinal strain, with maximum contracton shown as red and no-contraction shown blue.

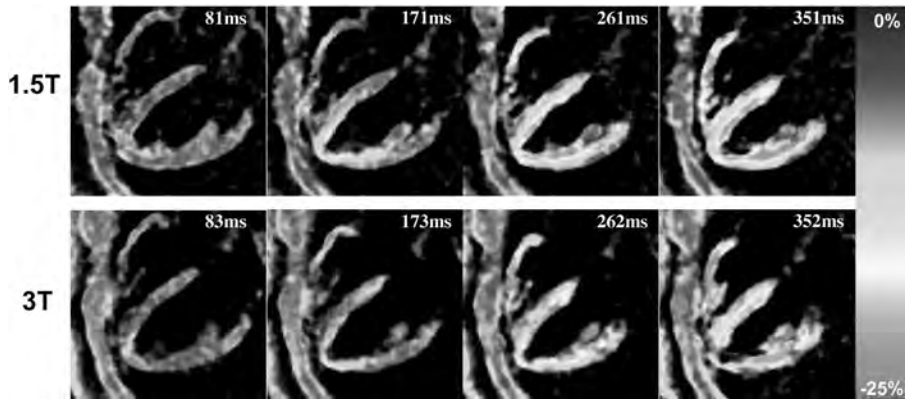

Figure 2. SENC functional image sequence (4 out of 19 for 1.5T and 4 out of 24 for 3T) in four-chamber view acquired on 1.5T and 3T systems. Both image series cover around 50% of the cardiac cycle. The color bar shows the scale of the Eulerian circumferential strain.

Results: Fig. 1 shows the cine SENC functional images (in the short-axis view) acquired on the 3 T system from one human subject. The image sequence shows a smooth evolution of the longitudinal strain in colors from blue (no contraction) to red (contraction). From the other human subject, two series (1.5 T and 3 T) of cine SENC functional image sequences in the four-chamber view are shown in Fig. 2. The two sequences show similar circumferential strain measurements on both left and right ventricles. The measured SNR of the septal and the lateral wall are 9.91 and 9.74 for 1.5 T system and 14.89 and 14.95 for 3 T system. This is corresponding to a 50% and 53% improvement of SNR on 3 T system.

Conclusion: Regional circumferential contraction and longitudinal shortening of both the left and right ventricles can be examined using SENC imaging at 3 T. 3 T system provides similar strain measurements as that acquired at 1.5 T system and offers improvements in SNR for SENC imaging.

ACKNOWLEDGMENTS

This research was supported by grant RO1 HL072704.

398. Instability of Perfusion Defect Size Over Time Despite Permanent Coronary Occlusion

Gauri S. Tilak, Li-Yueh Hsu, Andrew E. Arai, Anthony H. Aletras. *Laboratory of Cardiac Energetics, National Institutes of Health, Bethesda, MD, USA.*

Purpose: In a canine model of a non-reperfused acute myocardial infarction, we hypothesized that the area at risk observed on perfusion MRI approximately 6 hour into the occlusion would be of similar size to the hypoperfused area observed two days after later.

Methods: Eight mongrels underwent open chest permanent coronary occlusion of the left anterior descending (LAD) coronary artery. First pass rest perfusion CMR was performed approximately 6 hours after surgery (Day0) and again two days post-intervention (Day2). First pass perfusion imaging was performed with a multi-shot EPI FGRE perfusion sequence using slice interleaved TSENSE (Kellman et al., 2003) during contrast injection (Gd-DTPA, 0.1 mmol/kg) with the following parameters: field of view = 28 × 14 cm^2, matrix = 128 × 96, TE = 1.5 ms, TR = 7.2 ms, T_{SAT} = 50 ms. Three to four 8 mm slices were acquired to cover the left ventricle during each heartbeat. The size of perfusion defects was measured by computer assisted planimetry. All results are reported as % area of left ventricular (LV) slice. Circumferential shortening (CS) and radial thickening (RT) were measured with displacement encoding with stimulated echoes (DENSE) on Day0 and Day2 to quantify regional contractile function.

Results: Typical perfusion images acquired on Day0 and Day2 are shown in Figure 1. Histopathology depicting the infarcted territory is shown via negative TTC staining. On Day2, the apparent perfusion abnormality was 37 ± 4 percent LV compared to the 27 ± 3 perfusion defect imaged on Day0. These results were significantly different at ($p < 0.05$). In all 8 animals, the perfusion defect decreased in size over time. CS and RT regional contractile function as quantified by DENSE was not significantly different between Day0 and Day2 (CS: Day0 37.4 ± 4.5 Day2 36.5 ± 5.1, $p = 0.89$, RT: Day0 38.8 ± 4.6 Day2 36.1 ± 4.5, $p = 0.72$).

Conclusion: Our results indicate that perfusion territories do not remain stable two days following infarction in non-reperfused settings. Potentially, recruitment of collateral vessels or an early inflammatory response could contribute to the apparent decrease in the hypoperfused area over time. Note that the size of the hypokinetic region does not change significantly over the two day period despite the changes observed in the perfusion scans. The timing with which these perfusion changes take place is somewhat surprising since the first perfusion study was performed 6 hours into the infarction- a time one we had anticipated maximal recruitment of collateral circulation should have occurred. Time-course studies which depend on accurate determination of the area at

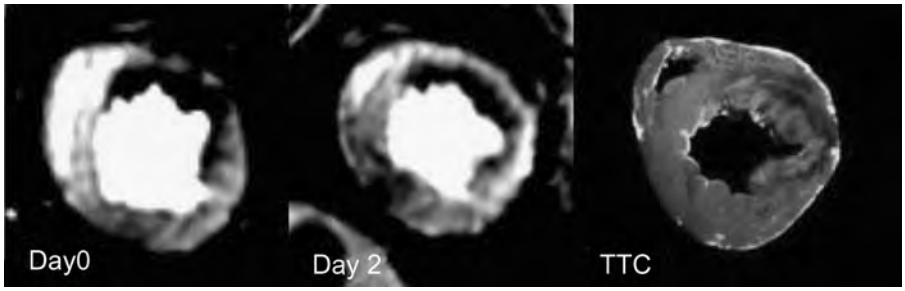

Figure 1.

risk can not rely on measurements other than those acquired during the first hours of the occlusion.

REFERENCE

Kellman, P., et al. (2003). *MRM.*

399. Imaging Infarct Expansion in Mice Using a Contrast-Enhanced Inversion Recovery MRI Sequence

Brent A. French, PhD, Ronald J. Beyers, MS, Florent C. Sureau, MS, Zequan Yang, PhD, Wesley D. Gilson, PhD, R Jack Roy, Stuart S. Berr, PhD, Frederick H. Epstein, PhD. *Biomedical Engineering, University of Virginia, Charlottesville, VA, USA.*

Introduction: Infarct expansion contributes importantly to left ventricular (LV) remodeling following large anteroapical myocardial infarction (MI). Transgenic and knockout mice can be used to elucidate the molecular mechanisms underlying these processes. We have previously used heavily T1-weighted contrast-enhanced gradient-echo MRI for infarct imaging by delayed hyperenhancement one day after experimental MI in mice.

Purpose: The goal of this study was to develop an inversion recovery (IR) sequence with adequate sensitivity to image delayed hyperenhancement throughout 4 weeks of infarct expansion and LV remodeling in mice post-MI.

Methods: An ECG-gated IR gradient echo sequence was implemented on a 4.7 T Varian scanner. To null nonenhanced myocardium at 4.7 T where the T1 of myocardium is approximately 1300 ms, parameters were TR = 3 s, TI = 450–480 ms, TE = 3 ms, flip angle = 90°. Six mice were imaged at baseline and 1, 3, 7, 14 days after experimental 60 min LAD occlusion followed by reperfusion and four mice were imaged at 28 days post-MI. IR imaging was performed 15–40 min after infusion of Gd-DTPA (0.3–0.6 mmol/kg). For each mouse, the entire LV was covered using 6–8 short-axis slices each 1 mm thick. Image analysis was performed in Matlab to determine LV volumes and mass as well as to determine infarct size, both as a percent of LV mass and percent circumferential extent.

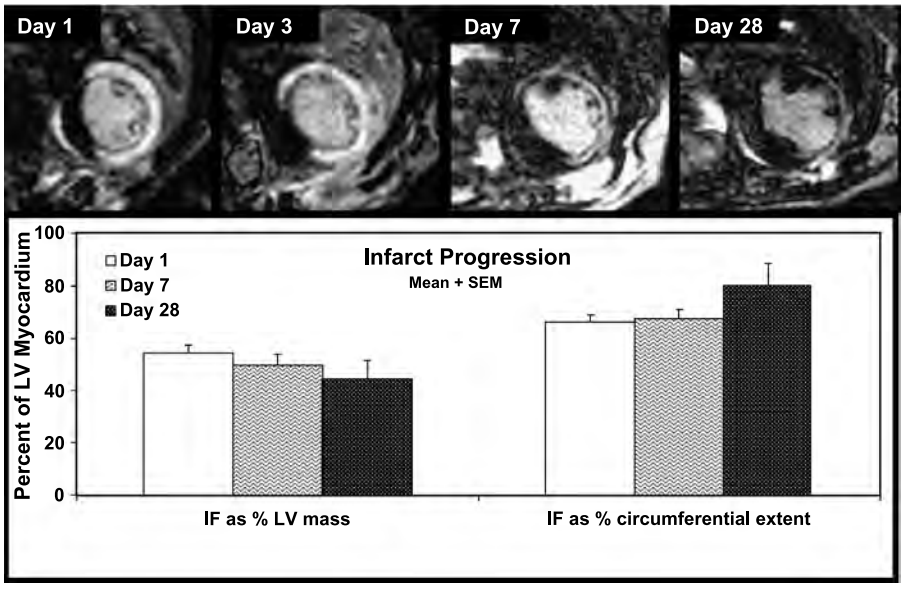

Figure 1.

Results: IR gradient echo MRI provided high contrast images depicting the temporal evolution of infarct expansion during the first 4 wks after MI. Example images at days 1, 3, 7 & 28 demonstrating infarct thinning, expansion and LV dilation are shown at the top of Fig. 1. The infarct-noninfarct contrast to noise ratio was 11.0 ± 0.7, 9.1 ± 0.5 & 11.8 ± 1.8 (mean ± SEM) at days 1, 7 & 28, respectively. As shown in the graph below, image analysis indicated a gradual 10% decline in infarct size as percent LV mass. Conversely, the circumferential extent of infarction increased by 14% during the same period of time.

Conclusions: This study represents the first time in which the standard method for infarct size assessment at early time points after MI (infarct as percent LV mass) has been related to the standard method for infarct size assessment at late time points after LV remodeling (circumferential extent of infarction). Furthermore, the results of this study provide the first direct serial evidence for both infarct expansion and infarct resorption in a mouse model of MI. These methods should prove useful in the serial assessment of the molecular mechanisms underlying infarct expansion and LV remodeling using transgenic and knockout mice in conjunction with mouse models of reperfused MI.

400. Diffusion Tensor MRI Sensitively Delineates Myocardial Infarction in Rat Heart without Exogenous Contrast Agents

Junjie Chen, MS, Wei Liu, ScD, Xiaoxia Yang, BS, Huiying Zhang, MS, Liz Lacy, BS, Samuel A. Wickline, MD, Xin Yu, ScD. *Cardiovascular MR Laboratories, Washington University, Saint Louis, MO, USA.*

Introduction: Water diffusivity in physiological tissue is sensitive to changes in the organization and structure of its molecular enviroment. Clinically, changes in apparent water diffusion contants have been used to evaluate stroke patients. After myocardial infarction (MI), myocardium undergoes structural changes including cell death, myofiber disarray and collagen deposition. Accordingly, diffusion tensor MRI (DTMRI) of formalin-fixed post-infarct heart showed increased water diffusivity and decreased diffusion anisotropy in the infarct zone Chen et al, 2002, 2003. In the present study, we aimed to define the potential of DTMRI for detecting MI in viable perfused hearts.

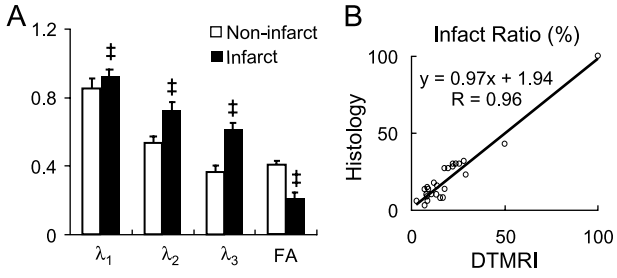

Figure 1.

Methods: MI was created in rats (n = 10) by permanent ligation of the left coronary artery. Four weeks after surgery, the hearts were excised and cannulated for retrograde perfusion. Subsequently, the hearts were perfusion-arrested in diastole with KCl. DTMRI of perfused (viable) hearts was performed on a Varian 4.7 T scanner. A multi-slice spin-echo sequence with diffusion sensitizing bipolar gradient was used. Diffusion weighted images were acquired on 7 short axis slices that covers the whole left ventricle. Diffusion encoding gradients were applied in 6 non-collinear directions. The b-value was 948 s/mm^2. Image voxel size was 156 μm × 156 μm × 1 mm. The apparent diffusion tensor was calculated from diffusion-weighted images. Diffusion anisotropy was analyzed with the use of fractional anisotropy (FA). The three eigenvalues (λ_1, λ_2, λ_3) and the trace of diffusion tensor were normalized by λ_{mean} of the residual water in the left ventricle. Infarct location and size were determined from the zones exhibiting greater increase in λ_3, which was defined objectively as the region where λ_3 was 2 SD above the mean relative to the remote, non-infarct myocardium. Following the DTI study, the hearts were sliced in 1 mm increments from base to apex along the LV long-axis to enable direct correlation of slice locations between MRI and histological analysis. Slices were stained with Masson's trichrome for identification of infarct scar tissue. The histological determined infarct size and ratio on each short-axis slice were correlated with the corresponding results from DTMRI.

Results: A three eigenvalues of diffusion tensor increased significantly in the infarct zone ($p < 0.001$ compared to that in non-infarct myocardium), indicating increased water diffusivity. The maximal increase (about 60%) was observed for λ_3. The FA decreased about 50% in infarct zone, indicating decreased diffusion anisotropy (Figure 1A). The infarct ratio measured by DTMRI showed strong correlation with that measured by histological analysis (Figure 1B, R = 0.97).

Conclusion: Within four weeks after MI, water diffusivity was increased and diffusion anisotropy was decreased significantly in the infarct zone of viable heart. The physical extent of increase in diffusivity was strongly correlated with histological determined infarct size. These findings were consistent with previous observations in fixed tissues. Increased extracellular space in infarct zone after the death of myocyte might account for the observed changes in water diffusivity and diffusion anisotropy. Furthermore, infiltration of spherically shaped cells (inflammatory cells, myofibroblasts, etc.) and collagen fiber disarray in scar tissue are potentially responsible for the decrease in diffusion anisotropy. We conclude from the results that DTMRI is sensitive to microscopic structural changes in post-infarct remodeling myocardium. Thus, DTMRI might permit direct assessment of infarct scar and cardiac structural remodeling without the need for exogenous contrast agent if it could be applied clinically.

REFERENCES

Chen, J., et al. (2003). *Am. J. Physiol.* 285:H946–H954.
Chen, J., et al. (2002). *JCMR* 4:68–69.

401. Differences in Contrast Agent Relaxivity in Blood and Myocardium at 1.5 T and 3 T

Puneet Sharma,[1] John N. Oshinski.[2] [1]*Biomedical Engineering, Georgia Tech, Atlanta, GA, USA,* [2]*Radiology, Emory University, Atlanta, GA, USA.*

Introduction: It is well known that relaxation rates (R_1) decrease at higher fields for most tissues. The longitudinal relaxivity of a contrast agent (r_1, $mM^{-1}\,s^{-1}$) is the change in relaxation rate (R_1, s^{-1}) per unit concentration of contrast agent ([CA], mM). Relaxivity is known to depend on the magnetic field strength (Rinck et al., 1999) *and* the macromolecular environment of the tissue compartment (Stanisz et al., 2000). As a result, the post-injection image contrast between blood and myocardium at 1.5 T cannot be assumed to be the same at 3 T. Knowledge of relaxivity behavior at higher fields will allow predictions of R_1 and image contrast differences between fields strengths in clinical applications such as delayed enhancement imaging.

Purpose: The purpose of this study was to quantify the relative change in gadodiamide (Gd-DTPA-BMA) relaxivity in blood and myocardium, and between 1.5 T and 3 T during steady-state conditions.

Methods: T_1 measurements were performed in ten healthy volunteers pre-contrast and every 5 minutes for 35 minutes after contrast administration (Gd-DTPA-BMA, 0.1–0.2 mmol/kg) at 1.5 T (Philips Intera) and 3 T (Siemens Trio). T_1 was calculated before contrast injection from an inversion recovery (IR), single-shot, balanced steady-state free precession (b-SSFP) sequence (FOV: 300 mm; 256 matrix; 112 lines; TR/TE/a = 2.5/1.2 ms/40 deg; 8 mm thickness) using five inversion times (TI): 400–1500 ms, and least-squares monoexponential fitting. Post contrast T1 values were determined from a 2-TI (150 and 650 ms) IR b-SSFP sequence with 3 heartbeat segment intervals (FOV: 300 mm; 256 matrix; 42 lines/segment; TR/TE/a = 3.0/1.5 ms/40 deg; 8 mm thickness). T_1 was calculated using a ratio estimation (Sharma et al., 2004). At each field strength, the T_1 data was used to determine the myocardium-to-blood partition coefficient (λ), which is related to the relative r_1, using the relationships (Wendland et al., 1997):

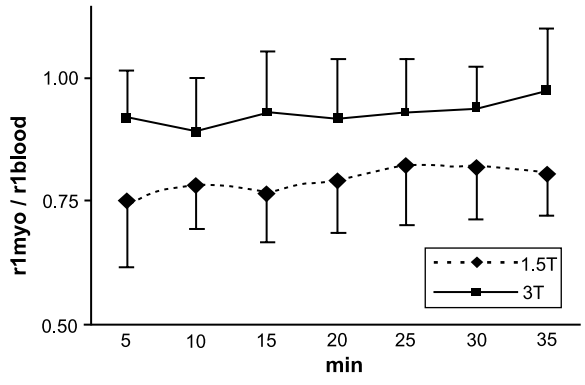

Figure 1.

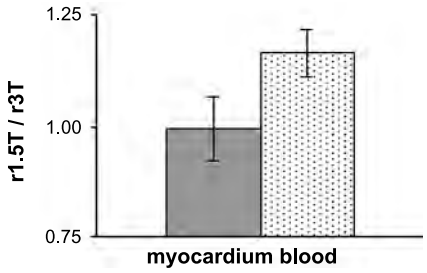

Figure 2.

$$R_1 = 1/T_1;\ \Delta R_1 = R_{1post} - R_{1pre} = r_1[Gd];$$
$$\lambda = \Delta R_{1myo}/\Delta R_{1blood} = K\, r_{1myo}/r_{1blood};$$

where [Gd] is the compartmental concentration of gadodiamide and K relates the fractional extracellular space of myocardium (0.35) and blood (0.60), and was assumed to be 0.58. The relative change in relaxivity between fields, $\Delta R1_{1.5\ T}/\Delta R1_{3\ T} = r_{1.5\ T}/r_{3\ T}$, was quantified separately for both myocardium and blood.

Results: The myocardium-to-blood partition coefficient remained constant from 5 to 35 minutes post-contrast at both 1.5 T (0.46 ±.06) and 3 T (0.54 ±.06), confirming an equilibrium Gd distribution between compartments. However, λ was significantly different between 1.5 T and 3 T ($p < 0.001$), despite using the same contrast agent dose for a given subject at each field strength. Hence, there was a significant difference in r_{1myo}/r_{1blood} between 1.5 T and 3 T (Fig. 1), suggesting r_1 is *both tissue and field dependent*, with Gd r_1 in myocardium around 20% lower than Gd r_1 in blood at 1.5 T, but only 10% lower at 3 T. The relative field-dependent change in compartmental r_1 is shown in Fig. 2. On average, $r_{1.5T}/r_{3T}$ was larger in blood (1.18 ±.10) than myocardium (1.01 ±.09). This implies that r_1 in blood decreases slightly at 3 T, while r_1 in myocardium remains relatively equal between 1.5 T and 3 T.

Conclusions: A constant Gd r_1 in myocardium suggests that Gd exerts the same enhancement effects at 1.5 T and 3 T, while the Gd effects in blood are greater at 1.5 T than 3 T. The lower Gd r_1 in blood at 3 T potentially enables greater tissue contrast with subendocardial infarcts.

REFERENCES

Rinck, P. A., et al. (1999). *Eur. Radiol.* 9:998–1004.
Stanisz, G. J., et al. (2000). *MRM* 44:665–667.

Sharma, P., et al. (2004). *JCMR* 6:346.
Wendland, M. F., et al. (1997). *MRM* 37:448–456.

402. In Vivo MR Imaging of Magnetically Labelled Human Embryonic Stem Cells After Itramyocardial Transplantation

Tommi Tallheden,[1] Ulf Nannmark, PhD,[2] Malin Lorentzon,[3] Olivier Rakotonirainy, PhD,[3] Anders Lindahl, MD, PhD,[4] Bassam Soussi, PhD,[3] Finn Waagstein, MD, PhD,[3] Elmir Omerovic.[3] [1]*Sahlgrenska University Hospital, Department of Clinical Chemistry and Transfusion Medicine, Gothenburg, Sweden,* [2]*Faculty of Odontology, Gothenburg, Sweden,* [3]*Sahlgrenska University Hospital, Wallenberg laboratory, Gothenburg, Sweden,* [4]*Sahlgrenska University Hospital, Department of Clinical Chemistry and Transfusion Medicine, Gothenburg, Sweden.*

Introduction: Human embryonic stem cells (hES) have emerged as a potentially new therapeutic approach for treatment of heart diseases. Methods.

Purpose: The aim of this study was to evaluate the feasibility of magnetic labelling and visualisation of hES with magnetic resonance imaging in vivo.

Methods: hES were established and expanded according to standard procedures. The cells were magnetically labelled by addition of SPIO (small particles of iron-oxide) agent dextran-coated ferrum-oxide particles (Endorem®) to the culture medium. Accumulation of SPIO in hES was assessed by Prussian Blue staining and electron microscopy. Viability of

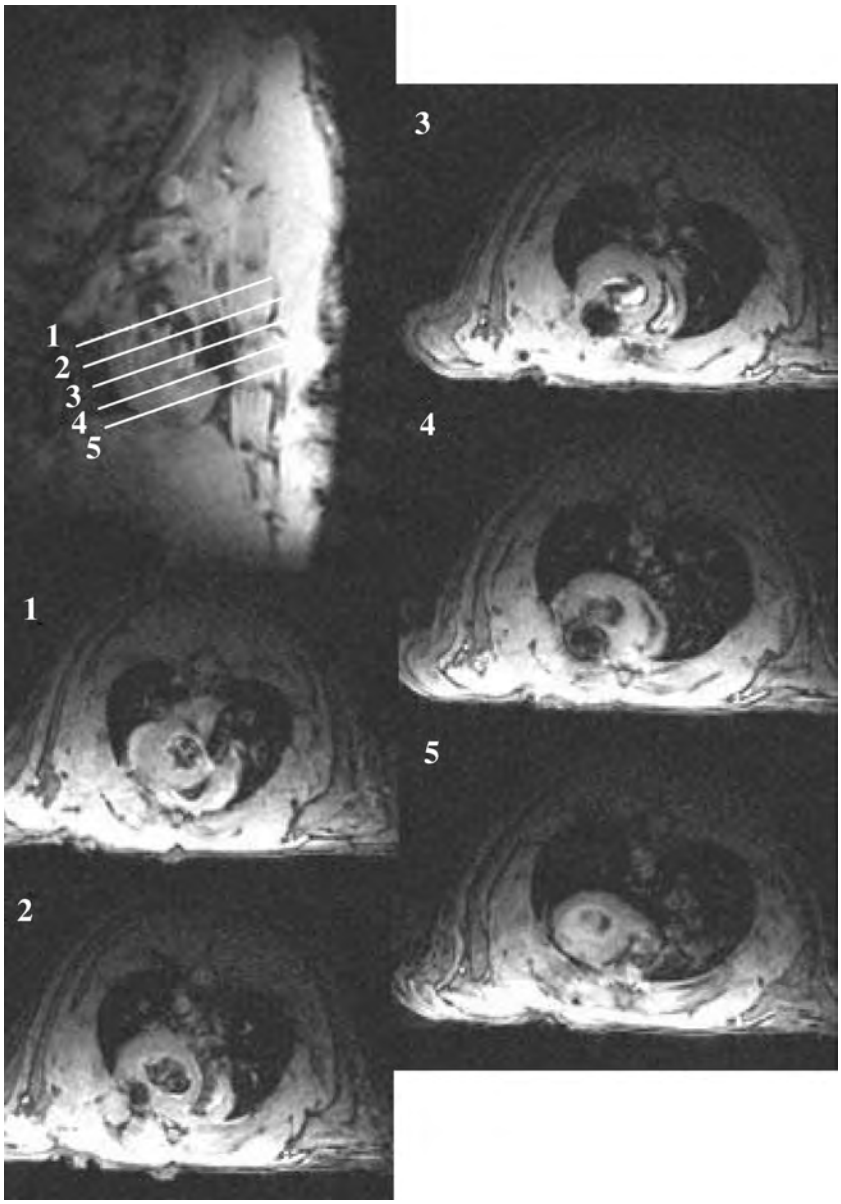

Figure 1.

the cells was assessed by trypan-blue. In vivo MR imaging was performed on 2.35 T Bruker Biospec magnet. Male Sprague-Dawely rats were used. Magnetically labeled hES (~ 300 000) were injected into anterior LV wall. Cardiac gated gradient echo pulse was used with the following parameters, FOV = 8 cm, matrix = 256 × 192, TR 150 ms, TE 8 ms. In vivo MRI was perforemed 24 h and 5 days after the transplantation.

Results: hES appeared to be unaffected by magnetic labelling and maintained their ability to proliferate and differentiate and in the culture. No agent for membrane permeabilisation was needed for facilitation of intracellular SPIO accumulation. Prussian Blue and electron microscopy have revealed numerous iron particles in the cytoplasm of hES. On T2-weighted images, the labelled cells have shown well-defined hyopintense areas at the site of injection in anterior LV wall both in vitro in the mouse heart (Figure 1) and in vivo in the rat heart (Figure 2).

Conclusions: It is feasible to magnetically label and visualise hES. MR visualisation of magnetically labelled hES may be a valuable tool for in vitro and in vivo tracking of hES.

403. Blood Pool Agent Demonstrates Prolonged Visualization of Microvascular Obstruction in Acute Myocardial Infarction

Oliver M. Weber, PhD,[1] Randall J. Lee, MD, PhD,[2] Alastair J. Martin, PhD,[3] Charles B. Higgins, MD,[1] Maythem Saeed, DVM, PhD.[1] [1]*Department of Radiology, University of California, San Francisco, San Francisco, CA, USA,* [2]*Department of Medicine, University of California, San Francisco, San Francisco, CA, USA,* [3]*Philips Medical Systems, Best, The Netherlands.*

Introduction: It has been shown that no-reflow zones (as determined 48–96 hours after reperfused coronary occlusion) denote irreversibly damaged tissue, the extent of which correlates well with infarct size (Kaul and Ito, 2004). Regions of microvascular obstruction (MO) can be seen briefly (90 seconds) in T1-sensitive perfusion sequences after bolus administration of extravascular contrast agents (Wu et al., 1998). Due to requirements on imaging speed, spatial resolution in these images is usually moderate at best. The transient effect also limits the time available for higher resolution MRI.

Purpose: To investigate the potential of the intravascular (blood-pool) contrast agent P792 (Vistarem, Guerbet Group, Aulnay Sous Bois, France) in delineating and sizing MO in reperfused acute myocardial infarction.

Methods: Experiments were performed on six farm pigs (30–32 kg). To create a myocardial infarction, a midsternal thoracotomy was performed and the left anterior descending coronary artery was dissected and occluded for 2 hours, followed by reperfusion. The chest was closed and sutured, and the animals were allowed to recover. Three to four days after surgery, MRI was performed under anesthesia on a 1.5 T clinical MR imager (Philips Medical Systems, Best, The Netherlands). Steady-state free-precession (SSFP; TR, 3.6 ms; TE, 1.8 ms; FOV, 260 mm; matrix, 176) and T1-weighted turbo-spin echo imaging (TR, 1 heart beat; TE, 20 ms; FOV, 240 mm; matrix, 176) was performed at baseline, for 40 minutes after administration of 0.026 mmol/kg Vistarem, as well as 20 minutes after administration of 0.1 mmol/kg Dotarem (Gd-DOTA; extravascular contrast agent; Guerbet) in short and long axis views. Images were processed in ImageJ (Research Services Branch, NIH, Bethesda, MD). Regions of interest were manually drawn in normal myocardium, at the rim of the infarct, and at the core of the infarct. Signal intensity (SI) and size were determined.

Table 1. Relative SI in infarcted zone (normal myocardium = 100)

	Core	Rim
P792-5 minutes	83 ± 12	122 ± 11[a]
P792-20 minutes	90 ± 11	133 ± 16[a]
P792-40 minutes	99 ± 12	145 ± 13[a,b]
Gd-DOTA-20 minutes	130 ± 44	153 ± 34[b]

[a] $p < 0.05$ vs. rim.
[b] $p < 0.05$ vs. normal.

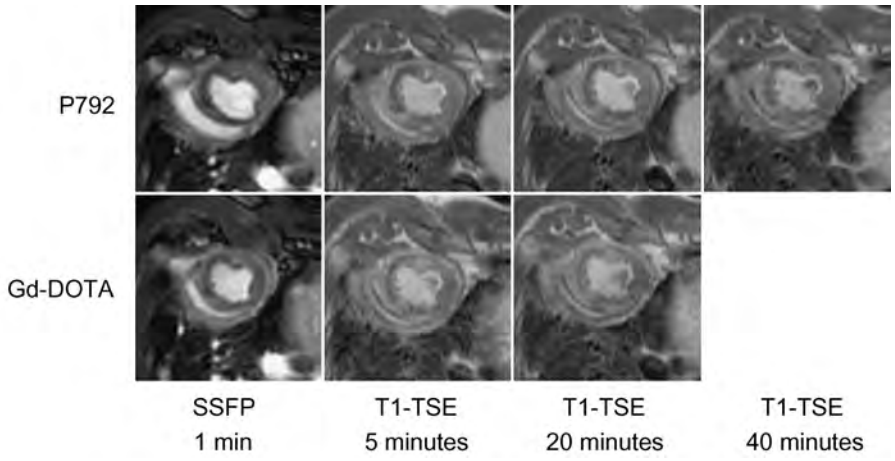

Non-parametric repeated measures analysis of variance (Friedman test) with Dunn's multiple comparisons post-test was performed at a significance level of 5%.

Results: Immediately after bolus injection of P792, SI on SSFP in the MO zone was 20 ± 9% lower than in the normally enhancing myocardium ($p = 0.015$). After Gd-DOTA, a signal loss of 12 ± 4% was observed ($p = 0.03$). SSFP and T1-weighted TSE showed similar hypo-enhanced areas (140 ± 40 mm^2 vs. 148 ± 42 mm^2; p = n.s.) 2–5 minutes after injection. The Table 1 summarizes SI on the T1-TSE images over time, expressed as percentage of SI in normal myocardium. The size if P792-enhanced region at 40 minutes was 18.8 ± 5.1% of the total LV mass. The reperfused region was more homogeneously enhanced 20 minutes after administration of Gd-DOTA (see Table 1). The Figure shows short axis images with MO in the septal wall.

Discussion: After injection of P792, both SSFP and T1-TSE showed MO as a hypo-enhanced region. The delineation persisted for more than 40 minutes. After injection of Gd-DOTA, only 1/6 animal showed minor underperfusion at the core, whereas 5/6 showed enhancement at the core, but less than at the rim.

Conclusion: P792 provided prolonged delineation of MO. It also showed higher occurrence rate of MO compared to the extravascular contrast agent. P792 is therefore suitable for predicting left ventricular remodeling.

ACKNOWLEDGMENTS

This study was supported by grants from NIH (RO1HL07295) and Guerbet Group, France.

REFERENCES

Kaul, S., Ito, H. (2004). Microvasculature in acute myocardial ischemia: part II: evolving concepts in pathophysiology, diagnosis, and treatment. *Circulation* 109:310–315.

Wu, K. C., Zerhouni, E. A., Judd, R. M., et al. (1998). Prognostic significance of microvascular obstruction by magnetic resonance imaging in patients with acute myocardial infarction. *Circulation* 97:765–772.

404. The Acute Cardiac Allograft Rejection is Heterogeneous and can be Non-invasively Monitored In Vivo with MRI by the Two-Pronged Methods

Yijen L. Wu, PhD,[1] Kazuya Sato, MD,[1] John B. Williams, PhD,[1] T. Kevin Hitchens, PhD,[1] Hsun-Hsien Chang, MS,[2] Jose Moura, PhD,[2] Chien Ho, PhD.[1] [1]*Pittsburgh NMR Center for Biomedical Research, Carnegie Mellon University, Pittsburgh, PA, USA,* [2]*Electrical and Computer Engineering Department, Carnegie Mellon University, Pittsburgh, PA, USA.*

Introduction: The current gold standard for diagnosing and staging rejection after organ transplantation is biopsy, which is not only invasive but also prone to sampling errors. The regiment for treating acute rejection after heart transplantation varies from center to center, partly because of lacking sensitive and reliable indexes for assessing the status of myocardial rejection. The goal of this study is to establish sensitive and reliable indexes with cardiac MRI for non-invasive and early detection of acute cardiac allograft rejection. We have used a novel two-pronged approach to detect acute cardiac allograft rejection using our rodent transplantation model. First, we use MRI to detect immune cell infiltration at the rejection sites by monitoring the accumulation of dextran-coated ultra-small superparamagnetic iron oxide (USPIO)-labeled immune cells in vivo. Second, we use tagging to detect regional myocardial functional loss resulting from acute rejection.

Methods:

1. Animal model: We developed a new abdominal heterotopic working heart and lung transplantation model in rats using DA to BN transplantation pairs. The transplanted hearts receive proper pressure pre-load and exhibit similar cardiac outputs and ventricular pressure close to those in native hearts.
2. MRI methods: EKG and respiration gated cine imaging was used to evaluate USPIO accumulation and cardiac function with the in-plane resolution of 156 μm. Tagging was achieved by a modified DANTE sequence. All MRI scans were performed on Bruker AVANCE 4.7-T system.
3. USPIO labeling: Immune cells, mostly macrophages, are labeled in vivo by direct intravenous injection of USPIO particles 1 day prior to MRI scans.

Results: We have previously shown that immune cells, particularly macrophages, accumulated in the rejection sites can be detected non-invasively with MRI by in vivo labeling immune cells with USPIO when severe rejection occurred in a non-working heart model. In our new heterotopic working heart model, we have found that at earlier rejection states, the accumulation of immune cells is spatially heterogeneous. The immune-cell-concentrated foci can be detected by $T2^*$-weighted MRI in vivo one day after administration of USPIO (Fig. 1). Patches of signal reduction are detectable, presumably caused by accumulation of USPIO-labeled immune cells, particularly macrophages. In addition, mildly to moderately rejected allografts exhibited spatial heterogeneity in contractility and it can be detected by cardiac tagging. Figure 2 shows tagging images for the previous 2 hearts and the extent of the twist and radial shortening can be quantified by displacement field (Fig. 2, C & F). The angles of the arrow heads represent the direction of motion whereas the length of the arrow heads represents the extent of the motion. The areas with impaired contractility revealed by tagging largely correlated with the USPIO-accumulated regions. Moreover, allografts that receive long-term immunosuppressant cyclosporine treatment and have only grade 1 B rejection, show detectable sub-regional changes of strain in localized small areas in LV wall. This

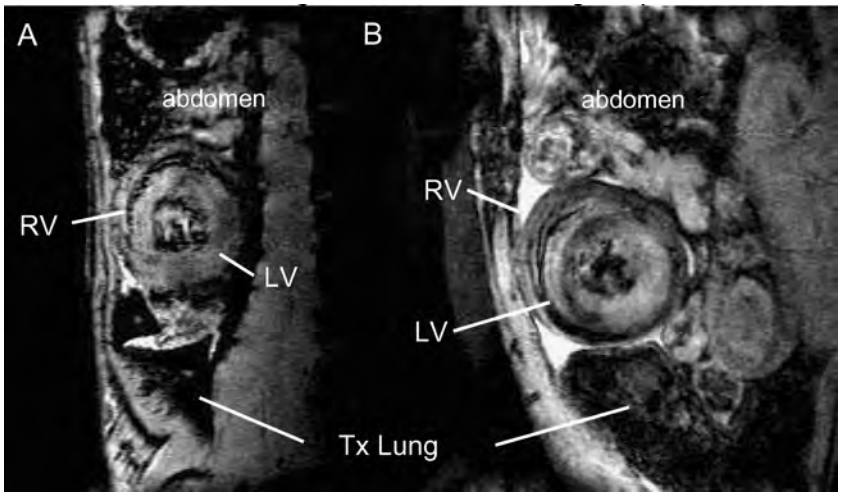

Figure 1. T2*-weighted image of 2 transplanted hearts 1 day after USPIO administration at (A) post-operational day (POD) 7 and (B) POD 6.

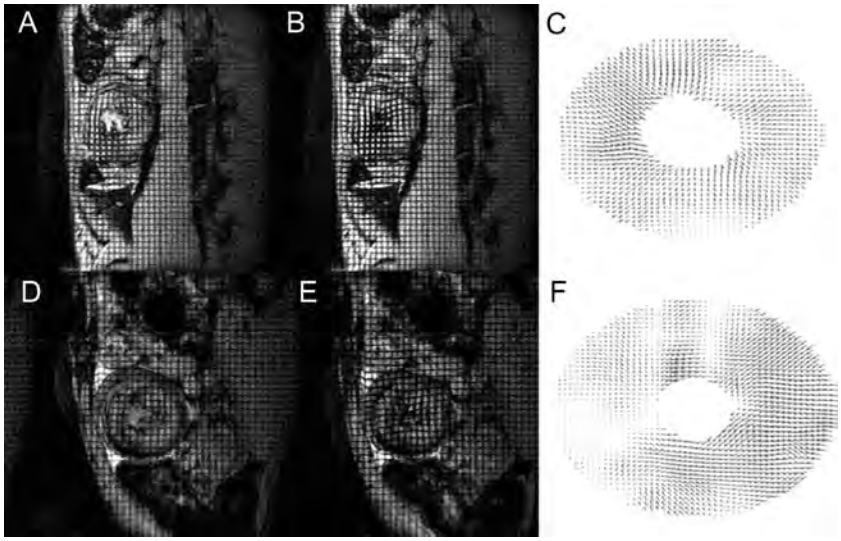

Figure 2. Tagging for heart A (A–C) at POD 7 and heart B (D–F) at POD 6 in Fig. 1. (A, D) end-diastole (B, E) end-systole (C, F) displacement field in a diastolic phase.

change is not detectable with mean strain measurement, or global systolic and diastolic functional evaluation.

Conclusions: Our data suggest that early rejection is spatially heterogeneous. The immune cell infiltrated foci can be detected non-invasively with in vivo USPIO labeling of immune cells whereas the regional functional loss can be measured by tagging and wall motion analysis. The two-pronged approach provides a potential non-invasive diagnostic tool for detecting early acute cardiac allograft rejection.

405. Assessment of Ion-Oxide Contrast Media (Resovist) for Visualization of MR-Guided Balloon Angioplasty

Sevim Yilmaz, MD,[1] Titus Kuehne, MD,[1] Dina Gelernte,[1] Bernhard Schnackenburg, PhD,[2] Julia J. Krueger, MD,[1] Eckart Fleck, MD,[2] Peter Lange, MD,[1] Eike Nagel, MD.[2]

[1]*Pediatric Cardiology, German Heart Institute, Berlin, Germany,* [2]*Department of Cardiology, German Heart Institute, Berlin, Germany.*

Introduction and Purpose: Successful MRI-guided balloon-angioplasty was reported by use of Gadolinium enhanced balloons and T1 weighted turbo field echo (TFE) MR fluoroscopy. However, optimal image quality for imaging cardiovascular anatomy is currently achieved by T1/T2* weighted steady state free precession (SSFP). Aim of this study was to assess the suitability of ion-oxide based MRI contrat media for balloon enhancement during SSFP based MR-fluoroscopy.

Methods: In in-vitro experiments plastic tubings were filled with different concentrations of the MRI contrast media Resovist (Schering, Germany). The ion-oxide based contrast media yields 500 mmolFe +/ml and was diluted with saline solution to a series of concentrations reaching

from 100% to 0.2% Resovist. For comparison, one tube was filled with 10% Gd-DPTA for optimum T1 effect. All tubing were imaged in a phantom using interactive real-time T1 weighted TFE and T1/T2* weighted SSFP for measuring signal intensity (SI) of the background (waterbath) and the tubings. For both, TFE and SSFP acquisition frame rate was 10 frames per second, slice thickness 6 mm, Matrix 256 × 256, FOV 200 × 200. In 4 in-vivo experiments angioplasty balloons (TayShak, diameter 12–20 mm) were advanced to the isthmus of the aorta and the aortic valve. There, the balloon was inflated with 100%, 10% and 1% Resovist and 10% Gd-DPTA. During inflation MR imaging was based on TFE and SSFP. SIs of the blood pool and the inflated balloon were measured. All measurements were repeated with different balloons 2 times in each animal.

Results: High concentration of Resovist (100% to 10%) produced in-vitro and in-vivo susceptibility artefacts that caused image distortion. Optimal signal contrast between the inflated balloon and its background (waterbath or aortic blood pool) was noted at concentration of 1% Resovist. At this concentration no image distortion due to susceptibility was noted. During SSFP SIs (unitless) were measured for the balloon in-vitro = 90 ± 9, balloon in-vivo = 97 ± 8, waterbath = 1252 ± 45 and blood pool aorta = 1387 ± 137, (background noise = 105 ± 23). Signal contrast between the balloon and the waterbath or aortic blood pool was excellent ($p < 0.001$). The balloon filled with 10% Gd-DPTA had SIs of 1185 ± 76 (in-vitro) and 1090 ± 66 9 (in-vivo) and thus produced no significant signal contrast to the waterbath or aortic blood pool ($p > 0.9$). During TFE, SI of the balloon filled with Gd-DPTA increased to 2120 ± 130. However, contrast-to-noise ratios of the waterbath and blood-pool decreased significantly ($p < 0.001$) and therefor reduced overall image quality. At concentration of 10% Resovist slight image distorsion occurred in the adjacent sourrounding of the inflated balloon. However, insertion of small amounts (1 ml) of 10% Resovist into the shaft of the catheter and the baloon produced local susceptibility artefacts that were easy perceptible to the observer and allowed for fast tracking of the catheter when moved through the abdominal or thoracal aorta.

Conclusions: The ion-oxide based MR contrast media Resovist is well suited for MR-guided balloon angioplasty of the aortic valve and isthmus. The use of SSFP and angioplasty ballons filled with ion-oxide contrast media allow for optimal imaging of cardivascular structures in combination with good image contrast between vascular blood pool and angioplasty balloon.

406. Interactive Real Time Imaging and Multi Coil Tracking

Sven Zuehlsdorff, PhD,[1] Peter Speier, PhD.[2] [1]*Siemens Medical Solutions, Chicago, IL, USA,* [2]*Siemens AG Medical Solutions, Erlangen, Germany.*

Introduction: The MR signal of small receiver coils can be used to determine the tip and track of interventional devices. In this work, an interactive gradient echo sequence with multi coil tracking capability was developed on a clinical 1.5 T scanner (Sonata, Siemens Medical Solutions, Erlangen, Germany). The imaging module supports both FLASH and trueFISP gradient timing. Projection data were acquired between consecutive images to determine the position of the tracking coils. Slice position and orientation were continuously updated in real time.

Material and Methods:

Imaging: The T2/T1 contrast of a trueFISP sequence is well suited to intravascular interventions (Duerk et al., 1998). The T1-weighted FLASH sequence is optimal for visualizing the bolus of contrast agent (Zuehlsdorff et al., 2004). This interactive sequence allows the image contrast to be changed interactively from FLASH to trueFISP. A nonselective saturation pulse prior each image could be applied optionally.

Tracking: Between consecutive images three non-selective projection data sets were acquired and the position of the tracking coils was determined (Domoulin et al., 1993). The slice position and orientation were changed in real time. Dependent on the number of independent micro coils, different tracking modes could be selected interactively:

Tip Tracking: The slice position was shifted with respect to one tracking coil position (Elgort et al., 2003).

Perpendicular: The slice orientation was adjusted perpendicular to two tracking coils and the slice was shifted to the first tracking coil.

Parallel: The slice contained two tracking coils. From the user interface, the slice could be freely rotated around the axis defined by the coils.

3D Plane: Three coils were defining slice position and orientation. The implemented algorithm contained a consistency check of the coil positions and performed a tracking mode with less constraints where required. The calculated slice orientation and position was displayed in the standard planning user interface of the scanner.

Phantom Experiments: In an initial phantom experiment a single micro coil and two independent receiver channels of an array coil were used for tracking. Small Cups of water simulated the localized signal of micro coils and compensated the unavailability of more micro coils.

In a second experiment the slice thickness was increased to 500 mm to acquire projection images (128 × 128 matrix, TE/TR = 1.82 ms/4.3 ms). The contrast was changed interactively to FLASH and the saturation recovery pulse was applied. 3 ml of contrast agent (Magnevist, Schering, Berlin, Germany) was injected into a water filled glove.

Results and Discussion:

Imaging: The bolus of contrast agent was clearly visualized at a frame rate of (1.8 Hz) using FLASH (Fig. 1). Previous

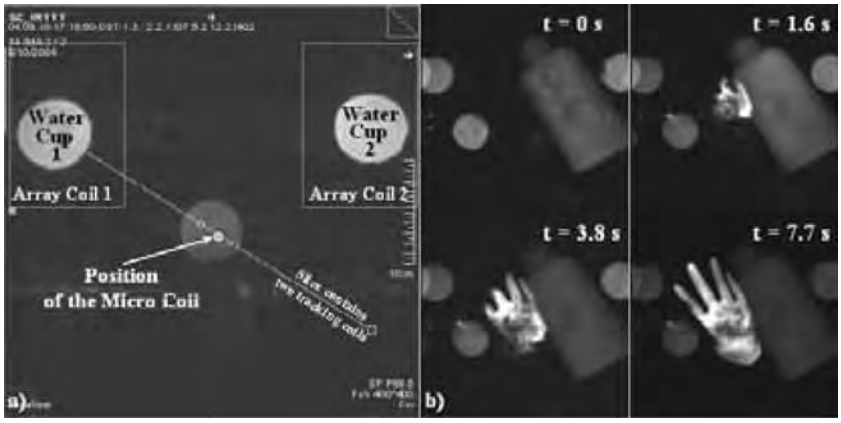

Figure 1. a) Parallel tracking mode. The slice contains two tracking coils and is displayed at the standard user interface on previously acquired images. b) Bolus of contrast agent: visualization using the FLASH imaging.

work has shown that the FLASH mode can be used to verify the position of a catheter and to monitor interventions like renal embolizations (Bock et al., 2004; Zuehlsdorff et al., 2004). This technique could be suitable for any contrast agent based intervention.

Tracking: The slice position and orientation was set and displayed correctly. A quantitative analysis would be possible by using only micro coils (Bock et al., 2004). The supported tracking modes can be used to track a catheter more accurately in blood vessels with a complicated course since position as well as orientation is updated in real time.

ACKNOWLEDGMENTS

The authors thank Daniel Elgort, Claudia M. Hillenbrand and Jeffrey L. Duerk for helpful discussion.

REFERENCES

Bock, M., et al. (2004). *JMRI* 19:580–589.
Domoulin, C. L., et al. (1993). *MRM* 29:411–415.
Duerk, J. L., et al. (1998). *JMRI* 8:203–208.
Elgort, D. R., et al. (2003). *JMRI* 18:621–626.
Zuehlsdorff, S., et al. (2004). *MRM* 52:214–218.

407. CMR at 3 Tesla Using a Large Flexible Surface Coil: Initial Experience

Krishna S. Nayak,[1] Padmini Varadarajan, MD,[2] Chia-ying Liu, PhD,[1] Samuel Valencerina,[3] Gerald M. Pohost, MD.[2]
[1]*Electrical Engineering, University of Southern California, Los Angeles, CA, USA,* [2]*Cardiovascular Medicine, University of Southern California, Los Angeles, CA, USA,* [3]*University Hospital Imaging Department, University of Southern California, Los Angeles, CA, USA.*

Introduction: The choice of receiver coils used in high-field CMR, such as at 3 T, is critical. Because of reduced RF penetration, a broader surface area is required. Too large an area requires imaging with a large FOV, which increases scan-time. This can often be reduced with parallel imaging, or k–t space techniques (if the additional FOV is relatively stationary). A simple solution is to use a single coil whose sensitivity profile barely covers the region of interest, minimizing the imaging FOV and therefore scan-time. We are in the process of testing a new 3 T CMR-dedicated system, and are examining several approaches to optimize image quality. Promising initial results were obtained with a flexible receiver coil that generates LV function studies at 3 T of diagnostic quality and coverage.

Purpose: To evaluate the usefulness of a large, single channel, flexible surface coil that wraps around the left chest for CMR imaging of the heart at 3 Tesla.

Methods: Experiments were performed on a GE Signa 3 T scanner (Excite 11) equipped with gradients supporting 40 mT/m amplitude and 150 T/m/s slew rate, and fast receiver. A general purpose 7 × 18 in flexible rectangular RF coil (FLEXGP) was used in all studies. Three healthy adult volunteers were scanned under a protocol approved by the Institutional Review Board of USC. Subjects were oriented supine with the flexible RF coil placed on the anterior and left lateral chest wall, and under the left axilla (see photo). Standard short axis, four chamber, and two chamber views were localized using the GE i-Drive real-time system. CINE loops of each view were acquired using a cine gradient echo sequence (“FastCARD”) and a cine steady-state free precession sequence (2D-FIESTA), both with TR < 4.8 ms. ECG gating was used in one subject, and plethysmographic gating was used in the other two subjects.

Results: Using this flexible surface coil approach, high quality images demonstrating the morphologic aspects of the